

Strong gravitational lensing of explosive transients

Masamune Oguri^{1,2,3}

¹Research Center for the Early Universe, University of Tokyo, Tokyo 113-0033, Japan

²Department of Physics, University of Tokyo, Tokyo 113-0033, Japan

³Kavli Institute for the Physics and Mathematics of the Universe (Kavli IPMU, WPI), University of Tokyo, Chiba 277-8582, Japan

E-mail: masamune.oguri@ipmu.jp

Abstract. Recent rapid progress in time domain surveys makes it possible to detect various types of explosive transients in the Universe in large numbers, some of which will be gravitationally lensed into multiple images. Although a large number of strongly lensed distant galaxies and quasars have already been discovered, strong lensing of explosive transients opens up new applications, including improved measurements of cosmological parameters, powerful probes of small scale structure of the Universe, and new observational tests of dark matter scenarios, thanks to their rapidly evolving light curves as well as their compact sizes. In particular, compact sizes of emitting regions of these transient events indicate that wave optics effects play an important role in some cases, which can lead to totally new applications of these lensing events. Recently we have witnessed first discoveries of strongly lensed supernovae, and strong lensing events of other types of explosive transients such as gamma-ray bursts, fast radio bursts, and gravitational waves from compact binary mergers are expected to be observed soon. In this review article, we summarize the current state of research on strong gravitational lensing of explosive transients and discuss future prospects.

Keywords: cosmology, gravitational lensing, transients

1. Introduction

Gravitational lensing is the deflection of light rays due to intervening inhomogeneous matter distributions in the Universe. The gravitational lensing effect is unambiguously predicted by Einstein's General Relativity, and has actually been used to test the validity of General Relativity as a gravitational theory. For instance, the deflection angle at the surface of the Sun is predicted to $1.7''$ in General Relativity, which was confirmed by observations during a solar eclipse in 1919 (see e.g., [1] for a historical review).

When the deflection angle is sufficiently large, it is possible that multiple images of a distant source are observed. In order for such *strong* gravitational lensing to be observed, a chance alignment of a background source and a foreground object that acts as a lens along the line-of-sight is needed. While the chance alignment of multiple stars is quite rare [2], strong gravitational lensing (strong lensing) is observed to be more common among galaxies and clusters of galaxies [3, 4]. Galaxies and clusters of galaxies are massive enough to split multiple images by more than an arcsecond on the sky, which can be resolved by astronomical observations in various wavelengths. Observations of such strong lensing events provide a unique opportunity to accurately measure the mass of the foreground lensing object, as well as to study the background object taking advantage of the magnification due to the lensing effect, as noted by Zwicky [3, 4].

Strong lensing was discovered for the first time in 1979 by Walsh *et al.* [5]. The background source is a quasar, which is a very bright active galactic nucleus powered by a supermassive black hole at the center of a galaxy. Quasars are bright enough to be detected even at cosmological distances, and their compact sizes suggest that their multiple images are well separated, which make them as an ideal source for strong lensing. In the first example, the quasar Q0957+561 at redshift $z = 1.4$ is split into two images separated by $6''$ due to the gravitational lensing effect of a foreground group of galaxies. The lensing interpretation was confirmed by the identical spectra of the two quasar images.

Strong lensing of background galaxies has also been discovered. Since galaxies are much larger in size than quasars, lensed galaxies often form giant arcs, which are highly elongated galaxy images due to strong lensing. Such giant arc was discovered for the first time

in the galaxy cluster A370 in the 1980s [6, 7].

Since the first discoveries, many strong lensing systems have been discovered in various surveys. To date, more than 100 strongly lensed quasars have been discovered from radio and optical surveys including Cosmic Lens All-Sky Survey [8, 9] and Sloan Digital Sky Survey Quasar Lens Search [10–12], from which evidence for the large value of cosmological constant has been obtained [13, 14]. In addition, hundreds of gravitationally lensed galaxies have been discovered in wide-field surveys including Sloan Digital Sky Survey [15–20], COSMOS [21, 22], Canada-France-Hawaii Telescope Legacy Survey [23], Herschel Astrophysical Terahertz Large Area Survey [24, 25], and South Pole Telescope [26, 27]. These strongly lensed galaxies are used e.g., to constrain the dark matter distribution in lensing galaxies as well as the initial mass function of stars (e.g., [28, 29]). A large number of gravitationally lensed distant galaxies have also been discovered by deep imaging of central regions of massive clusters of galaxies with *Hubble Space Telescope* [30–32]. Recently, more strong lens systems are being found in various surveys such as Gaia [33–35], Dark Energy Survey [36–39], Kilo-Degree Survey [40], Pan-STARRS1 [41], and Subaru Hyper Suprime-Cam survey [42, 43].

One important application of strong lensing comes from *time delays* between multiple images. The arrival time difference between multiple images is naturally expected as they travel through different paths, which serves as a very useful probe of the Universe. For instance, in 1964 Sjur Refsdal proposed to use measurements of time delays to constrain the Hubble constant H_0 , which is one of the most fundamental cosmological parameters [44]. This is possible because H_0 determines the absolute length scale of the Universe, and therefore changes the time delay between images by changing the difference of the light ray paths.

In order to measure time delays between multiple images, sources have to be time-variable. Quasars are suited for this application, because they are known to change their brightness, presumably due to the variation of the gas inflow and accretion disk instabilities. Indeed the time delay for the first gravitationally lensed quasar Q0957+561 is measured to be 417 days [45], and subsequently time delays have been measured for more than 20 quasar lens systems [46–48]. In combination with detailed modeling of mass distributions of lensing galaxies, now quasar lens

time delays constrain H_0 at better than 3% precision [49–52].

Recently measurements of H_0 attract a lot of attention given a possible tension among them. One of the most traditional methods to measure H_0 is the so-called distance ladder (e.g., [53–55]), with the most recent measurement yielding the best-fit value of $H_0 = 74.03 \pm 1.42$ km/s/Mpc including systematics [56]. On the other hand, H_0 can also be inferred from observations of cosmic microwave background anisotropies, yielding $H_0 = 67.4 \pm 0.5$ km/s/Mpc assuming the standard Λ -dominated cold dark matter model [57]. The discrepancy between these two measurements might suggest new physics such as additional relativistic particle species, or might be attributed to unknown systematic errors in either or both of these two measurements. While the latest measurement of H_0 from 6 quasar lens time delays is $H_0 = 73.3^{+1.7}_{-1.8}$ km/s/Mpc [52] and is consistent with the distance ladder result, more accurate and precise measurements of H_0 from time delays as well as the exploration of a possible dependence of the constraints on redshifts are important to understand the origin of the H_0 tension.

In fact, the Refsdal’s original proposal assumed to use strong lensing of supernovae, rather than quasars, to measure H_0 from time delays. Because of the relatively small number of distant supernovae observed so far, strong lensing of supernovae has not been discovered until recently, which is the reason why strongly lensed supernovae have not been used to obtain competitive constraints on H_0 . However, strong lensing of supernovae has several advantages over strong lensing of quasars, as will be discussed below. These advantages make strongly lensed supernovae an alternative powerful probe of the Universe.

In addition to supernovae, there are other types of explosive transients known, including gamma-ray bursts, fast radio bursts, and gravitational waves from compact binary mergers. Here we refer “explosive” transients to as astronomical events with relatively short time scales, which we adopt in order to distinguish them from long term variable objects such as quasars. These transients are observed at cosmological distances, and therefore are subject to strong lensing applications. A notable difference of these transients from supernovae is that their typical time scales of light curves, seconds or milliseconds, are much shorter than the time scale of supernova light curves, a month to several months. The shorter time scales indicate that the measurement precision of time delays is much better and that they can in principle probe much smaller mass scale of the lensing object for which a typical time delay is much shorter.

In most applications of strong lensing, we

can assume geometric optics, which is a good approximation when the wavelength is sufficiently small compared with the scale of the structure of interest. However, there are cases where we have to take account of wave optics effects, which is more fundamental than the geometric optics (e.g., [58]). Wave optics effects produce interesting observable features such as the interference pattern, which may provide additional useful information on the lensing object. In order for this effect to be observed, the source must be sufficiently compact compared to the lens, as the finite source size smears the interference pattern. Since these explosive transients have compact sizes as compared with quasars and galaxies, strong lensing of explosive transients may open up the possibility of using wave optics effects as additional applications.

In this review article, we focus on strong lensing of explosive transients, which will be discovered in large numbers in the future. We discuss how these events can be used to address several outstanding questions in modern cosmology, such as the nature of dark matter and dark energy. In addition, strong lensing can be used to understand these explosive transients better, with the help of gravitational lensing magnification. We also discuss the prospect for detecting these events in the future. We note that this review article focuses on a limited aspect of strong lensing, and in fact there are many reviews and textbooks [58–69] that are useful to cover the broader aspects of strong lensing.

The rest of this review article is organized as follows. In Section 2, we briefly review basic theory of strong lensing. In Section 3, we summarize explosive transients that we discuss in this review article. In Section 4, we discuss possible applications of strong lensing of these explosive transients. In Section 5, we summarize observations so far and also present future prospects. We give a brief summary in Section 6. Unless otherwise stated, we assume a flat cosmological model with matter density $\Omega_M = 0.3156$, cosmological constant $\Omega_\Lambda = 0.6844$, and the dimensionless Hubble constant $h = 0.6727$ [70].

2. The basics of strong gravitational lensing

2.1. Multiple images and the Einstein radius

We begin with a brief overview of the formulation of strong lensing. While the path of light rays in arbitrary matter distributions in the Universe is calculated by the geodesic equation in General Relativity, which is a differential equation that connects the path of light ray (i.e., null geodesics) to the space time metric, in most astronomical situations where deflection angles are small we can apply weak-field approximation to linearize the geodesic equation and obtain the so-

called lens equation. Although the weak-field limit does not apply to the source regions for e.g., binary black hole mergers, in the far-field gravitational lensing regime considered in this article the weak-field limit is still valid. The lens equation can be regarded as mapping between positions of the source (that would be observed in absence of the gravitational lensing effect) and the image (that is actually observed) on the sky. In the analysis of strong lensing, it is also common to assume that the deflection is dominated by a single object along the line-of-sight whose size is thin as compared with cosmological distances, although in some cases line-of-sight mass structures are not negligible. Under these approximations, the gravitational lensing effect is fully described by the following lens equation

$$\beta = \theta - \alpha(\theta), \quad (1)$$

where two-dimensional vectors β and θ denote positions of the source and the image on the sky, respectively, and α is the deflection angle

$$\alpha(\theta) = \frac{1}{\pi} \int d\theta' \frac{\theta - \theta'}{|\theta - \theta'|^2} \kappa(\theta'), \quad (2)$$

where κ , which is sometimes referred to as convergence, is essentially the projected surface mass density distribution of the lensing object $\Sigma(\theta)$ normalized by the critical surface density Σ_{cr}

$$\kappa(\theta) = \frac{\Sigma(\theta)}{\Sigma_{\text{cr}}} = \frac{1}{\Sigma_{\text{cr}}} \int_{-\infty}^{\infty} dz \rho(\theta, z), \quad (3)$$

$$\Sigma_{\text{cr}} = \frac{c^2}{4\pi G} \frac{D_{\text{os}}}{D_{\text{ol}} D_{\text{ls}}}, \quad (4)$$

where ρ is the three-dimensional density profile of the lensing object, z denotes the line-of-sight direction, c is the speed of light, G is the gravitational constant, and D_{os} , D_{ol} , and D_{ls} are angular diameter distances (see e.g., [71] for the definition) from the observer to the source, from the observer to the lens, and from the lens to the source, respectively. We note that the integrand in Equation (2) is the deflection angle from a differential mass element such that the integral sums over deflection angles from different mass elements. Figure 1 shows a schematic illustration of a gravitational lens system, including definitions of the angles involved in the lens equation.

Given the mass distribution of the lens, the lens equation (1) predicts the image position θ for the source position β . Importantly, the lens equation is in general nonlinear in θ , which suggests that multiple θ can satisfy the lens equation for a given β . These multiple solutions of the lens equation correspond to multiple images. Such multiple images can be

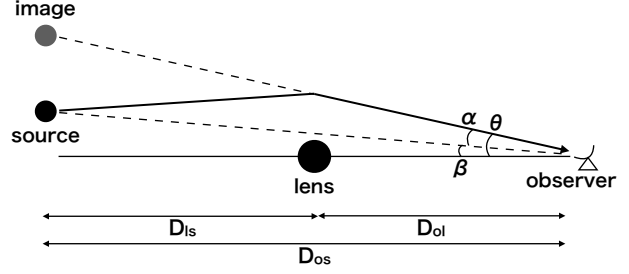


Figure 1. Schematic illustration of a gravitational lens system.

produced where the deflection angle α is sufficiently large, i.e., in high density regions such as centers of galaxies and clusters of galaxies.

Gravitational lensing not only changes the observed position on the sky, but also changes the observed brightness of the source. The change of the brightness is determined by the Jacobi matrix from the lens equation

$$A(\theta) = \frac{\partial \beta}{\partial \theta}, \quad (5)$$

from which the magnification μ of each image is computed as

$$\mu(\theta) = \frac{1}{\det A(\theta)}. \quad (6)$$

This means that the image at θ is magnified by a factor of $|\mu(\theta)|$. The sign of μ corresponds to the parity of the image such that the parity of the image is flipped when μ is negative.

Equation (6) indicates that magnification factors formally diverge at points satisfying $\det A(\theta) = 0$. These points in the image plane form closed curves, which are called critical curves. Corresponding curves in the source plane obtained via the lens equation (1) are called caustics. These curves are important in strong lensing studies because they are closely related to the image multiplicity. When a source is located far from caustics, there is only one image. Once a source crosses a caustic, the number of images increases or decreases by 2. Therefore, we can infer the number of images and image configuration by checking the position of a source with respect to caustics. We show an example in Figure 2, in which we can see 5 images as the source crosses caustics twice (see also [72]).

When the mass distribution of the lensing object is spherically symmetric (i.e., $\kappa(\theta) = \kappa(\theta)$), the deflection angle (2) reduces to

$$\alpha(\theta) = \frac{\theta}{\theta} \alpha(\theta) = \frac{2\theta}{\theta^2} \int_0^\theta d\theta' \theta' \kappa(\theta'), \quad (7)$$

and therefore the lens equation (1) reduces to the one-dimensional equation

$$\beta = \theta - \alpha(\theta). \quad (8)$$

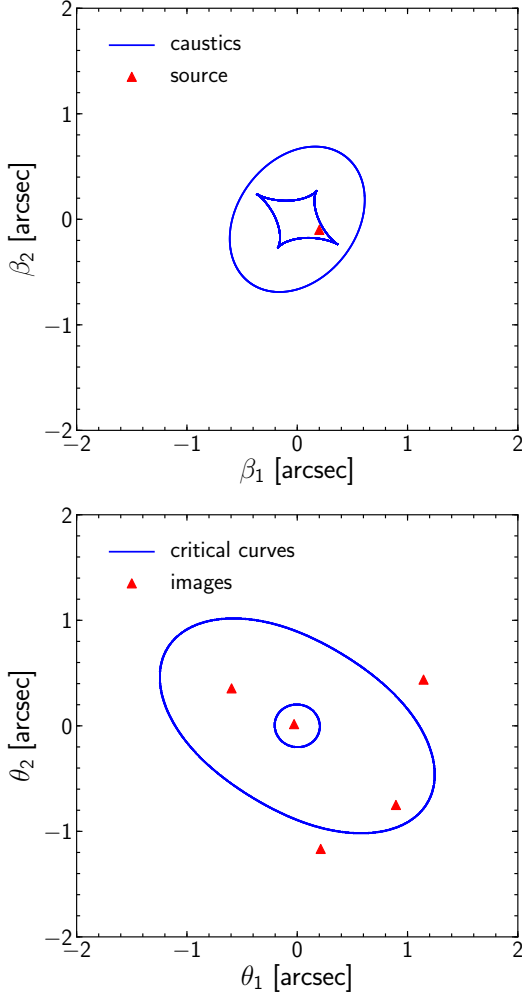


Figure 2. An example of the configuration of multiple images produced by strong lensing. The upper panel show the location of the source and caustics in the source plane, $\beta = (\beta_1, \beta_2)$. The lower panel show multiple images and critical curves in the image plane $\theta = (\theta_1, \theta_2)$. In this example, 5 images are produced. The lens equation is solved using `glafic` [73].

This indicates that in the limit of $\beta \rightarrow 0$ the lensed image forms a ring with the radius θ_{Ein} that satisfies

$$\theta_{\text{Ein}} - \alpha(\theta_{\text{Ein}}) = 0. \quad (9)$$

This radius θ_{Ein} is called the Einstein radius. We can rewrite equation (9) to obtain

$$M(< \theta_{\text{Ein}}) = D_{\text{ol}}^2 \int_0^{\theta_{\text{Ein}}} d\theta' 2\pi\theta' \Sigma(\theta') = \pi D_{\text{ol}}^2 \theta_{\text{Ein}}^2 \Sigma_{\text{cr}}, \quad (10)$$

which indicates that the Einstein radius probes the total projected mass of the lensing object within the Einstein radius, as long as lens and source redshifts are known.

In fact, equation (10) has important implications. It has been known that image separations between

multiple images are typically twice the Einstein radius, which is approximately true even when the lens mass distribution is not spherically symmetric. This means that we can estimate the Einstein radius from observations of multiple images (see also Figure 2). We can then use equation (10) to translate the observed Einstein radius into the total projected mass within the Einstein radius $M(< \theta_{\text{Ein}})$. Remarkably, the relation given by equation (10) does not depend on the radial density profile of the lens object. Therefore, $M(< \theta_{\text{Ein}})$ is one of the most robust quantities we can extract from observations of strong lensing, and hence plays a central role in the strong lens analysis.

It is useful to present Einstein radii for some lens mass distributions. For instance, the simplest mass model is a point mass lens with mass M , $\rho(\mathbf{r}) = M\delta(\mathbf{r})$. From equation (10), the Einstein radius is found to

$$\theta_{\text{Ein}} = \frac{1}{D_{\text{ol}}} \sqrt{\frac{M}{\pi \Sigma_{\text{cr}}}} \sim 1.63'' \times 10^{-6} \left(\frac{M}{M_{\odot}} \right)^{1/2} \left(\frac{D_{\text{ol}} D_{\text{os}} / D_{\text{ls}}}{3.06 \text{ Gpc}} \right)^{-1/2} \quad (11)$$

where distances (Gpc stands for gigaparsec) are normalized to values at the lens redshift $z_1 = 0.5$ and the source redshift $z_s = 1.0$. Another lens model that is commonly used is a singular isothermal sphere (SIS) model whose three-dimensional radial density profile is given by $\rho(r) = \sigma^2 / 2\pi G r^2$, where σ is the velocity dispersion. The Einstein radius of the SIS model is computed as

$$\theta_{\text{Ein}} = \frac{4\pi\sigma^2}{c^2} \frac{D_{\text{ls}}}{D_{\text{os}}} \sim 0.492'' \left(\frac{\sigma}{200 \text{ km s}^{-1}} \right)^2 \left(\frac{D_{\text{ls}} / D_{\text{os}}}{0.426} \right), \quad (12)$$

where the distances are again normalized to values at the lens redshift $z_1 = 0.5$ and the source redshift $z_s = 1.0$.

The so-called Navarro-Frenk-White (NFW) profile [74, 75] is yet another mass profile that is commonly used in the analysis of strong lensing. The NFW profile is used to model the density profile of dark matter halos, with its three-dimensional radial density profile given by $\rho(r) \propto r^{-1}(r + r_s)^{-2}$, where r_s is the scale radius. While the deflection angle of the spherical NFW profile can be computed analytically (e.g., [76]), no simple analytical expression for the Einstein radius is known. Figure 3 shows the relation between the halo mass and the Einstein radius for the NFW profile. It is found that the Einstein radius is sensitive to not only the halo mass but also the concentration parameter $c_{\text{vir}} = r_{\text{vir}}/r_s$, where r_{vir} is the virial radius. Since its inner density profile is not very steep, the Einstein radius for the NFW profile encloses relatively little of the total halo mass.

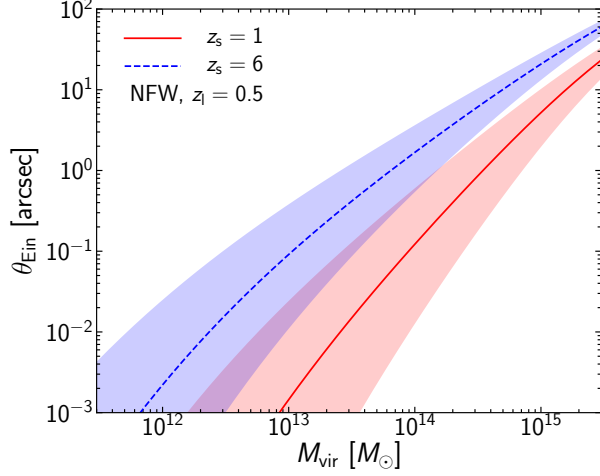


Figure 3. The Einstein radius θ_{Ein} as a function of the halo mass M_{vir} for an NFW profile. The lens redshift is fixed to $z_l = 0.5$, whereas source redshifts of $z_s = 1$ (solid red) and 6 (dashed blue) are considered. Here the mass-concentration relation presented in [77] is adopted. The shaded regions represent the uncertainty of θ_{Ein} originating from 1σ scatter ($\sigma_{\ln c} = 0.3$) of the concentration parameter.

2.2. Time delays

The light comprising the multiple images produced by strong lensing travels different paths, and hence take different amounts of time to propagate to us. The arrival time difference between multiple images can be observed if the source is time-variable such as quasars and explosive transients. The time delay for each image is computed as

$$\Delta t = \frac{1+z_l}{c} \frac{D_{\text{ol}} D_{\text{os}}}{D_{\text{ls}}} \left[\frac{(\theta - \beta)^2}{2} - \phi(\theta) \right], \quad (13)$$

where $\phi(\theta)$ is the lens potential that is related to the deflection angle as

$$\alpha = \nabla_{\theta} \phi. \quad (14)$$

The time delay involves contributions both from a geometric delay originating from different path lengths and a gravitational time delay originating from the gravitational potential of the lens. Note that we can observe only the time delay between different images e.g., we can observe $\Delta t_{ij} = \Delta t_i - \Delta t_j$ for image i and j .

Again, it is useful to present time delays for some lens models such as point mass lens and SIS. Using equation (13), we can rewrite Δt_{ij} as

$$\Delta t_{ij} = \Delta t_{\text{fid}} \Phi(\theta_i, \theta_j), \quad (15)$$

$$\Delta t_{\text{fid}} = \frac{1+z_l}{c} \frac{D_{\text{ol}} D_{\text{os}}}{D_{\text{ls}}} \theta_{\text{Ein}}^2, \quad (16)$$

$$\Phi(\theta_i, \theta_j) = \frac{(\theta_i - \beta)^2}{2\theta_{\text{Ein}}^2} - \frac{(\theta_j - \beta)^2}{2\theta_{\text{Ein}}^2} - \frac{\phi(\theta_i)}{\theta_{\text{Ein}}^2} + \frac{\phi(\theta_j)}{\theta_{\text{Ein}}^2}. \quad (17)$$

The factor Δt_{fid} represents a typical size of the time delay for the lens, and $\Phi(\theta_i, \theta_j)$ is a $\mathcal{O}(1)$ function that represents the dependence of the time delay on the image configuration. For instance, if the multiple image configuration is *symmetric*, we have $|\theta_i| \sim |\theta_j|$ and $|\beta| \sim 0$, leading to $\Phi(\theta_i, \theta_j) \sim 0$. Put another way, time delays are larger when the image configuration is more asymmetric, and are smaller when the image configuration is more symmetric.

We can also reinterpret the gravitational lensing effect from this expression of the time delay [78, 79]. Fermat's principle in geometric optics states that a light ray takes a path with a stationary path length. This immediately suggests that observed images should satisfy the following condition

$$\nabla_{\theta} \Delta t = 0. \quad (18)$$

By inserting equation (13) to equation (18) it is easily found that we can recover the lens equation (1) from this condition.

The typical time delay value is encapsulated by Δt_{fid} . Using equation (10), Δt_{fid} is rewritten as

$$\Delta t_{\text{fid}} = (1+z_l) \frac{4GM(<\theta_{\text{Ein}})}{c^3}, \quad (19)$$

which suggests that Δt_{fid} is on the order of the light crossing time of the “gravitational radius” for the mass defined by $M(<\theta_{\text{Ein}})$. Again, by normalizing distances to those at the lens redshift $z_l = 0.5$ and the source redshift $z_s = 1.0$, Δt_{fid} is estimated as

$$\Delta t_{\text{fid}} \sim 128 \text{ day} \times \left(\frac{\theta_{\text{Ein}}}{1''} \right)^2 \left[\frac{(1+z_l) D_{\text{ol}} D_{\text{os}} / D_{\text{ls}}}{4.59 \text{ Gpc}} \right]. \quad (20)$$

Therefore, for typical galaxy-scale strong lens systems with $\theta_{\text{Ein}} \sim 0.5'' - 1''$, we expect time delays on the order of a month to a few months. For reference, by inserting the typical Einstein radius of a solar mass compact object (see equation 11), $\theta_{\text{Ein}}/1'' = 10^{-6}$, to equation (20), we obtain $\Delta t_{\text{fid}} \sim 1.1 \times 10^{-5}$ sec for the fiducial distances. More generally, from equation (19) we can estimate Δt_{fid} for a point mass lens with mass M as

$$\Delta t_{\text{fid}} \sim 1.97 \times 10^{-5} \text{ sec} \times (1+z_l) \left(\frac{M}{M_{\odot}} \right), \quad (21)$$

which can also be applicable to other lens models if we replace M to $M(<\theta_{\text{Ein}})$.

On the other hand, the function $\Phi(\theta_i, \theta_j)$ depends on the assumed mass model. For a point mass lens,

$$\Phi(\theta_i, \theta_j) = \ln \left(\frac{\theta_j}{\theta_i} \right) + \frac{\theta_j^2 - \theta_i^2}{2\theta_i \theta_j}, \quad (22)$$

and for an SIS lens

$$\Phi(\theta_i, \theta_j) = \frac{2(\theta_j^2 - \theta_i^2)}{(\theta_j + \theta_i)^2}, \quad (23)$$

where $\theta_i = |\theta_i|$ and $\theta_j = |\theta_j|$. Again, no simple analytic expression of Φ for the NFW profile is known.

As mentioned in Section 1, time delays provide a powerful means of measuring the Hubble constant H_0 , which is sometimes referred to as time delay cosmography. Given that θ_{Ein} is well constrained from the data, observations of time delays between multiple images put direct constraints on the distance ratio $D_{\text{ol}}D_{\text{os}}/D_{\text{ls}}$, which is inversely proportional to H_0 , but only if Φ is accurately known. The examples above already indicate that values of Φ depend on the underlying lens mass model, which implies that accurate determinations of lens mass distributions are a key for successful time delay cosmography.

When multiple images are observed, we can constrain the lens mass distribution from positions and flux ratios of multiple images. However, in most cases these constraints are insufficient to robustly constrain the lens mass distribution, and we need additional constraints. For instance, host galaxies of quasars or any explosive transients are also expected to be lensed into extended arcs, which may provide useful additional constraints (e.g., [80]). Furthermore, the velocity dispersion of the lensing galaxy, which can be observed by deep spectroscopy of the lensing galaxy, is sometimes used as additional constraints on the lens mass distribution (e.g., [81]).

However, there is a fundamental difficulty in the strong lensing analysis, which originates from various degeneracies inherent to the lens equation. One such example is the mass-sheet degeneracy [82], in which the following transform is considered

$$\phi(\theta) \rightarrow (1 - \kappa_{\text{ext}})\phi(\theta) + \kappa_{\text{ext}} \frac{\theta^2}{2}, \quad (24)$$

$$\beta \rightarrow (1 - \kappa_{\text{ext}})\beta, \quad (25)$$

where κ_{ext} is constant. It is straightforward to see that this transform keeps the lens equation (1) unchanged. This transform corresponds to an operation that rescales the mass of the lensing object and instead inserts a constant mass sheet κ_{ext} . Importantly, this transform also changes time delays (13) between any multiple image pairs as

$$\Delta t_{ij} \rightarrow (1 - \kappa_{\text{ext}})\Delta t_{ij}, \quad (26)$$

which indicates that H_0 estimated from *observed* time delay should scale as $H_0 \rightarrow (1 - \kappa_{\text{ext}})H_0$. Therefore, H_0 measured from time delays is subject to the uncertainty of κ_{ext} that cannot be constrained from

strong lensing observations. As we will discuss later, one way to break the degeneracy is to observe the magnification factor μ , because the transform changes μ as

$$\mu \rightarrow (1 - \kappa_{\text{ext}})^{-2}\mu. \quad (27)$$

Note that this transform does not change the ratio of magnification factors between multiple images.

This mass-sheet degeneracy implies other approximate degeneracies. For instance, for a power-law mass model with $\phi \propto r^\beta$ ($\beta = 1$ corresponds to an SIS profile), the change of β around $\beta = 1$ can be approximated by the mass-sheet transform with $1 - \kappa_{\text{ext}} = 2 - \beta$ (e.g., [83]), which implies that the Hubble constant from time delays is sensitive to the radial slope of the density profile of the lensing object, which is difficult to be constrained from strong lensing observations. Furthermore, the mass-sheet transform is generalized to the source-position transform [84, 85], which is essentially a global mapping of the source plane that keeps observed image positions unchanged. In order to measure H_0 robustly from time delays, it is essential to explore these degeneracies carefully, and to make use of additional observational constraints that can break these degeneracies.

2.3. Microlensing and Substructure lensing

While calculations of multiple image positions and time delays so far assumed that the lens mass distribution is smooth, this assumption is in fact not valid. Small scale structures in lensing objects often affect strong lensing observables significantly, and therefore should be taken into account.

One such example is microlensing by stars in lensing galaxies (see e.g., [86–88]). The contribution to the lens potential includes both dark and baryonic matter in the lensing object, and some fraction of the baryonic matter consists of stars. Lensing by these individual stars can significantly affect magnifications of individual multiple images if the source size is comparable or smaller than the Einstein radii of the stars (see e.g., [89, 90]).

To illustrate the sensitivity of microlensing variabilities on the source size, in Figure 4 we show examples of flux variabilities as a function of the source size R_{src} , which is computed using the GPU-Enabled, High Resolution cosmological MicroLensing parameter survey (GERLUMPH) microlensing magnification maps [91, 92]. It is clear that microlensing variabilities are suppressed at $R_{\text{src}} \gtrsim R_{\text{Ein}}$ due to the large source size, where $R_{\text{Ein}} = D_{\text{os}}\theta_{\text{Ein}}$ is the Einstein radius of the microlens in the source plane.

Strong lensing allows us to probe the small-scale structure of the dark matter distribution as well. In the standard cold dark matter (CDM) model, the dark

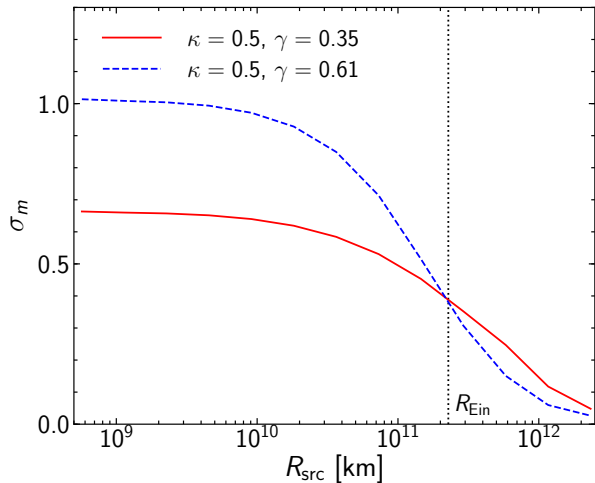


Figure 4. Flux variabilities σ_m (the standard deviation in magnitude) due to microlensing as a function of the source size, which are computed using the GERLUMPH microlensing magnification maps [91, 92] with the smooth matter fraction of 0.5. Note that the distributions of flux variabilities are not Gaussian particularly for small source sizes. We show results both for positive parity (convergence $\kappa = 0.5$ and shear $\gamma = 0.35$) and negative parity ($\kappa = 0.5$ and $\gamma = 0.61$) cases. The source is assumed to have a top-hat profile with the radius R_{src} . We assume $z_l = 0.5$, $z_s = 1$, and the microlens mass $M = 0.3 M_\odot$ to convert the simulation results into physical units. For comparison, the Einstein radius in the source plane is indicated by a vertical dotted line.

matter distribution in galaxies and clusters is predicted to be lumpy rather than smooth. In the CDM model, the mass function of such substructures extends to very small masses in which no star is formed (e.g., [93]). The detection of very small mass substructures in observations therefore serves as a critical test of the CDM model (e.g., [94]).

Substructures can be detected by strong lensing via flux ratios between multiple images [95]. This is because substructures can affect the magnification of one of multiple images to produce anomalous flux ratios that cannot be reproduced by mass models assuming smooth mass distributions. However, in order to study the abundance of substructures from flux ratio anomalies, lensing by substructures should be distinguishable from microlensing by stars in lensing galaxies, because microlensing also changes flux ratios between multiple images as discussed above. One way to overcome this issue is to use sources whose sizes are sufficiently large so that they are insensitive to microlensing (see Figure 4).

In addition to flux ratios, substructures affect time delays between multiple images as well, particularly for time delays between multiple images with small angular separations, such as merging image pairs near the critical curve [46, 96]. This is because the smaller

time delays between such merging pairs make them more sensitive to perturbations.

2.4. Lensing rates

Strong lensing is a rare event that occurs only when the light ray from a distant object passes through (or near) high density regions such as centers of galaxies and clusters. The chance probability of strong lensing can be calculated as long as the mass distribution and abundance of putative lensing objects are known. From the density profile one can derive the lensing cross section, i.e., the area on the sky within which strongly lensed multiple images are produced, which is on the order of θ_{Ein}^2 .

Historically, strong lensing probabilities are calculated assuming lensing by galaxies. For instance, the detailed calculation in Turner *et al.* [97] indicates that strong lensing events are dominated by those due to field elliptical galaxies. They also show that strong lensing probabilities are a steeply increasing function of the source redshift. Calculations of strong lensing probabilities have been improved partly due to improved measurements of velocity dispersion functions of galaxies in observations [13, 14, 98–106].

It has been known that clusters of galaxies also produce strong lensing. While individual clusters have larger lensing cross sections than galaxies, clusters are much less abundant than galaxies. Narayan and White [107] discussed the image separation distribution in the standard CDM cosmology to argue that the contribution of clusters to the total strong lensing probability is small but non-negligible. This calculation has been updated following the improved knowledge of the density profiles and the abundance of clusters [108–122].

As briefly mentioned in Section 2.1, N -body simulations of the structure formation in the CDM model have revealed that the density profile of dark matter halos is universal and is well approximated by the NFW profile [74, 75]. As shown in Figure 3, the Einstein radius of the NFW profile is a steep function of the halo mass such that it becomes too small for galaxy-scale dark matter halos, $M_{\text{vir}} \lesssim 10^{13} M_\odot$, which appears to contradict observations in which there are many strong lens systems with $\theta_{\text{Ein}} \sim 1''$ due to isolated galaxies.

This issue is resolved by taking proper account of the baryonic component. Dissipative cooling of gas makes the spatial distribution of stars much more compact than that of dark matter. At the galaxy scale this effect is more efficient such that the total density profile of dark matter and the baryonic component resembles an SIS profile that was also mentioned in Section 2.1. Indeed calculations based on this idea successfully reproduce the observed image separation

distribution of strong lenses for a wide mass range from the galaxy to cluster scales [23, 123–133], which suggest that the contribution of clusters to the total strong lensing probability is ~ 1 –10% and that strong lensing events are dominated by those due to single galaxies.

In practice, we need to take account of selection effects when we compare expected strong lensing probabilities with observations. The best-known example is the magnification bias [134], which originates from the fact that in any survey objects are detected only above some flux threshold. Because of gravitational lensing magnifications, faint objects that fall below the threshold in absence of gravitational lensing can in fact be observed thanks to the magnification. This effect increases the observed strong lensing rates and hence should be taken into account. For sources with the flux f and differential number counts $N(f) = dN/df$, the magnification bias factor B is computed as

$$B = \frac{1}{N(f)} \int_{\mu_{\min}}^{\infty} \frac{d\mu}{\mu} \frac{dP}{d\mu} N(f/\mu), \quad (28)$$

where $dP/d\mu$ denotes the magnification probability distribution. As a simple example, assuming power-law number counts $N(f) \propto f^{-\alpha}$ and an SIS lens for which $dP/d\mu = 8/\mu^3$ ($\mu > \mu_{\min} = 2$), we can compute B as

$$B = \frac{2\alpha}{3 - \alpha}. \quad (29)$$

From this expression it is found that steeper number counts (larger α) lead to the larger magnification bias factor.

In addition to the magnification bias, there are other possible selection effects. Multiple images with large differences in their fluxes are difficult to be identified in observations, and any cut on the flux ratio of multiple images reduces the strong lensing probability. For lens systems with small Einstein radii, image separations of multiple images can be too small to be resolved in observations, depending on the spatial resolutions of observations. Also when the size of the source is comparable or larger than the Einstein radius, the gravitational lensing effect on the source is quite inefficient. These effects remove strong lenses with small image separations from the sample, leading to the smaller strong lensing probability. Therefore, depending on the threshold on the image separation, they can significantly change the relative contribution of cluster lenses to the whole strong lens sample. In order to make fair comparisons with observations, any theoretical calculations of strong lensing probabilities should take proper account of these selection effects.

Here we present some examples of calculations of strong lensing probabilities, following recent calculations presented in Oguri [135]. In short, we compute

strong lensing probabilities due to single galaxies, because galaxies dominate the total strong lensing probability as discussed above. The strong lensing probability $P_{\text{sl}}(z_s)$ for a source at redshift z_s is computed as

$$P_{\text{sl}}(z_s) = \int_0^{z_s} dz_1 \frac{d^2V}{dz_1 d\Omega} \int_0^{\infty} d\sigma \frac{dn}{d\sigma} B\sigma_{\text{sl}}(\sigma), \quad (30)$$

where $d^2V/dz_1 d\Omega$ is the comoving volume element per redshift and steradian, $dn/d\sigma$ is the velocity dispersion function of galaxies, $\sigma_{\text{sl}}(\sigma)$ is the strong lensing cross section in units of steradian for galaxies at redshift z_1 with the velocity dispersion σ , and B encapsulates various selection effects such as the magnification bias. To compute the strong lensing cross section, we assume that the mass distribution of lensing galaxies follow a Singular Isothermal Ellipsoid, which is an extension of an SIS to include the ellipticity in the projected mass distribution. We also add external shear perturbation. The velocity dispersion function $dn/d\sigma$ is taken from the one measured in the Sloan Digital Sky Survey [136] with the redshift evolution predicted by the Illustris cosmological hydrodynamical simulation [137]. The strong lensing probability is derived in the Monte-Carlo approach in which many lenses and sources are randomly generated and the lens equation is solved numerically using **glafic** [73]. Interested readers are referred to [135] for more details.

Figure 5 shows the strong lensing probability $P_{\text{sl}}(z_s)$ computed with the setup described above, without any selection bias i.e., $B = 1$. As noted in e.g., [97], the strong lensing probability is a steeply increasing function of the source redshift at low redshifts, $z \lesssim 1$. The dependence on the redshift becomes somewhat weaker at higher redshifts. The redshift dependence mainly comes from the total volume, $\int_0^{z_s} dz_1 d^2V/dz_1 d\Omega$ in equation (30), which suggests that the redshift dependence is $\propto z_s^3$ at low redshifts. We find that the strong lensing probability shown in Figure 5 is crudely approximated by the following functional form

$$P_{\text{sl}}(z_s; B = 1) \approx \frac{(5 \times 10^{-4}) z_s^3}{(1 + 0.41 z_s^{1.1})^{2.7}}, \quad (31)$$

which may be useful for quick estimates of the occurrence of strong lensing events in various situations.

As discussed above, in most cases we have to take account of the magnification bias, which can significantly enhance the strong lensing probability. For instance, the radio source sample used in Cosmic Lens All-Sky Survey [8, 9] approximately has power law number counts with $\alpha = 2.1$, which leads to, from equation (29), the magnification bias factor of $B \sim 4.8$ for an SIS lens.

The magnification bias factor is larger when number counts are steeper. An extreme example

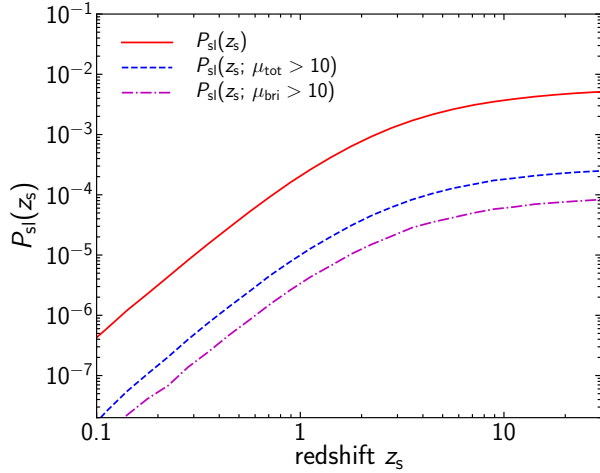


Figure 5. Strong lensing probabilities $P_{\text{sl}}(z_s)$ defined by equation (30) as a function of the source redshift z_s . See the text for the setup of the calculations. The solid line shows strong lensing probabilities without any selection bias (i.e., $B = 1$), whereas dashed and dash-dotted lines show probabilities of strong lensing with the total magnification $\mu_{\text{tot}} > 10$ and the magnification of the brightest image $\mu_{\text{bri}} > 10$, respectively.

is found in the bright ends of number counts or luminosity functions. For many types of sources, there are exponential cutoffs in their number counts or luminosity functions, and beyond those exponential cutoffs the magnification bias is infinitely large as without gravitational lensing magnifications we would not expect any sources observed far beyond the cutoffs. Therefore at these luminosity or flux ranges, almost all the observed sources are strong lensing events, suggesting that the strong lens search among such brightest sources is highly efficient. A good example of this is brightest galaxies in the submm wavelength, which indeed have been found to be dominated by strong lensing (e.g., [24]).

In Figure 5, we also show probabilities of strong lensing events with magnifications $\mu > 10$. Since magnification probabilities are approximately $dP/d\mu \propto \mu^{-3}$ for most situations, we naively expect $P_{\text{sl}}(z_s) \propto \mu_{\text{min}}^{-2}$. In our fiducial case without the selection effect we have $\mu_{\text{min}} \approx 2$, suggesting that the larger magnification threshold of $\mu_{\text{min}} = 10$ leads to $\approx 1/25$ smaller strong lensing probabilities (i.e., $B \approx 1/25$), which appears to hold approximately in Figure 5.

However, there are some subtleties in computing the magnification bias. The magnification factor used in the calculation of the magnification bias can be either the total magnification of all the multiple images, μ_{tot} , or the magnification of one of the multiple images. To illustrate this point, in Figure 5 we consider two cases, one is $\mu = \mu_{\text{tot}}$ and the other is

the magnification of the brightest image, $\mu = \mu_{\text{bri}}$, which clearly make a quantitative difference. The choice should be made depending on the strong lens search strategy in the observations. If multiple images are unresolved when searching for strong lensing the total magnification should be used, whereas multiple images are well resolved, either the magnification of the brighter or the fainter image should be used.

In the case of strong lensing of explosive transients, there may be another selection bias associated with time delays. A transient survey is conducted during some period, and we may miss some of the multiple images that fall outside the survey period. This effect is more significant for multiple images with longer time delays. This time delay bias [138] may also be important in future statistical analysis of lensed explosive transients.

2.5. Wave optics effects

In this review article, thus far we implicitly assumed geometric optics in all the calculations of gravitational lensing. Indeed, geometric optics serve as an excellent approximation in most astronomical situations of interest. However, there are some exceptional cases where wave optics effects play a crucial role (e.g., [139–145]), especially for strong lensing of explosive transients that is the topic of this review article. Here we briefly review the wave aspect of gravitational lensing theory. For more details, see e.g., [58, 146].

We consider the propagation of monochromatic waves $\psi(\mathbf{x}, t) = \tilde{\psi}(\mathbf{x})e^{-2\pi i f t}$ with frequency f . In the presence of a weak gravitational field that is characterized by the gravitational potential $U(\mathbf{x})$ ($|U| \ll 1$), the propagation equation is

$$(\nabla^2 + \omega^2)\tilde{\psi} = 4\omega^2 U\tilde{\psi}, \quad (32)$$

with $\omega = 2\pi f$. Defining the amplification factor as

$$F = \frac{\tilde{\psi}^{\text{L}}}{\tilde{\psi}}, \quad (33)$$

where $\tilde{\psi}^{\text{L}}$ and $\tilde{\psi}$ denote wave amplitudes with and without gravitational lensing, respectively, we obtain the diffraction integral formula for the amplification factor of gravitationally lensed waves in the expanding Universe as a function of frequency f and the source position β

$$F(f, \beta) = \frac{1 + z_1}{c} \frac{D_{\text{ol}} D_{\text{os}}}{D_{\text{ls}}} \frac{f}{i} \int d^2\theta \exp[2\pi i f \Delta t(\theta, \beta)], \quad (34)$$

where Δt is the arrival time defined by equation (13). This formula allows us to compute both amplitude and phase shifts of the wave due to gravitational lensing. Note that the wave intensity is amplified by $|F|^2$. We

can simplify this equation by defining the dimensionless parameter w using Δt_{fid} defined in equation (16)

$$w = 2\pi f \Delta t_{\text{fid}} = 2\pi f \frac{1+z_1}{c} \frac{D_{\text{ol}} D_{\text{os}}}{D_{\text{ls}}} \theta_{\text{Ein}}^2. \quad (35)$$

From equation (19), it is found that w is also expressed as

$$w = 2\pi f (1+z_1) \frac{4GM(<\theta_{\text{Ein}})}{c^3}. \quad (36)$$

By defining $\hat{\theta} = \theta/\theta_{\text{Ein}}$ and $\hat{\beta} = \beta/\theta_{\text{Ein}}$, we can rewrite equation (34) as

$$F(f, \beta) = \frac{w}{2\pi i} \int d^2 \hat{\theta} \exp \left[iwT(\hat{\theta}, \hat{\beta}) \right], \quad (37)$$

where T is similar to Φ defined in equation (17) and is described as

$$T(\hat{\theta}, \hat{\beta}) = \frac{(\hat{\theta} - \hat{\beta})^2}{2} - \frac{\phi(\hat{\theta})}{\theta_{\text{Ein}}^2}, \quad (38)$$

which is also dimensionless.

The geometric optics limit corresponds to $f \rightarrow \infty$. In this limit, we can evaluate equation (37) using the stationary phase approximation, where only critical points satisfying

$$\nabla_{\hat{\theta}} T(\hat{\theta}, \hat{\beta}) = 0, \quad (39)$$

contribute to the integral in equation (37). This is same as equation (18) and hence the lens equation, indicating that the contributions comes from only multiple image positions $\hat{\theta}_j$. In this limit we can approximate equation (37) as

$$F(f, \beta) \approx \sum_j \frac{1}{i} |\det A(\theta_j)|^{-1/2} \exp \left[iwT(\hat{\theta}_j, \hat{\beta}) + \frac{i\pi\sigma_s}{4} \right], \quad (40)$$

where j runs over multiple images, $A(\theta)$ is the Jacobi matrix defined in equation (5), and σ_s is the signature of A i.e., the number of positive eigenvalues minus the number of negative eigenvalues. Given the definition of the magnification factor (6), we can simplify this further as

$$F(f, \beta) \approx \sum_j |\mu(\theta_j)|^{1/2} \exp \left[iwT(\hat{\theta}_j, \hat{\beta}) - i\pi n_j \right], \quad (41)$$

where $\mu(\theta)$ is the (signed) magnification factor and $n_j = 0, 1/2$, and 1 correspond to the cases where θ_j is a minimum, saddle, and maximum point of $T(\theta)$, respectively. From this expression, we can derive the amplification of the wave intensity as

$$|F(f, \beta)|^2 \approx \sum_j |\mu(\theta_j)| + 2 \sum_{j < k} |\mu(\theta_j) \mu(\theta_k)|^{1/2} \cos [w\Phi(\theta_j, \theta_k) - \pi \Delta n_{jk}], \quad (42)$$

where $\Phi(\theta_j, \theta_k)$ is defined in equation (17) and $\Delta n_{jk} = n_j - n_k$. The first term in the right hand side of equation (42) agrees with magnifications in the geometric optics, whereas the second term represents wave optics effects and is the interference between multiple images. In the limit $f \rightarrow \infty$, however, this term rapidly oscillates such that e.g., averaging over a small finite source size easily eliminates this term.

We caution that equation (42) is valid only approximately, and in order to take full account of wave optics effects we should evaluate equation (37) directly. For instance, in the case of a point mass lens, the amplification can be computed analytically [147, 148]

$$|F(f, \beta)|^2 = \frac{\pi w}{1 - e^{-\pi w}} \left| {}_1F_1 \left(\frac{i}{2} w, 1; \frac{i}{2} w \hat{\beta}^2 \right) \right|^2, \quad (43)$$

where ${}_1F_1$ is the confluent hypergeometric function. In this case, the dimensionless parameter w reduces to

$$w = 2\pi f \frac{4GM(1+z_1)}{c^3} \approx 1.24 \times 10^{-4} (1+z_1) \left(\frac{M}{M_\odot} \right) \left(\frac{f}{\text{Hz}} \right). \quad (44)$$

Equation (43) indicates that the maximum amplification at $\hat{\beta} = 0$ is

$$|F(f, \beta = 0)|^2 = \frac{\pi w}{1 - e^{-\pi w}}, \quad (45)$$

which becomes $|F(f, \beta = 0)|^2 \rightarrow 1$ for $w \rightarrow 0$. This is essentially diffraction of waves i.e., any obstacle whose size is much smaller than the wavelength does not affect the propagation of waves. From this expression it is found that the gravitational lensing magnification becomes quite inefficient for $w \lesssim 1$ due to wave optics effects. We note that the similar analytic expression of the amplification factor for an SIS lens is also available [149]

$$|F(f, \beta)|^2 = \left| \sum_{n=0}^{\infty} \frac{\Gamma(1+n/2)}{n!} g(w, \hat{\beta}) \right|^2, \quad (46)$$

$$g(w, \hat{\beta}) = \left(2we^{(3\pi/2)i} \right)^{n/2} {}_1F_1 \left(-\frac{n}{2}, 1; \frac{i}{2} w \hat{\beta}^2 \right), \quad (47)$$

where the dimensionless parameter w for an SIS reduces to

$$w = 2\pi f (1+z_1) \frac{1}{c} \left(\frac{4\pi\sigma^2}{c^2} \right)^2 \frac{D_{\text{ol}} D_{\text{ls}}}{D_{\text{os}}}. \quad (48)$$

Equations (42) and (43) suggest that the gravitational lensing amplification shows an oscillating behavior as a function of the source position or the frequency of waves. Figure 6 shows some examples. If

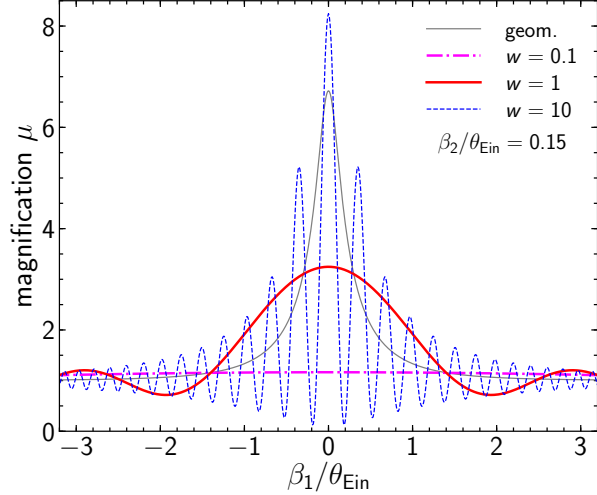


Figure 6. The magnification factor for a point mass lens in wave optics, which is computed from equation (43), as a function of the source position. Here we fix $\beta_2/\theta_{\text{Ein}} = 0.15$ and change β_1 to see how the magnification factor change as a function of the source position $\beta = (\beta_1, \beta_2)$, for $w = 0.1$ (dash-dotted magenta), 1 (thick solid red), and 10 (dashed blue), where w is the dimensionless parameter defined by equation (44). The magnification factor for the geometric optics case is shown by the thin solid gray line.

observed, it provides a direct evidence of wave optics effects in action. As mentioned above, however, wave optics effects may be suppressed due to the finite source size (e.g., [149]). Here we discuss the finite source size effect using equation (42), from which it is found that the oscillating behavior comes from $w\Phi$. For reasonably small β , equations (22) and (23) imply that $\Phi \sim (\hat{\theta}_j - \hat{\theta}_i) \sim \hat{\beta} = \beta/\theta_{\text{Ein}}$. Therefore the width of interference oscillations in the source plane is on the order of θ_{Ein}/w . In order for the interference pattern to be observed, the source size in the angular unit, $\beta_s = R_s/D_{\text{os}}$, should satisfy $\beta_s \lesssim \theta_{\text{Ein}}/w$.[‡] This condition yields

$$R_s \lesssim \frac{D_{\text{os}}\theta_{\text{Ein}}}{w}. \quad (49)$$

In the case of the point mass lens, this condition is expressed as

$$R_s \lesssim 2.24 \times 10^{15} \text{ km} \left(\frac{1+z_1}{1.5} \right)^{-1} \times \left(\frac{M}{M_\odot} \right)^{-1/2} \left(\frac{f}{\text{Hz}} \right)^{-1} \left(\frac{D_{\text{os}}D_{\text{ls}}/D_{\text{ol}}}{0.949 \text{ Gpc}} \right)^{1/2}, \quad (50)$$

where distances are normalized to values at the lens redshift $z_1 = 0.5$ and the source redshift $z_s = 1.0$.

[‡] Near the fold caustic, the time delay between merging image pairs scales as $\Delta t \propto \beta^{3/2}$, where β here is the distance from the caustic. Therefore, in this situation this condition should be modified as $(\beta_s/\theta_{\text{Ein}})^{3/2} \lesssim 1/w$.

To summarize, wave optics effects suppress the gravitational lensing magnification when $w \lesssim 1$ due to diffraction, where w is defined in equation (35). On the other hand, when $w \gtrsim 1$, the gravitational lensing magnification exhibits oscillating behavior as a function of the source position or the wave frequency, which can be observed only when the source size R_s satisfies the condition given by equation (49). We will discuss specific examples in Section 4.4.

3. Explosive transients

3.1. Supernovae

A supernova is an explosion associated with the death of a star. Observations of supernovae have a long history, for example some supernovae that took place in the Milky Way were observed even in the naked eye and were recorded in the literature. Here we provide a brief overview of supernovae. Interested readers are referred to reviews (e.g., [150]) and textbooks (e.g., [151]) for more details.

Observationally there is a great deal of diversity in properties of supernovae, including their light curves and spectral features. First, supernovae are classified based on the presence or absence of hydrogen lines. Supernovae without hydrogen lines are classified as Type I, whereas those with hydrogen lines are classified as Type II. Type I supernovae are further divided into subclasses based on the presence or absence of a singly ionized silicon line (SiII) such that those with the strong silicon line are Type Ia and those with the weak or no silicon line are Type Ib/c. Type II supernovae are also classified into e.g., Type IIP, IIL, and IIn, depending on their shapes of the light curves and/or the presence or absence of narrow line features in their spectra.

We can classify supernovae on more physical basis, depending on their explosion mechanisms. Type Ia supernovae are thought to be thermonuclear explosions of white dwarfs near the Chandrasekhar mass, $\approx 1.4M_\odot$. The explosion of a white dwarf is triggered by the matter accretion from a companion star. There is a long controversy whether the companion star is a non-degenerate star such as a red giant or a main sequence star (single degenerate scenario) or the companion star is also a white dwarf i.e., a Type Ia supernova is triggered by the merger of two white dwarfs (double degenerate scenario). See e.g., a review by Maoz *et al.* [152] for more details on this topic. On the other hand, both Type Ib/c and Type II supernovae are thought to be produced by the core collapse of massive stars. There are several possible mechanisms to trigger the explosion, including the development of an iron core that exceeds the Chandrasekhar and leads to the collapse and bounce of the core. After the bounce the

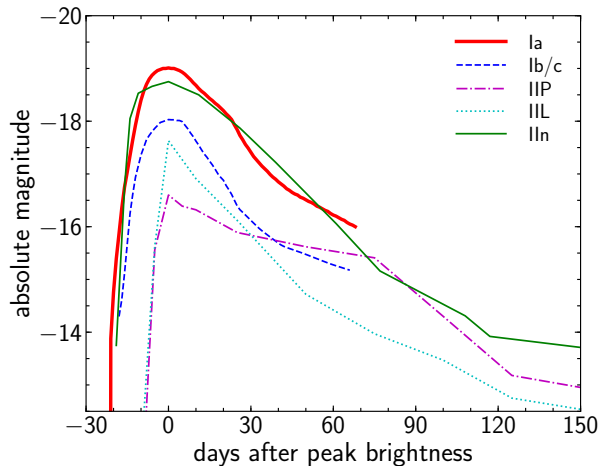


Figure 7. Light curves of various types of supernovae. We show template light curves of Ia (thick solid red), Ib/c (dashed blue), IIP (dot-dashed magenta), IIL (dotted cyan), and IIn (thin solid green). The light curve templates in V-band are taken from the webpage https://c3.lbl.gov/nugent/nugent_templates.html. Absolute magnitudes at the peaks correspond to typical magnitudes for these supernova types [154].

outgoing shock is heated by neutrino emitted from the core, which is thought to be a key ingredient for the successful explosion. Extensive numerical simulations to understand the explosion mechanism of core-collapse supernovae are ongoing (see e.g., [153]).

Figure 7 shows template light curves of various supernovae. It is found that supernovae are luminous. Peak luminosities of luminous supernovae are comparable to galaxy luminosities, which indicate that we can observe supernovae out to high redshifts, $z \gtrsim 1$. The Figure also indicates that the typical time scale of the light curves is a month, if we define the time scale by the full-width-half-maximum (FWHM) of the light curve. Their shapes are simple with a rise and a fall, although details are different for different types of supernovae. We note that these are template light curves in the supernova rest frame. Observed light curves of supernovae at cosmological distances are stretched due to cosmological dilation by a factor of $1+z$, which indicates that we expect the time scale of a few months in the observer frame for supernovae at $z \sim 1-2$.

Studies of supernovae are important in several ways. For instance, supernovae are associated with the death of stars, and therefore their rates as a function of galaxy type or redshift reflect the cosmic history of star formation. Supernovae are produced only when masses of progenitor stars fall in a particular range, from which we can obtain information on the stellar initial mass function. One of the most important applications of supernovae is the measurement of the cosmic expansion. It is known that peak luminosities

of Type Ia supernovae are quite similar, which is particularly true if the empirical relation between peak luminosities and widths of light curves is taken into account [155]. This “standardizable candle” nature of Type Ia supernovae allows us to measure luminosity distances to supernovae. Combining the distance measurements with redshift information, one can constrain the Hubble constant H_0 as well as the cosmic expansion history out to sufficiently high redshifts. For instance, luminosity distance measurements out to $z \sim 1$ with Type Ia supernovae led to the direct confirmation of the accelerated expansion of the Universe and hence the significant amount of dark energy in the Universe [156, 157]. Type Ia supernovae also play a crucial role in the measurement of H_0 with the so-called distance ladder method (e.g., [53]).

Because of their importance, a number of supernova surveys have been conducted, including Supernova Legacy Survey [158], Sloan Digital Sky Survey II Supernova Survey [159], Palomar Transient Factory [160], Hubble Space Telescope Cluster Supernova Survey [161], Pan-STARRS Medium Deep Survey [162], All-Sky Automated Survey for Supernovae [163], Dark Energy Survey Supernova Program [164], and Hyper Suprime-Cam Transient Survey [165]. The total number of supernovae discovered by now amounts to $O(10^4)$ both for Type Ia supernovae and for core-collapse supernovae (e.g., [166]).

These supernova surveys also revealed new classes of supernovae. Among others, an interesting class of supernovae relevant for this review article is a superluminous supernova (e.g., [167, 168]). One of the first examples of this class, SN 2005ap, was discovered by the Texas Supernova Survey in 2005 [169]. Superluminous supernovae, whose origin is yet to be known but is believed to be associated with the deaths of very massive stars, have peak absolute magnitudes less than -21 , and hence are much more luminous than normal Type Ia and core-collapse supernovae (see Figure 7). Their light curves are also wider, with the typical time scale of up to ~ 100 days in the rest frame rather than a month. Thanks to their bright luminosities, they can be observed out to very high redshifts of $z \gtrsim 2$ (e.g., [170, 171]).

Finally, we summarize event rates and sizes of supernovae, which are important for strong lensing studies. Li *et al.* [172] derived supernova rates in the local Universe as $R_{\text{SNIa}} = (3.0 \pm 0.6) \times 10^4 \text{ Gpc}^{-3} \text{ yr}^{-1}$ for Type Ia and $R_{\text{SNcc}} = (7.1 \pm 1.6) \times 10^4 \text{ Gpc}^{-3} \text{ yr}^{-1}$ for core-collapse (i.e., Type Ib/c and Type II). We note that these comoving rates increase toward higher redshifts, mainly due to the increase of the cosmic star formation rate density from $z \sim 0$ to ~ 2 . Quimby *et al.* [173] estimated the rate of superluminous supernovae at $z \sim 0.2$ to $R_{\text{SLSN}} = (1.99^{+1.37}_{-0.86}) \times$

$10^2 \text{ Gpc}^{-3}\text{yr}^{-1}$. The size of a supernova changes with time because of the dynamical evolution of the photosphere. In the case of supernovae, the ejecta is expected to enter the homologous expansion phase, in which the radial expansion velocity is proportional to the radius, after a few times of the expansion time scale. Initially the photospheric radius increases as the ejecta expands, and then it decreases as the density of the ejecta decreases. As a result, the photospheric radius is $\sim 10^{10} \text{ km}$ at around the peak of the light curve (e.g., [174]).

3.2. Gamma-ray bursts

Gamma-ray bursts are very energetic explosions that are observed in the gamma-ray band. Their durations are quite short, $< 100 \text{ sec}$, and such high energy prompt emission is followed by afterglow emissions observed from the X-ray to radio wavelength range. Gamma-ray bursts were discovered for the first time in 1960s by the Vela satellites [175], but their origin was totally unknown at that time. Later the Burst and Transient Source Experiment (BATSE) on the Compton Gamma Ray Observatory observed many gamma-ray bursts to show that their distribution on the sky is isotropic, which supports the extragalactic origin of gamma-ray bursts [176]. Detections of the afterglow emissions [177] led to identifications of their host galaxies, which confirm that gamma-ray bursts indeed lie at cosmological distances [178]. Now gamma-ray bursts are detected regularly by the *Swift* satellite [179] as well as the Fermi Gamma-ray Space Telescope [180, 181]. Here we summarize basic properties of gamma-ray bursts, see reviews [182–184] for more details.

From the analysis of gamma-ray bursts detected by the BATSE, it is found that gamma-ray bursts are classified into two classes, long (or long-soft) and short (or short-hard) gamma-ray bursts [185]. They are divided based on the duration of the emission, such that gamma-ray bursts with their durations longer and shorter than 2 sec are classified into long and short gamma-ray bursts, respectively. Figure 8 shows examples of light curves of both long and short gamma-ray bursts. The clear difference of the durations between short and long gamma-ray bursts is seen. It is also seen that the light curve of the long gamma-ray burst is complicated with several subpeaks. Indeed shapes of light curves of different long gamma-ray bursts are quite different with each other. So far > 5000 long gamma-ray bursts and > 1000 short gamma-ray bursts have been discovered mainly by Compton Gamma Ray Observatory, the *Swift* satellite, and Fermi Gamma-ray Space Telescope.

Long gamma-ray bursts are thought to be caused by the death of massive stars, because of the following

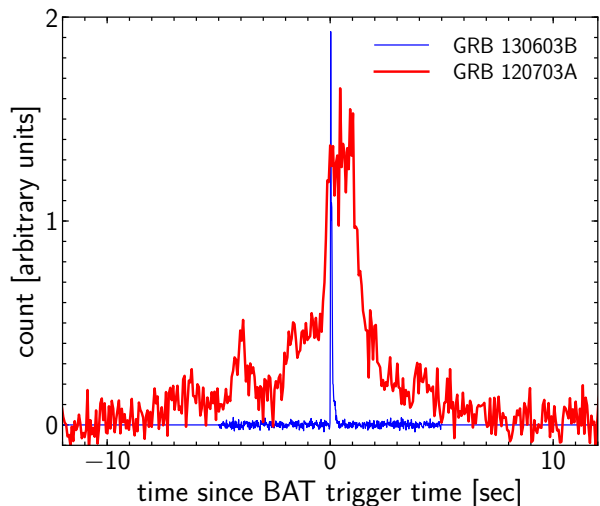


Figure 8. Examples of light curves of short (GRB 130603B, thin blue) and long (GRB 120703A, thick red) gamma-ray bursts observed by the Burst Alert Telescope (BAT) on the *Swift* satellite [179]. The light curves are rescaled so that their peak counts roughly match.

reasons. First, in most cases host galaxies of long gamma-ray bursts are young star-forming galaxies in which many massive stars are recently formed (e.g., [186]). Second, it was found that some gamma-ray bursts are accompanied by core-collapse supernovae that are also thought to be caused by the death of massive stars (e.g., [187, 188]). In this scenario, gamma-ray emissions can be explained by a relativistic ejecta due to a strong relativistic jet that is launched after the core-collapse. However, for this scenario to work, the central engine that drives the relativistic jet is needed, although the true nature of the central engine is still yet to be understood (e.g., [189] for a review).

The connection of long gamma-ray bursts to star formation suggests that observations of long gamma-ray bursts may help understand the star formation history in the Universe. An advantage of long gamma-ray bursts is their very high luminosities that allow us to observe them out to very high redshifts. Indeed, the redshift distribution of long gamma-ray bursts detected in *Swift* has the median of $z \approx 2$ [184, 190], and extends out to $z \sim 9.4$ [191]. Regarding the rate of long gamma-ray bursts, from the *Swift* gamma-ray burst sample Wanderman and Piran [192] derived the local rate of $R_{\text{LGRB}} = 1.3^{+0.6}_{-0.7} \text{ Gpc}^{-3}\text{yr}^{-1}$ for $L > 10^{50} \text{ erg s}^{-1}$. The comoving rate increases with redshift as $(1+z)^{2.1^{+0.5}_{-0.6}}$ at $z < 3$, and decreases as $(1+z)^{-1.4^{+2.4}_{-1.0}}$ at $z > 3$. We note that this is the rate of events that we can observe i.e., gamma-ray bursts with the jet orientations aligned with the line-of-sight directions. In order to derive the true event

rate in the Universe we have to apply for the beaming factor correction, which would make the long gamma-ray burst rate about two orders of magnitude higher.

On the other hand, short gamma-ray bursts are thought to have a different origin, because of their markedly different properties from those of long gamma-ray-bursts. For example, in many cases host galaxies of short gamma-ray bursts are elliptical galaxies with little star formation (e.g., [193]) in contrast to star-forming host galaxies of long gamma-ray bursts. In addition, the association of short gamma-ray bursts with supernovae is lacking (e.g., [194]). A promising scenario that explains these properties is that short gamma-ray bursts are caused by binary mergers of compact objects such as neutron stars and black holes. This scenario is confirmed by the discovery of gravitational waves from a binary neutron star merger, GW170817, for which the associated short gamma-ray burst GRB 170817A was detected (see also Section 3.4). From BATSE, *Swift*, and Fermi short gamma-ray samples, Wanderman and Piran [195] derived the local rate of $R_{\text{SGRB}} = 4.1^{+2.3}_{-1.9} \text{ Gpc}^{-3} \text{ yr}^{-1}$ for $L > 5 \times 10^{49} \text{ erg s}^{-1}$. The comoving rate rapidly increases with increasing redshift, at least out to $z \sim 1$.

There have been many proposals to use gamma-ray bursts as standardizable candles to probe the cosmic expansion history (see e.g., [196] for a review), just like Type Ia supernovae. Many luminosity correlations that can be used to standardize gamma-ray bursts are proposed, including the correlation between the time variability and the luminosity [197], the isotropic energy and the rest-frame peak energy [198], the luminosity and the rest-frame peak energy [199], and the peak energy and the collimated energy [200]. Cosmology with gamma-ray bursts is potentially very powerful as the Hubble diagram can be extended to very high redshifts out to $z > 8$.

The size of the emission region has also been studied in the literature (e.g., [201–203]). The size is estimated as

$$R_{\text{em}} \sim \Gamma^2 c \Delta t_{\text{var}}, \quad (51)$$

where $\Gamma = \{1 - (v/c)^2\}^{-1/2}$ is the Lorentz factor of the ejecta with velocity v and Δt_{var} is the variability time scale. The Lorentz factor is thought to be typically $\mathcal{O}(100)$. From observed variabilities of light curves, we have $R_{\text{em}} \sim 10^{13} \text{ cm}$ for short gamma-ray bursts and $R_{\text{em}} \sim 10^{14} \text{ cm}$ for long gamma-ray bursts, albeit with large uncertainties. Due to the relativistic effect, the transverse extent of the emission region R_{tv} differs from R_{em} by a factor of Γ i.e.,

$$R_{\text{tv}} \sim \frac{R_{\text{em}}}{\Gamma}, \quad (52)$$

which suggests that, assuming $\Gamma \sim 300$, $R_{\text{tv}} \sim 3 \times 10^{10} \text{ cm} = 3 \times 10^5 \text{ km}$ for short gamma-ray bursts and

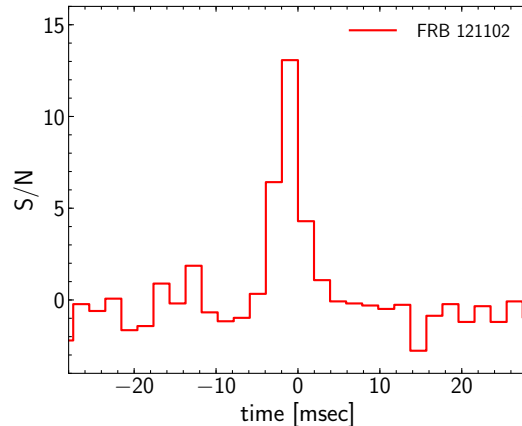


Figure 9. An example of light curves of fast radio bursts. Here we show a dedispersed, averaged pulse profile of FRB 121102 detected with the Arecibo Observatory [212].

$R_{\text{tv}} \sim 3 \times 10^{11} \text{ cm} = 3 \times 10^6 \text{ km}$ for long gamma-ray bursts, again with large uncertainties. Since the size that is relevant for strong lensing is R_{tv} , in what follows we refer to R_{tv} as the size of gamma-ray bursts. We note that these sizes are for gamma-ray prompt emissions, and sizes of X-ray and optical afterglows should be three or more orders of magnitude larger than the values mentioned above.

3.3. Fast radio bursts

Fast radio bursts, which are transient radio pulses with the time scale of a millisecond, are a new class of transients that was identified relatively recently (see [204, 205] for recent reviews). The first example of fast radio bursts was discovered with the Parkes Observatory in 2007 by Lorimer *et al.* [206]. Discoveries of additional four events by Thornton *et al.* [207] support the astrophysical origin of fast radio bursts. Thanks to Canadian Hydrogen Intensity Mapping Experiment (CHIME) [208] and Australian Square Kilometre Array Pathfinder (ASKAP) [209], the number of known fast radio bursts is now rapidly increasing, and is reaching $\mathcal{O}(100)$ [210, 211]. An example of the light curve is shown in Figure 9.

A key quantity that characterizes each fast radio burst is the dispersion measure. Because of dispersive effects, electromagnetic waves propagate through a plasma with different speeds at different frequencies. More specifically, electromagnetic waves with frequency ν have the following delay of the arrival time

$$\Delta t = \frac{e^2}{2\pi m_e c} \frac{\text{DM}}{\nu^2} \approx 4150 \text{ sec} \left(\frac{\nu}{\text{MHz}} \right)^{-2} \left(\frac{\text{DM}}{\text{cm}^{-3} \text{ pc}} \right), \quad (53)$$

where DM is the dispersion measure, which is

essentially the column density of free electron along the line-of-sight

$$\text{DM} = \int_0^d n_e dl, \quad (54)$$

where d is the distance to the fast radio burst. Since the Universe is ionized at $z \lesssim 6$, a large contribution from the intergalactic medium (IGM) to the observed DM after subtracting the Galactic contribution is expected. A useful approximation that relates the DM from the IGM and redshift z is [204]

$$\text{DM}_{\text{IGM}} \approx 1000 \times z \text{ cm}^{-3} \text{ pc}, \quad (55)$$

which is reasonably accurate at least out to $z \sim 2$.

The dispersion measures of fast radio bursts discovered so far are typically $100 - 1000 \text{ cm}^{-3} \text{ pc}$ after subtracting the Galactic contribution, which suggest their redshifts of $\approx 0.1 - 1$ according to equation (55). A complication is that there may also be contributions from host galaxies and local environments. For example, if the source is surrounded by a dense plasma, the contribution of the local environment to DM can be as large as $\sim 1000 \text{ cm}^{-3} \text{ pc}$ and hence can be comparable or larger than DM from the IGM. Therefore the redshift estimated by equation (55) should be taken as the upper limit of the source redshift.

Accurate distances to fast radio bursts are obtained if their host galaxies are successfully identified. However, identifications of host galaxies have been challenging due to limited localization capabilities. The host galaxy was recently identified for the first time for a repeating fast radio burst, which represents a rare class of fast radio bursts with repeating pulses. So far only ten repeating fast radio bursts, FRB 121102 [213], FRB 180814.J0422+73 [214], and some more new repeating FRBs [215] have been identified. In the case of FRB 121102, its host galaxy is identified to be a low-metallicity, low-mass dwarf galaxy at $z = 0.193$ [216], which confirms the extragalactic origin of fast radio bursts.

Very recently, host galaxies have been identified for non-repeating fast radio bursts as well. A luminous galaxy at $z = 0.3214$ has been identified as a host galaxy of the non-repeating fast radio burst FRB 180924 detected by ASKAP [217]. A massive galaxy with a relatively low specific star-formation rate at $z = 0.66$ has been identified as a host galaxy of FRB 190523 detected by the Deep Synoptic Array ten-antenna prototype [218]. These results highlight the possibility of the association of fast radio bursts with relatively old stellar populations.

The mechanism to produce these fast radio bursts is still unknown. Many progenitor models that explain fast radio bursts have been proposed (see [204] for a

summary). The statistical analysis of a large sample of fast radio bursts is a key for discriminating these different scenarios. Another important clue will be obtained by identifying many host galaxies. For example the host galaxy of FRB 121102 implies the connection between fast radio bursts and massive star formation, although it is also unknown whether repeating and non-repeating fast radio bursts have the same origin.

The volumetric rate of fast radio bursts is also still very uncertain, although it gives another important clue to the origin. Assuming that observed fast radio bursts are distributed out to $z \sim 1$, we crudely obtain $R_{\text{FRB}} \sim 2 \times 10^3 \text{ Gpc}^{-3} \text{ yr}^{-1}$ [204]. The recent study by Lu and Piro [219] suggests an order of magnitude higher rate, $\sim 3 \times 10^4 \text{ Gpc}^{-3} \text{ yr}^{-1}$ (see also [220]). In either case, the high event rate of fast radio bursts is a great promise for the future.

The size of the emission region of fast radio bursts is poorly constrained. The direct upper limit of $R_{\text{tv}} < 0.7 \text{ pc} \sim 2 \times 10^{13} \text{ km}$ is obtained from observations of the repeating fast radio burst FRB 121102 with European VLBI Network [221], although this constraint is not quite tight. Tighter constraints of the size will greatly help discriminate different progenitor models.

3.4. Gravitational waves

The existence of gravitational waves was predicted by Albert Einstein in 1916 on the basis of General Relativity. Gravitational waves are essentially the propagation of fluctuations of curvature in spacetime, but the strain amplitude is so small that its detection has been quite challenging. The first direct detection [222] was made in 2015 by the Advanced Laser Interferometer Gravitational-Wave Observatory (Advanced LIGO; [223]). The event named GW150914 was produced by a merger of a binary black hole with masses $\sim 36 M_{\odot}$ and $\sim 29 M_{\odot}$ located at redshift $z \sim 0.09$. Figure 10 shows the waveform of GW150914, which was detected both in the Hanford and Livingston detectors. The slight offset of the arrival times and the relative amplitudes between the two detectors contain information on the position of the gravitational wave source on the sky. Since then, the study of gravitational waves is progressing rapidly. See e.g., [224, 225] for details of theory and experiments of gravitational waves.

Gravitational waves that are detectable with Advanced LIGO are thought to be produced from mergers of binary black holes, binary neutron stars, and black hole-neutron star binaries. Since Advanced LIGO can detect gravitational waves in the frequency range $f \sim 10^1 - 10^4 \text{ Hz}$, only gravitational waves at the final inspiraling and merging stages are observed.

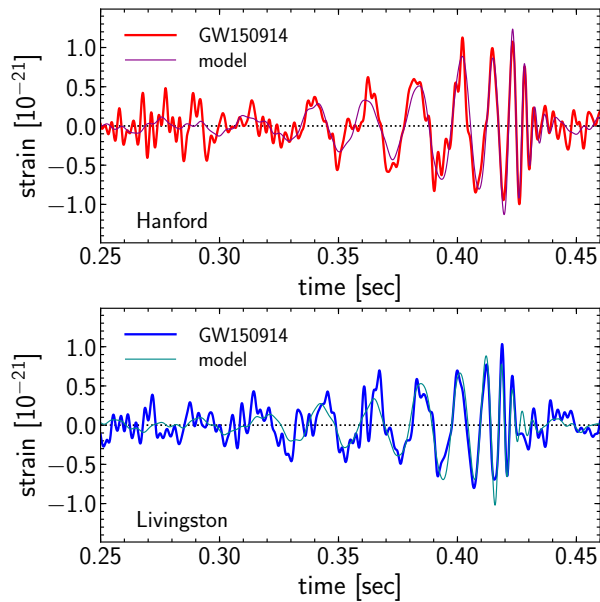


Figure 10. The first gravitational wave event GW150914 [222] observed by Advanced LIGO. This event was detected by both Hanford (*upper*) and Livingston (*lower*) detectors. The observed waveform (*thick*) is plotted together with the best-fitting model (*thin*).

After the discovery of GW150914, there are more than 10 gravitational wave observations from binary black hole mergers out to $z \sim 0.5$ with the total mass ranging from $\sim 20 M_\odot$ to $\sim 80 M_\odot$ (e.g., [226] for the summary of the second observing run, and there are more observations from the third observing run). The first observation of gravitational waves from a binary neutron star merger was reported in 2017 [227]. Currently there is no confirmed observation of a black hole-neutron star binary merger.

We can measure various properties of merging binaries from observations of gravitational waves. One of the most important quantities that can be accurately constrained from observations of gravitational waves is the (redshifted) chirp mass

$$\mathcal{M}_z = (1+z)\mathcal{M} = (1+z) \frac{(m_1 m_2)^{3/5}}{(m_1 + m_2)^{1/5}}, \quad (56)$$

where m_1 and m_2 are masses of two compact objects that constitute the binary. The chirp mass is constrained very well because the orbital evolution during inspiraling at a given frequency depends only on the chirp mass at the leading-order. The degeneracy between m_1 and m_2 is broken by the analysis of the waveform around the merger and ringdown phase. In addition, we can obtain information on the spin from the analysis of the waveform.

Importantly, we can also measure the luminosity distance D_L to the binary from observations of

gravitational waves. This is because the frequency and its time evolution of a merging binary constrain the chirp mass accurately, which in turn predicts the amplitude of gravitational waves emitted from the binary. Since the propagation of gravitational waves decreases the amplitude as D_L^{-1} , the observation of the strain amplitude of gravitational waves directly constrains D_L . On the other hand, the redshift is not directly measured by gravitational wave observations. Therefore, the redshift of $z \sim 0.09$ for GW150914 was in fact the value *inferred* from the luminosity distance measurement.

Redshifts of gravitational wave sources are obtained directly if we successfully identify their host galaxies. However the identification of a host galaxy is challenging, mainly because of the poor angular resolution of gravitational wave observations. In the case of GW150914, the error circle of the arrival direction has an area of 600 deg^2 , which is too wide to pinpoint its host galaxy. One way to improve the localization accuracy is to detect gravitational waves with more detectors, as demonstrated by observations of GW170814 [228] whose arrival direction was constrained to an area of 60 deg^2 thanks to the detection by Advanced Virgo [229] in addition to two detectors of Advanced LIGO. In the near future KAGRA [230] and LIGO India will join the observing run, which allows us to localize gravitational wave sources to a few square degrees, although this is still insufficient for determining host galaxies from gravitational wave observations alone in most cases.

Therefore, we usually rely on observations of electromagnetic counterparts for secure identifications of host galaxies. The search for electromagnetic counterparts for binary black hole mergers have been unsuccessful so far, which implies that electromagnetic counterparts for binary black hole mergers are weak if at all exist. On the other hand, as already mentioned in Section 3.2, binary neutron star mergers are a prominent candidate of the central engine of short gamma-ray bursts. Shortly after observations of the first neutron star merger event GW170817 [227] a likely counterpart in gamma-ray, GRB 170817A, was discovered by the Fermi satellite [231]. The gamma-ray burst was observed 1.7 sec after the coalescence. Subsequently, electromagnetic counterparts in other wavelengths such as X-ray, ultraviolet, optical, infrared, and radio were identified [232]. From these observations, the host galaxy of GW170817 is identified to NGC 4993 at $z = 0.0098$.

Such identification of a host galaxy opens up a new application in cosmology. As emphasized above, gravitational wave observations directly measure the luminosity distance to the source. Together with the redshift information from the host galaxy, one can

constrain the distance-redshift relation and hence the Hubble constant [233]. This application, which is sometimes referred to as a standard siren, provides a powerful means of deriving accurate constraints on the Hubble constant because of the simple and well understood physics behind the method. In the specific case of GW170817, the Hubble constant is constrained to $H_0 = 70_{-8.0}^{+12.0}$ km/s/Mpc only from a single event [234].

The current estimate of event rates of compact binary mergers from gravitational wave observations depends on the prior on the mass distribution. From the analysis of Advanced LIGO and Advanced Virgo First and Second Observing Runs [226], the event rate for binary black hole (BBH) mergers is constrained to $R_{\text{BBH}} \sim 9.7 - 101 \text{ Gpc}^{-3}\text{yr}^{-1}$ and that for binary neutron star (BNS) mergers to $R_{\text{BNS}} \sim 110 - 3840 \text{ Gpc}^{-3}\text{yr}^{-1}$, which are obtained by combining results from different priors on the mass distribution. Since any black hole-neutron star (BHNS) binary merger was not observed in those observing runs, only the upper limit of $R_{\text{BHNS}} < 610 \text{ Gpc}^{-3}\text{yr}^{-1}$ is obtained. While the redshift evolution of the event rates is not yet constrained from the observations, theoretical models generally predict that the comoving rates increase toward higher redshifts out to $z \sim 2 - 10$ (e.g., [235, 236]).

The size of gravitational wave sources is effectively the orbital radius. Since the gravitational wave frequency f is related to the angular velocity Ω of the binary orbit as $f = \Omega/\pi$, from Kepler's law we obtain the size R for a binary system of compact objects with equal masses $m_1 = m_2 = m$ as

$$R = \left(\frac{2Gm}{\pi^2 f^2} \right)^{1/3} \approx 3000 \text{ km} \left(\frac{m}{M_\odot} \right)^{1/3} \left(\frac{f}{\text{Hz}} \right)^{-2/3}, \quad (57)$$

which indicates that the size is quite small. Setting $m \sim 10 - 40 M_\odot$ and $f \sim 10 - 1000 \text{ Hz}$, the size of gravitational waves from binary black hole mergers detected by Advanced LIGO is $\sim 20 - 700 \text{ km}$, and assuming $m \sim 1.4 M_\odot$ the size of gravitational waves from binary neutron star mergers detected by Advanced LIGO is $\sim 10 - 200 \text{ km}$.

3.5. Summary of explosive transients

Table 1 gives a summary of explosive transients discussed in previous Sections. Some quantities that characterize each transient and are relevant for discussions of strong lensing are listed. For comparison, the size of the quasar accretion disk depends on the black hole mass, but for typical quasars with black hole masses $M \sim 10^8 - 9 M_\odot$ the size of the optical emission region is found to be $\sim 10^{10-11} \text{ km}$ and that of the X-ray emission region is $\sim 10^{9-10} \text{ km}$

(e.g., [237]). Therefore the sizes of these explosive transients are comparable or much smaller than that of quasars.

4. Applications

4.1. Introduction

In this Section, we discuss possible applications of strong lensing of explosive transients that are introduced in Section 3. We emphasize advantages of these new strong lensing events as compared with more traditional strong lensing such as strong lensing of quasars.

4.2. Time delay cosmography

As emphasized in Section 1, time delay cosmography, which is made so far mostly using variabilities in lensed quasars, is becoming more and more important, because of the apparent tension of H_0 between the distance ladder (e.g., [56]) and *Planck* cosmic microwave background measurements (e.g., [57]). Thus an independent measurement from gravitational lens time delays is very important. Furthermore, time delays actually measure the time delay distance, which is a combination of three angular diameter distances, $D_{\text{ol}}D_{\text{os}}/D_{\text{ls}}$, as shown in equation (13). The time delay distance depends not only H_0 but also other cosmological parameters such as Ω_M and dark energy equation of state parameter w_{de} . Since the dependence of the time delay distance on cosmological parameters differs considerably from those of other cosmological probes, time delays provide unique cosmological information that is highly complementary to other cosmological probes (e.g., [238, 239]).

In addition to the measurements of source and lens redshifts, key observations that lead to precise measurements of H_0 from time delays include (see e.g., [66] for more discussions); (i) precise time delay measurements, (ii) precise measurements of image positions, (iii) detailed measurements of a lensed host galaxy to constrain the lens potential, (iv) the measurement of the stellar velocity dispersion of the lensing galaxy, and (v) the proper understanding of the structure along the line-of-sight. In the future, we will be able to measure H_0 at the high precision by combining many strong lens systems, but in order to assure the high accuracy we need to keep various systematics under control. In what follows, we discuss possible systematics and argue how strong lensing of explosive transients mitigate some of the systematics.

Strong lensing of explosive transients can definitely improve the point (i) above. Since H_0 is inversely proportional to the time delay, ideally we want to measure time delays at a percent level in order for the

Table 1. Summary of explosive transients discussed in this review article. See the text in each Section for details and references.

Type	Subclass	Number	z_{\max}	Wavelength (f [Hz])	Time scale	Local rate [Gpc ⁻³ yr ⁻¹]	Size [km]
Supernova (Section 3.1)	Ia	$\mathcal{O}(10^4)$	~ 2	optical ($\sim 10^{14-15}$)	~ 30 days	$\sim 3 \times 10^4$	$\sim 10^{10}$
	core-collapse	$\mathcal{O}(10^4)$	~ 2	optical ($\sim 10^{14-15}$)	~ 30 days	$\sim 7 \times 10^4$	$\sim 10^{10}$
	superluminous	$\mathcal{O}(100)$	~ 4	optical ($\sim 10^{14-15}$)	~ 100 days	~ 200	$\sim 10^{10}$
Gamma-ray burst (Section 3.2)	long	> 5000	~ 9	γ ($\sim 10^{18-23}$)	a few sec	~ 1	$\sim 10^{6-7}$
	short	> 1000	~ 3	γ ($\sim 10^{18-23}$)	$< \text{sec}$	$\sim 1 - 10$	$\sim 10^{5-6}$
Fast radio burst (Section 3.3)	...	$\mathcal{O}(100)$	$\sim 3?$	radio ($\sim 10^9$)	$\sim \text{msec}$	$\sim 10^{3.5-4.5}$	$< 10^{13}$
Gravitational wave (Section 3.4)	BBH	> 10	~ 0.5	LIGO band ($\sim 10^{1-4}$)	$\lesssim \text{sec}$	$\sim 10 - 100$	~ 100
	BNS	≥ 1	$\sim 0.05?$	LIGO band ($\sim 10^{1-4}$)	$\lesssim \text{sec}$	$\sim 100 - 4000$	~ 100
	BHNS	0	...	LIGO band ($\sim 10^{1-4}$)	$\lesssim \text{sec}$	< 600	~ 100

measurement errors not to degrade cosmological constraints. In the case of strong lensing of quasars, due to the stochastic nature of the quasar light curve, the robust measurement of time delays requires monitoring of lensed quasar images for many years. Microlensing due to stars in lensing galaxies, which we will discuss in more detail later, add additional variability to the light curve, making the robust measurement even more challenging. As a result, reliable measurements of quasar time delays require ~ 10 yr monitoring observations, and the resulting accuracy on time delay measurements is on the order of ~ 1 day (e.g., [240–242]).

In contrast, since light curves of explosive transients introduced in Section 3 are simple, we do not need monitoring much beyond the time delay. In the case of gamma-ray bursts, fast radio bursts, and gravitational waves, their time scales of light curves are less than ~ 1 sec, which indicates that time delays can be measured with an accuracy better than ~ 1 sec, much better than current measurements with lensed quasars. This point has been discussed in [243–246] for gravitational waves, in [247] for gamma-ray burst, and in [248] for fast radio bursts. Repeated observations of very precise time delay measurements with repeating fast radio burst may allow us to directly measure the cosmic expansion [249]. We also expect accurate and robust measurements of time delays for strong lensing of supernovae, even though the time scale of their light curves is $\gtrsim 30$ days, because of their simple and well-known light curves [138, 250, 251].

However, one complication that may affect the accuracy and precision of time delay measurements

is microlensing, which refers to flux variabilities due to stars in lensing galaxies (see Section 2.3). Table 1 indicates that size of the explosive transients tend to be smaller than R_{Ein} , which suggests the importance of microlensing in strong lensing of explosive transients (see also Figure 4).

The microlensing effect can be time dependent due to the transverse motions as well as the change of the size of the emitting region with respect to time, and therefore can distort the light curve in a non-trivial manner, which is particularly significant for strong lensing of supernovae [252]. Recent studies discuss possible ways to mitigate the effect of microlensing on supernova lensing [253–256], which indicates that a percent level measurement of time delays is possible even in the presence of microlensing by taking advantage of multiband light curves.

However, an exception is strong lensing of gravitational waves. Thanks to their long wavelength, microlensing variabilities are suppressed by wave optics effects. This is obvious from equation (44), as it is found $w \lesssim 0.1$ for $M \sim 1 M_{\odot}$ and $f \lesssim 10^3$ Hz, for which diffraction is quite effective. The effect of microlensing by stars in lensing galaxies on strong lensing of gravitational waves have been studied by [257–259], in which it is concluded that microlensing can modify the waveform significantly only for highly magnified sources. In high magnification regions, the effective Einstein radius of each microlens is enhanced by the macro model magnification, which leads to an increase of w for the same mass of the microlens. Put another way, due to diffraction

microlensing by normal stars in lensing galaxies is not effective for strong lensing of gravitational waves with moderate magnifications, which is more common. This insensitivity to microlensing can be seen as an advantage for the application of gravitational wave lensing for cosmology.

Strong lensing of explosive transients can also improve points (iii) and (iv) mentioned above. Quasars are very bright so that they outshine their host galaxies and sometimes lensing galaxies as well. Such bright quasar images make detailed measurements of shapes of lensed host galaxies very difficult. In contrast, for transient events, we can always use images before the transient event happens or after it fades away to measure shapes of lensed host galaxies accurately. This point is emphasized in [250] for strong lensing of supernovae and [243] for strong lensing of gravitational waves. The images without bright lensed sources also make it easier to conduct deep spectroscopy of lensing galaxies to measure velocity dispersion profiles including resolved two-dimensional velocity dispersion maps [260].

On the other hand, point (ii) above may be challenging in some cases. This is because of poor angular resolutions of observations for detecting some of the explosive transients, including gamma-ray bursts, fast radio bursts, and gravitational waves. One way to obtain accurate astrometry of lensed images is to identify their counterparts in other wavelengths, in particular optical. Such optical counterparts are known to be available at least for gamma-ray bursts and gravitational waves from binary neutron star mergers, and deep high-quality observations of multiple images of the optical counterparts enable us to determine the image position on the order of milliarcseconds, which is required for precise time delay cosmography [261]. For fast radio bursts, very accurate measurements of image positions may be possible using high-resolution radio imaging such as VLBI [221], although this may be practical only for strong lensing of repeating fast radio bursts [248].

Finally, strong lensing of these explosive transients may provide new information that is not available for traditional strong lens systems. One such example is magnification factors that are available for strong lensing of Type Ia supernovae. For traditional quasar strong lensing, we cannot measure magnification factors directly because intrinsic magnitudes of lensed quasars are unknown. In contrast, the standardizable candle nature of Type Ia supernovae allows us to directly measure the magnification factors, which break the mass-sheet degeneracy and related degeneracies (see Section 2.2). The idea to use strong lensing of Type Ia supernovae to break the H_0 -slope degeneracy and to obtain accurate H_0 measurements has been

proposed in [262]. Accurate measurements of H_0 may be possible also by strong lensing of Type Ia supernovae due to clusters [263–265]. Inversely, we can use strong lensing of Type Ia supernovae to calibrate their absolute magnitudes [266]. Again, an obstacle is microlensing which can change the total magnification of each lens system considerably in some cases [252, 267]. Similarly, the standard siren nature of gravitational waves can add useful information to time delay cosmography.

4.3. Test of Fundamental Physics

The measurements of the propagation speed for different particle types or energies provide an important means of testing fundamental physics. For instance, the violation of weak equivalence principle leads to different propagation speeds between e.g., photons and neutrinos (e.g., [268]). The violation of Lorentz invariance, which is predicted by some quantum gravity theories, results in an energy dependent dispersion to photons and changes the propagation speed of photons as a function of the energy (e.g., [269]). Moreover, some modified gravity theories predict the propagation speed of gravitational waves that differs from the speed of light (e.g., [270]).

These effects can be tested by observations of explosive transients (e.g., [231, 269, 271, 272]), by checking arrival time differences between different particle types or energies. However the observed arrival time difference consists of both the intrinsic time delay and the time delay caused by the different propagation speeds. The former is usually unknown or poorly constrained, which makes the result somewhat uncertain. One interesting way to overcome this intrinsic time delay is to make use of strong lensing. This is because the contribution of the intrinsic time delay vanishes if we compare the difference of time delays between multiple images among different particles or energy. This idea has been applied to strong lensing of gamma-ray bursts [273] and gravitational waves [274–277]. A caveat is that the difference between the propagation speeds of gravitational waves and their electromagnetic counterparts might also be caused by wave optics effects (Section 2.5) in gravitational lensing, because the propagation of gravitational waves is not affected by small intervening matter due to diffraction [278].

Another test of fundamental physics includes the time variation of fundamental constants such as the gravitational constant and the speed of light. Strong lensing may also help for this type of test as such time variation changes strong lensing observables such as time delays (e.g., [279]).

4.4. Compact dark matter

There have been long discussions on whether dark matter is composed of unknown elementary particle or compact objects such as primordial black holes (PBHs). The possibility of compact dark matter has been tested with various observations including microlensing in and around the Milky Way (see [280] for a review), from which constraints on the abundance of compact dark matter are derived as a function of the mass of compact dark matter.

Strong lensing of explosive transients helps improve these constraints. For instance, strong lensing or microlensing of gamma-ray bursts and their afterglow emissions have been studied extensively as a means of testing the compact dark matter scenario [281–291]. The ideas include the search for echo signals in gamma-ray bursts and the modification of the afterglow light curve due to the size dependence of microlensing.

When the mass of compact dark matter is very small, from $\sim 10^{-13} M_\odot$ to $\sim 10^{-16} M_\odot$ wave optics effects (Section 2.5) become important even in gamma-ray. In this case, the interference between multiple images induces an oscillating feature in the photon energy spectrum. The application of this effect to gamma-ray bursts, which is referred to as femtolensing, was proposed in [139] (see also [292, 293]). This method has been applied to Fermi Gamma-ray Burst Monitor data to place useful constraints on the abundance of compact dark matter in the mass range mentioned above [294]. However, the finite source size effect, which has been ignored before, is in fact crucial in this application [149]. The recent study by Katz *et al.* [203] revisited constraints from femtolensing taking full account of the finite source size effect to find that a useful constraint on the abundance of compact dark matter cannot be placed from the currently available data.

The search for echo signals due to strong lensing is possible also with other explosive transients. For instance, the possibility of using fast radio bursts to constraint compact dark matter with $M \gtrsim 20 M_\odot$ has been proposed in [295] and subsequently studied in [296, 297]. For the mass of $\sim 20 M_\odot$, we expect to observe multiple bursts separated by a typical time delay of a few milliarcseconds. It is found that ongoing experiments such as CHIME can place meaningful constraints on the abundance of compact dark matter in that mass range. Wave optics effects in strong lensing of fast radio bursts and its application to the compact dark matter search were discussed in [298] and also noted in [295].

Although the similar search is possible with strong lensing of gravitational waves, their long wavelengths and compact sizes indicate that wave optics effects

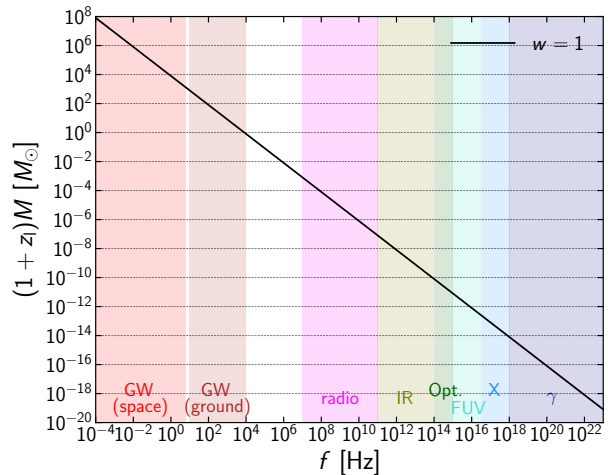


Figure 11. The relation between the frequency f and the (redshifted) mass $(1 + z_l)M$ of a point mass lens for the dimensionless parameter $w = 1$, where w is defined in equation (44). The region below the solid line corresponds to the case that the gravitational lensing magnification is significantly suppressed due to the diffraction, which is one of wave optics effects.

definitely play an important role (Section 2.5). Again, equation (44) indicates that we need compact dark matter with the mass $M \gtrsim 10 - 100 M_\odot$ to avoid diffraction and to observe strong lensing magnifications. When the mass is near the threshold, the signal-to-noise ratio of lensed waveforms shows an oscillatory behavior as the frequency sweeps up due to wave optics effects, which can be regarded as a smoking gun signature of strong lensing [140]. Strong lensing of gravitational waves by compact objects is recently revisited after the first direct observation of gravitational waves from binary black hole mergers, including the rate estimate and expected constraints on the abundance of compact dark matter [299–303].

The compact dark matter scenario can be tested with strong lensing of supernovae as well. In particular, strong lensing of Type Ia supernovae by compact dark matter produces a non-Gaussian tail in their apparent magnitude distribution for a given redshift, from which useful constraints on compact dark matter for a wide mass range $M \gtrsim 0.01 M_\odot$ are obtained [304].

In testing the compact dark matter scenario with strong lensing, wave optics effects and the finite source size effect sometimes become very important. To guide future studies along this line, we revisit these effects introduced in Section 2.5 and discuss them more quantitatively.

First, an important parameter that controls wave optics effects is the dimensionless parameter w defined in equation (44). When $w < 1$, diffraction originating from wave optics effects becomes so effective that the gravitational lensing magnification is highly suppressed

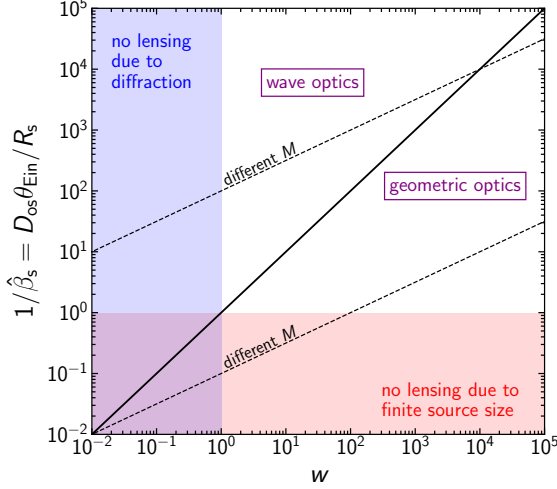


Figure 12. The schematic illustration of regions relevant for geometric optics and wave optics. The solid line shows $w = 1/\hat{\beta}_s$, where w is defined in equation (44) and $\hat{\beta}_s = R_s/(D_{os}\theta_{Ein})$ is the source size normalized by the Einstein radius. The region above the solid line corresponds to the situation where the interference pattern due to wave optics effects may be observed, whereas the region below the solid line corresponds to the situation that the geometric optics approximation is relevant. The shaded regions show $w < 1$ and $1/\hat{\beta}_s < 1$, for which the gravitational lensing magnification is significantly suppressed due to diffraction and the finite source size effect, respectively. The dotted lines show the direction along which parameter values change by changing the lens mass M .

i.e., $\mu \sim 1$ irrespective of the impact parameter. In Figure 11, we show the relation between the frequency f and the (redshifted) lens mass $(1+z_1)M$ that satisfy $w = 1$ for the case of a point mass lens. We note that the similar relation holds for other lens mass models, once M is replaced to the enclosed mass within the Einstein radius (see equation 36). The region below the line in Figure 11 corresponds to $w < 1$, and hence to diffraction. Figure 11 clearly demonstrates that wave optics effects are particularly important for gravitational waves.

As discussed in Section 2.5, in order for the interference pattern due to wave optics effects to be observed, the source must be sufficiently compact. This condition (equation 49) is given as $w \lesssim 1/\hat{\beta}_s$, where $\hat{\beta}_s = R_s/(D_{os}\theta_{Ein})$ is the source size R_s normalized by the Einstein radius. We illustrate this condition in Figure 12. The region above the line $w = 1/\hat{\beta}_s$ corresponds to the situation where the interference pattern due to wave optics effects may be observed. We note that this is just a necessity condition, and in order for the interference pattern to be observed other conditions such as the frequency band should also be met [146]. We also note that in regions with $w < 1$ and $1/\hat{\beta}_s < 1$ the gravitational lensing magnification is significantly suppressed due to

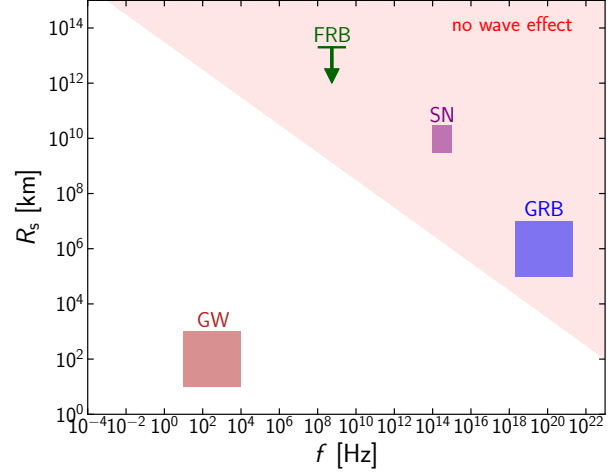


Figure 13. Sizes and observed frequency of various explosive transients (see also Table 1). The shaded region in the upper right corner does not satisfy the condition given by equation (58), which means that wave optics effects are never observed in this region irrespective of the lens mass. We note that the boundary depends on redshifts, and in this example we assume $z_1 = 0.5$ and $z_s = 1.0$.

diffraction and the finite source size effect, respectively. Therefore in these regions we do not observe any gravitational lensing effect.

Figure 12 has several important implications. Since w and $1/\hat{\beta}_s$ depend on the mass M of a point mass lens as $w \propto M$ and $1/\hat{\beta}_s \propto \sqrt{M}$, respectively, parameter values change along the direction indicated by the dotted lines. This indicates that in the limit $M \rightarrow \infty$ the parameter values always fall in the geometric optics region, which is one of the reasons why the geometric optics approximation is valid in most astronomical situations. Figure 12 also suggests that the interference pattern due to wave optics effects may be observed only when $1/\hat{\beta}_s > 1$ at $w = 1$, as in the case of the upper dotted line in Figure 12. In contrast, in the case of the lower dotted line in Figure 12, the geometric optics approximation is valid in all the parameter range of interest. Even though at the small mass end w becomes smaller than unity, at $w \sim 1$ the magnification is already strongly suppressed by the finite source size effect ($1/\hat{\beta}_s \ll 1$), suggesting that the effect of diffraction is unobservable. From equations (44) and (50), the necessity condition that the interference pattern is observed for some lens masses is written as

$$R_s \lesssim 3.05 \times 10^{13} \text{ km} \left(\frac{1+z_1}{1.5} \right)^{-1/2} \left(\frac{f}{\text{Hz}} \right)^{-1/2} \times \left(\frac{D_{os}D_{ls}/D_{ol}}{0.949 \text{ Gpc}} \right)^{1/2}, \quad (58)$$

where distances are again normalized to values at the lens redshift $z_1 = 0.5$ and the source redshift $z_s = 1.0$.

We can check whether the condition given by equation (58) is satisfied for explosive transients summarized in Table 1. The result summarized in Figure 13 suggests that gravitational waves indeed satisfy the condition, and therefore are ideal site to search for wave optics effects in strong lensing. Based on the current understanding of their sizes, gamma-ray bursts do not satisfy the condition, and therefore the so-called femtolensing does not occur efficiently. Another interesting target to search for wave optics effects in strong lensing is fast radio bursts for which sizes are poorly constrained. If the size of fast radio bursts is sufficiently compact, we may be able to detect the interference pattern in strong lensing of fast radio bursts for lens masses of $M \gtrsim 10^{-5} M_\odot$ [295, 298, 305].

4.5. Structure of dark matter and galaxies

Normal lensing objects such as galaxies and clusters consist of both dark and luminous matter. Precise measurements of the dark matter distribution in galaxies and clusters serve as an important test of dark matter scenario as well as galaxy formation models. Gravitational lensing is unique in that it probes the total projected mass of the lensing galaxy robustly. While distributions of dark matter and baryon in lensing objects have been studied in detail using lensed galaxies and quasars (e.g., [63, 64] for reviews), strong lensing of explosive transients can shed new light on these applications.

For instance, strong lensing of various transients can be discovered by monitoring massive clusters of galaxies, which are known to be efficient lenses. Time delays obtained from measurements of multiple images of explosive transients break degeneracies in mass models reconstructed from multiple image positions of strongly lensed galaxies [306]. In Section 5.1.3, we present a specific example of this application in the case of a strongly lensed core-collapse supernova. If the background sources are standardizable candles such as Type Ia supernovae, we can directly measure magnification factors that break the mass-sheet degeneracy [307], as is clear from equation (27), and other mass model degeneracies. This application is possible even when background sources are not multiply imaged (e.g., [308–310]).

As discussed in Section 2.3, strong lensing provides an important means of studying substructures in lensing galaxies, which serve as a critical test of the CDM model. Gravitational lensing of gravitational waves offers an alternative approach, as it is insensitive to microlensing due to wave optics effects as discussed in Section 4.2.

Substructures can be probed also by perturbations on time delays between merging pairs of multiple images (see Section 2.3). However, the smaller time

delays suggest that their precise measurements have been difficult for quasar lenses. Strong lensing of explosive transients, on the other hand, can improve time delay measurements significantly due to the short time scale of their light curves, leading to much more accurate estimates of the effect of substructures on time delays. This point was discussed in [311] for strong lensing of gravitational waves.

Finally, using gravitational waves we may be able to detect substructures more directly. Lensing by substructures with masses $\sim 10^{3-6} M_\odot$ can induce interference pattern in waveforms, as in the case of microlensing by compact dark matter discussed in Section 4.4. This possibility has been explored in [312].

4.6. The nature of explosive transients

As discussed in Section 3, the true nature of the explosive transients that are considered in this review article is yet to be fully understood. Strong lensing may help reveal their true nature by taking advantage of its magnifying power as well as its power to resolve fine structures of sources.

First, the result in Section 2.4 indicates that the strong lensing probability is a steep function of the source redshift. Therefore, we can constrain the redshift distribution of explosive transients from their strong lensing probabilities. The idea was used in [313] to constrain the redshift distribution of gamma-ray bursts. The similar idea was proposed for fast radio bursts in [314].

Since strong lensing magnifies background sources, it enables us to observe very distant events that cannot be observed without the gravitational lensing magnification. Therefore, we can constrain the supernova rate at very high redshifts by observations of strongly lensed supernovae at such high redshifts [138, 315, 316]. The search of lensed high-redshift supernovae can be conducted efficiently by monitoring massive clusters of galaxies [317–322].

The example above immediately suggests that the gravitational lensing magnification modifies the observed distribution of explosive transients. This may be particularly important for gravitational waves from binary black hole mergers for which redshifts are not directly measured in most cases. Instead, as discussed in Section 3.4, from gravitational wave observations one can measure the luminosity distance to the source. However, in presence of gravitational lensing magnification μ , the observed luminosity distance is modified as

$$D_L^{\text{obs}} = \frac{\bar{D}_L}{\sqrt{\mu}}, \quad (59)$$

where \bar{D}_L is the luminosity distance to the source in absence of gravitational lensing (i.e., the luminosity

distance to the source redshift computed assuming a homogeneous and isotropic Universe) and D_L^{obs} is the luminosity distance measured from observations of gravitational waves. Therefore, for highly magnified events $\mu \gg 1$, the redshift inferred from the luminosity distance is biased low. The bias in the estimated redshift directly affects the estimate of the chirp mass via equation (56). Indeed it is pointed out that strong lensing magnification produces an apparent tail in the high mass end of the observed chirp mass distribution [323]. Furthermore, strong lensing of gravitational waves produce multiple images, some of which are *demagnified*. Such demagnified images can be observed as apparently very high redshift events, and hence produce a tail at the high end of the observed redshift distribution [135]. These examples highlight the critical importance of gravitational lensing for the interpretation of observed distributions of gravitational waves.

When multiple images of explosive transients are produced, in a sense we observe the transients multiple times with some time differences. If we can predict the appearance of trailing images, it opens up interesting applications such as the detailed monitoring of early light curves. This possibility was noted in [138] for strong lensing of supernovae, and was explored in detail in [324]. A particularly interesting feature in the early light curves of supernovae is the so-called shock breakout, which is a luminous emission with very short time scale.

Strong lensing can also be used to resolve fine structures of sources by e.g., taking advantage of the size dependence of microlensing as shown in Figure 4. The ideas to resolve the jet structure of gamma-ray sources with strong lensing have been explored in [325–330]. For strong lensing of repeating fast radio bursts, one can measure the change of time delays between multiple images, from which the motion of fast radio burst sources is measured [331].

5. Past observations and future prospects

5.1. Past observations

5.1.1. Strong lensing of supernovae: Before discoveries. The expected event rates of strongly lensed supernovae in various supernova surveys have been computed [124, 250, 332–335], which suggest that future surveys that are aimed at finding many supernovae at $z \gtrsim 1$ should also be able to find strongly lensed supernovae. One of the most comprehensive predictions before the first discoveries has been made in [105], in which it was argued that Pan-STARRS1 [336, 337] can find $\mathcal{O}(1)$ strongly lensed supernovae, whereas Large Synoptic Survey Telescope (LSST) [238] can find more than 100 strongly lensed supernovae.

We can efficiently search for strongly lensed supernovae by monitoring plausible sites, such as galaxy-galaxy strong lens systems [338] and massive clusters [339–342]. The latter search led to discoveries of some supernovae behind clusters, which are magnified but not multiply imaged [308–310, 343–345]. Giraud [346] reported a possible strongly lensed variable source in a pair of arclets in the cluster Cl 0302+1658, but interpreted it as an active galactic nucleus rather than a supernova.

5.1.2. Discovery of PS1-10afx. Pan-STARRS1 Medium Deep Survey (see [337]) is a time-domain survey with a typical cadence of 3 days. The total survey area is $\sim 70 \text{ deg}^2$ and the typical 5σ depth of nightly stacks is 23 mag. PS1-10afx is a new peculiar transient from Pan-STARRS1 Medium Deep Survey reported by Chornock *et al.* [347]. PS1-10afx turned out to be a very bright supernova at $z = 1.388$ with an unusually fast light curve and a red color, from which it was concluded that it is a new type of a hydrogen-deficient superluminous supernova.

However, Quimby *et al.* [348] re-examined the photometric and spectroscopic data of PS1-10afx and proposed a new interpretation: PS1-10afx is a normal Type Ia supernova that is magnified by a factor of ~ 31 due to strong gravitational lensing. In this case, the magnification factor can be estimated directly thanks to the standardizable nature of a Type Ia supernova. The lack of any signature of multiple images in both the supernova images and the light curve is easily explained by the small image separation between multiple images, $\theta < 0.4''$. This scenario, however, requires the presence of a foreground galaxy that acts as a lens, which was not clearly seen in the follow-up images of the supernova host galaxy taken after PS1-10afx faded away.

Quimby *et al.* [349] presented a new evidence that supports the lensing interpretation of PS1-10afx. They obtained a deep spectrum of the host galaxy with Keck telescope and detected a foreground galaxy at $z = 1.117$ in the spectrum of the host galaxy at $z = 1.388$. This indicates that there are two galaxies that are superposed and blended in the ground-based images. The analysis indicates that the foreground galaxy well explains the small image separation and time delay that are need to be compatible with the observed property of PS1-10afx. In addition, the discovery of a lensed Type Ia supernova from Pan-STARRS1 Medium Deep Survey is in good agreement with the expected rate [105] that is extended to include events with unresolved multiple images. The comparison of theoretical expectations suggests that PS1-10afx is likely to consist of four multiple images, although these images were not resolved.

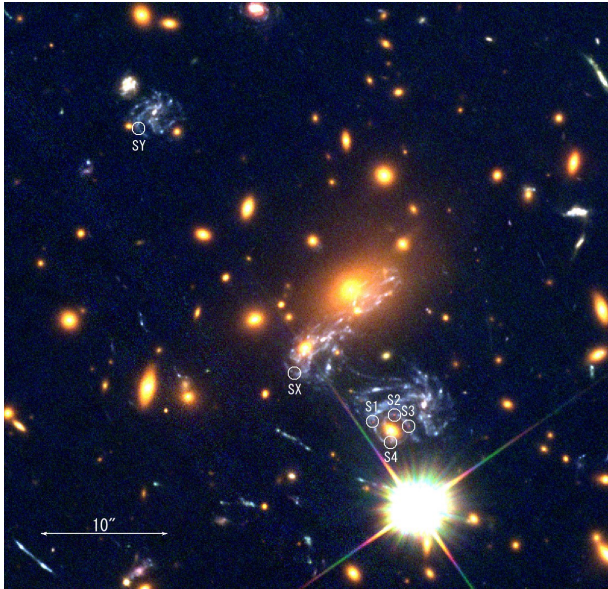


Figure 14. Locations of 6 multiple images of the strongly lensed Type II supernova SN Refsdal [350] at the core of the massive cluster MACS J1149.6+2223. The image shows a color-composite *Hubble Space Telescope* image taken in the *Hubble* Frontier Fields program [31]. Originally the 4 multiple images S1–S4 are detected, and about 1 year after the discoveries of S1–S4 the appearance of the new image SX was observed [351]. The image SY is never observed but predicted to have appeared $\gtrsim 10$ years before the appearance of S1–S4.

5.1.3. Discovery of SN Refsdal. Kelly *et al.* [350] reported the discovery of SN Refsdal at $z = 1.49$, which is the first strongly lensed supernova discovered with resolved multiple images and time delay measurements. It was discovered during *Hubble Space Telescope* observations of the cluster MACS J1149.6+2223 at $z = 0.54$, one of six clusters targeted by the *Hubble* Frontier Fields program [31] that is aimed at studying distant Universe with help of gravitational lensing magnifications due to massive clusters of galaxies. Specifically, SN Refsdal was discovered by the Grism Lens-Amplified Survey from Space program [352], a follow-up program to acquire near-infrared grism spectra of massive galaxy clusters including the *Hubble* Frontier Fields clusters.

Figure 14 shows locations of multiple images of SN Refsdal. Originally the 4 images S1–S4 that were produced around an elliptical member galaxy of the cluster were reported in [350]. The host galaxy of the supernova is a face-on spiral galaxy at $z = 1.49$ that are multiply imaged by the foreground cluster as shown in Figure 14, which immediately suggests that additional multiple images in addition to the observed 4 images should exist. This possibility was noted in [350] with estimated time delays on the order of years.

Soon after the discover was reported, many predictions of expected time delays between multiple

images of SN Refsdal have been made [353–359]. Thanks to deep imaging of the *Hubble* Frontier Fields program, there are more than 100 multiple images of background galaxies identified for this cluster, which allow us to reconstruct the mass distribution in a reliable manner. These predictions agree in that there are two additional images in addition to the observed image S1–S4. Although one of the images, SY, is predicted to have appeared $\gtrsim 10$ years before the appearance of S1–S4 and hence cannot be confirmed by future observations, the other image SX is predicted to appear in the future, which is a falsifiable prediction with future monitoring observations (see Figure 14 for the locations of SX and SY on the sky). However, there was a considerable scatter in the predictions of the appearance of SX, ranging from about half year to 2 years from the appearance of S1–S4. The large difference of predictions of time delays despite a large number of multiple images is partly due to the complex nature of the cluster mass distribution. This, in turn, implies that the observation of the reappearance of SX provides a unique opportunity to check and improve our understanding of the cluster mass distribution that is dominated by dark matter.

Since the images S1–S4 were discovered in 2014 October, SX has been expected to appear sometime in 2015–2016. Monitoring follow-up observations of this cluster with *Hubble Space Telescope* indeed detected the new image SX at the position exactly predicted by mass models [351]. From the observation, the time delay between S1 and SX is measured to ~ 350 days, which is in excellent agreement with several model predictions, in particular those made with *glafic* [73, 353, 357] and *GLEE* [359–361]. These successful predictions of the appearance of the image SX support the validity of strong lensing mass reconstruction techniques adopted so far (see also [362] for another validation using simulated clusters). From the follow-up monitoring observations, time delays between images S1–S4 were also measured [363] and were found to agree with model predictions reasonably well (see also [355]). Based on the observed light curve and spectrum, SN Refsdal was classified as an SN 1987A-like Type II supernova [364], and therefore the magnification factor was not directly measured. The total magnification of all the 6 images is predicted to be ~ 74 by a best-fit mass model of [357].

If mass distributions of clusters are well understood and the systematics inherent to strong lens mass reconstructions are kept under control, we may be able to use SN Refsdal-like events to constrain H_0 . Estimates of the constraining power using SN Refsdal indicates that we can constrain H_0 from a single SN Refsdal-like event with $\sim 10\%$ accuracy or even better [365, 366], although the accuracy may be degraded

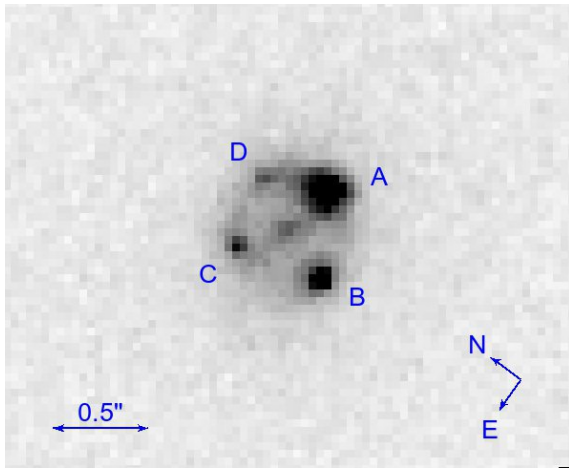


Figure 15. The *Hubble Space Telescope* F814W image of the strongly lensed Type Ia supernova iPTF16geu [368]. The 4 supernova images are marked by A–D.

by a factor of a few or more if we relax prior assumptions on the cluster mass distribution [367].

5.1.4. Discovery of iPTF16geu. Goobar *et al.* [368] reported the discovery of iPTF16geu, which is the first strongly lensed Type Ia supernova with resolved multiple images, from the intermediate Palomar Transient Factory [369] that is a massive time-domain survey with the limiting magnitude of $R \sim 20.5$ using a camera covering the 7.26 deg^2 field-of-view on the 48-inch Oschin telescope at Palomar Observatory. Figure 15 shows the follow-up *Hubble Space Telescope* image of iPTF16geu, in which a Type Ia supernova at $z = 0.409$ is strongly lensed into 4 multiple images due to a foreground galaxy at $z = 0.216$. As in the case of PS1-10afx, the standardizable nature of a Type Ia supernova enables the direct measurement of the total magnification of iPTF16geu to ~ 52 . Since the foreground galaxy is a relatively low mass galaxy with the velocity dispersion of $\sim 160 \text{ km s}^{-1}$, the maximum image separation between multiple images is small, $\sim 0.6''$. A gravitationally lensed host galaxy is clearly visible particularly in follow-up Keck near-infrared images.

Mass modeling of iPTF16geu has been conducted in More *et al.* [370]. Although the supernova image positions and lensed host galaxy are fitted well by a simple model that consists of Singular Isothermal Ellipsoid plus an external shear, it was found that flux ratios between the multiple images predicted by mass models differ considerably from observed flux ratios. These anomalous flux ratios have been attributed to microlensing in [370]. It was also found that predicted time delays between the multiple images are less than a day, making measurements of time delays in

observations very challenging.

The effect of microlensing on iPTF16geu has been revisited by [267, 371], who conclude that microlensing alone cannot explain the anomalous flux ratios. Possible explanations include the too simplistic assumption on the macro mass model and an additional perturbation on the flux ratios by substructures in the lensing galaxy. On the other hand, recent mass modeling by Mörtzell *et al.* [372] concluded that the anomalous flux ratio can be reconciled with microlensing if the radial density profile of the lensing galaxy is shallower than the isothermal model.

The observed light curves of iPTF16geu have been analyzed by Dhawan *et al.* [373] to confirm very short time delays between images, $\lesssim 1$ day. Specifically, time delays with respect to the brightest image are measured to -0.23 ± 0.99 , -1.43 ± 0.74 , and 1.36 ± 1.07 days. They also studied the dust extinction of multiple images, and derived the extinction-corrected total magnification factor of $\mu = 67.8_{-2.9}^{+2.6}$. In a companion paper by Johansson *et al.* (in prep.), they provide the first time delay measurement based on spectroscopic measurements.

The high total magnification of ~ 52 even before the extinction correction is partly explained by the selection effect, which will be discussed in detail in Section 5.2. However, it has been found from detailed comparisons with theoretically expected distributions that the observed magnification is higher than expected given its redshift, even if we take account of the selection effect [368, 370, 374]. This issue may be related with the anomalous flux ratios mentioned above. It is of great importance to understand the cause of the anomalous flux ratios and the high total magnification for the future use of strongly lensed Type Ia supernovae for cosmology.

5.1.5. Implications of the first discoveries for search methods. Table 2 summarizes properties of the three strongly lensed supernovae presented in this review article. Two out of the three events have very small image separations such that they are barely resolved in ground-based imaging observations. Such unresolved events were not included in the calculation of [105]. If we can identify these unresolved strong lensing events from the survey data in a timely manner, we may be able to increase the number of strongly lensed supernovae discovered in future time-domain surveys to enhance their power for cosmological and astrophysical studies.

Based on the discovery of PS1-10afx, Quimby *et al.* [349] proposed a new method to identify strongly lensed Type Ia supernovae, utilizing a color-magnitude diagram of supernovae. Specifically, it was found that strongly lensed Type Ia supernovae are

Table 2. Summary of strongly lensed supernovae discussed in this review article. See the text in each Section for details and references. N_{img} indicates the number of multiple images, m_{peak} is an observed peak magnitude (the total magnitude for PS1-10afx and iPTF16geu, and the magnitude of the brightest image for SN Refsdal), μ_{tot} is the total magnification factor of all the multiple images, which is directly measured from the observation for Type Ia, θ_{max} is the maximum image separation between any multiple image pairs, and Δt_{max} is the maximum time delay between any multiple image pairs. Note that the values listed here can be either observed or model predicted ones.

Name	Type	z_s	z_l	N_{img}	m_{peak}	μ_{tot}	θ_{max}	Δt_{max}
PS1-10afx (Section 5.1.2)	Ia	1.388	1.117	4?	$i \sim 22$	~ 31	$< 0.4''$	< 4 days
SN Refsdal (Section 5.1.3)	II	1.49	0.54	6	$i \sim 27$	~ 74	$\sim 32''$	~ 6000 days
iPTF16geu (Section 5.1.4)	Ia	0.409	0.216	4	$i \sim 19$	~ 52	$\sim 0.6''$	$\lesssim 1$ days

well separated from unlensed supernovae in i -band magnitude versus $r - i$ color diagram, which allows us to identify unresolved strong lensing candidates relatively securely. Rapid follow-up observations of these candidates may lead to measurements of time delays for these strong lensing events. It was argued that this approach can significantly increase the number of strongly lensed supernovae discovered by LSST.

Goldstein and Nugent [375] proposed a slightly different approach, in which strongly lensed Type Ia supernova candidates are identified by identifying supernovae near elliptical galaxies whose absolute magnitudes computed from the redshifts of the elliptical galaxies are brighter than those of Type Ia supernovae. This search method is based on the fact that lensing galaxies are dominated by elliptical galaxies. This method also enables rapid identifications of unresolved strong lensing events and potentially increases the number of strongly lensed supernovae discovered by LSST (see also [374]).

Even if multiple images of strongly lensed supernova are barely resolved, we may still be able to see its signature by carefully checking the morphology of the supernova image to see if it is really consistent with the Point Spread Function. The possibility of finding strong lensed supernovae by checking the ellipticity of the supernova image is discussed in [376].

Recent work by Wojtak *et al.* [377] explored how effective such new strategy to find unresolved strongly lensed supernovae is in ongoing and future time-domain surveys. It was found that finding unresolved strongly lensed supernovae increases the number of strongly lensed supernovae drastically for shallow surveys such as Palomar Transient Factory, whereas the increase of the number is modest for deep time-domain surveys such as LSST.

5.1.6. Strong lensing of gamma-ray burst. One of the most comprehensive discussions on the detectability of strong lensing of gamma-ray bursts has been presented in [378]. Although the *Swift* satellite may be able to detect strongly lensed gamma-ray bursts, it is

argued that detecting multiple image pairs is unlikely because of its inefficient duty cycle and the limited sky coverage, $\sim 50\%$ (see also [379]). Fermi Gamma-ray Burst Monitor has more sky coverage and therefore may be suited to search for multiple image pairs in this regard.

Despite some explicit attempts to search for lensed image pairs in the gamma-ray burst catalogs for a wide range of time delays [380–383], no secure candidate of multiply imaged gamma-ray bursts has been identified so far. The latest search by Hurley *et al.* [383] makes use of the gamma-ray burst sample detected by *Konus-Wind* [384], which has the high duty cycle and large sky coverage, to search for lensed image pairs. Based on the absence of any candidate of strongly lensed gamma-ray burst, an upper limit of the lensing probability of 0.0033 is placed. A caution is that microlensing can distort light curves of strongly lensed gamma-ray bursts (e.g., [385]), which may affect the efficiency of searching for multiple image pairs based on the similarity of the light curves.

5.1.7. Strong lensing of fast radio burst. While some estimates of expected event rates of strongly lensed fast radio bursts have been presented in the literature (e.g., [248, 314]), so far no systematic search for strong lensing of fast radio bursts has been made. Since the number of observed fast radio bursts is very rapidly increasing, the future search in real catalogs will be interesting.

5.1.8. Strong lensing of gravitational waves. The expected rates of strongly lensed gravitational waves have been computed both for ground based experiments (e.g., [135, 386–391]) and space based experiments (e.g., [135, 141, 392, 393]). These calculations suggest that a large number of strongly lensed gravitational waves from compact binary mergers will be discovered in future third-generation ground-based experiments as well as future space-based gravitational wave experiments.

The expected rates of strongly lensed gravitational waves in the previous and ongoing Advanced LIGO observing runs are predicted to be small (e.g., [135,

389–391]). However, Broadhurst *et al.* [394, 395] made an interesting claim that roughly half of gravitational waves from binary black hole mergers detected by Advanced LIGO are in fact strongly lensed ones. As discussed in Section 4.6, estimated redshifts and chirp masses of highly magnified gravitational wave events are biased if gravitational lensing is not taken into account, such that highly magnified high redshift events are observed as low redshift events with very large chirp masses. Therefore, binary black holes with relatively high masses of $\sim 30 M_\odot$, if interpreted as highly magnified events, are in fact binary black hole systems with moderate masses, $\sim 10 M_\odot$. In order for such events to contribute to the current observation, the redshift evolution of the event rate must be very strong such that the event rate at $z \sim 1 - 2$ is several orders of magnitude higher than the local event rate.

For highly magnified strong lensing events, we expect a pair of images with similar waveforms [396], which are observed with a typical time difference of less than a day [135]. While the absence of such pair events in Advanced LIGO observations may disfavor the lensing scenario mentioned above, it is possible that such counterimages are missed due to the relatively low duty cycle (“glitches” in the data stream) as well as the effect of the Earth rotation that changes the sensitivity to a source located in a given position on the sky as a function of time [397]. These issues are mitigated by increasing the number of detectors in operation.

Gravitational lensing also rotates the polarization plane of gravitational waves, which results in the modification of the antenna pattern function. This effect, however, appears to be negligibly small in most situations given the small deflection angles due to gravitational lensing [398].

There are some attempts to explicitly search for strongly lensed gravitational wave events among sub-threshold signals, but no promising candidate of strong lensing events is identified [399, 400]. Since strong lensing of gravitational waves may be produced by foreground galaxy clusters, the search of strong lensing events can also be conducted around known massive clusters within error circles of observed gravitational wave events [401, 402].

5.2. Expected event rates

Here we present some discussions on expected event rates of strongly lensed explosive transients. Our strategy here is to provide simple and concise estimates of strong lensing rates for various explosive transients in a unified manner. Since we do not fully take account of the luminosity distributions and selection functions, these estimates are not very accurate, but a reward of this simple approach is that the parameter dependence is clearer that leads to the better understanding of

differences of expected strong lensing rates in different setups. Our approach here is also complementary to detailed calculations of event rates of strong lensing taking full account of the luminosity distributions and the selection effects, e.g., [105, 374, 377] for strong lensing of supernovae and [135, 389] for strong lensing of gravitational waves.

We start with the strong lensing probabilities derived in Section 2.4. The strong lensing probability as a function of the source redshift, $P_{\text{sl}}(z_s)$ defined by equation (30), is computed following the Monte-Carlo approach [135] assuming single galaxies as lensing objects. The galaxy mass distribution is modeled by a Singular Isothermal Ellipsoid plus an external shear (see Section 2.4 for more details). Since groups and clusters of galaxies are not included in the calculation, these strong lensing probabilities are likely to be underestimated, although their contribution of the strong lensing probability to the total strong lensing probability is thought to be subdominant as discussed in Section 2.4, especially for strong lensing of explosive transients whose sizes are compact.

Given the strong lensing probabilities, we can compute the expected observed rate of strongly lensed explosive transients at $z < z_{\text{max}}$ as

$$R_{\text{sl}}(< z_{\text{max}}) = \Omega_{\text{sky}} \int_0^{z_{\text{max}}} dz_s \frac{d^2 V}{dz_s d\Omega} \frac{R(z_s)}{1 + z_s} P_{\text{sl}}(z_s), \quad (60)$$

where $R(z)$ is the comoving rate density of explosive transients as a function of redshift and Ω_{sky} is the sky area of the survey. The factor $(1 + z)^{-1}$ takes account of the time dilation effect, since $R(z)$ is usually defined as the event rate in the rest frame of the transients.

We compute R_{sl} in the following setup. We compute expected observed rates in all sky by setting $\Omega_{\text{sky}} = 4\pi$. Since strong lensing events with sufficiently magnified are of more interest and total magnification factors tend to be high for known strongly lensed supernovae (see Table 2), we focus on strong lensing events with $\mu_{\text{tot}} \gtrsim 10$ by setting the selection bias, $B = 1/25 = 0.04$ (see also the discussion in Section 2.4). For simplicity, the event rate of explosive transients is assumed to have the following redshift dependence

$$R(z) = R^{\text{loc}}(1 + z)^{\alpha_z}, \quad (61)$$

where R^{loc} is the local event rate and α_z parametrizes the redshift evolution. See Table 1 for the current estimates of R^{loc} for various explosive transients. In many cases, the redshift evolution of event rates of explosive transients traces the global star formation history of the Universe, for which the rate increases toward higher redshifts out to $z \sim 2$, with the slope corresponding to $\alpha_z \approx 2$. With these assumptions, the

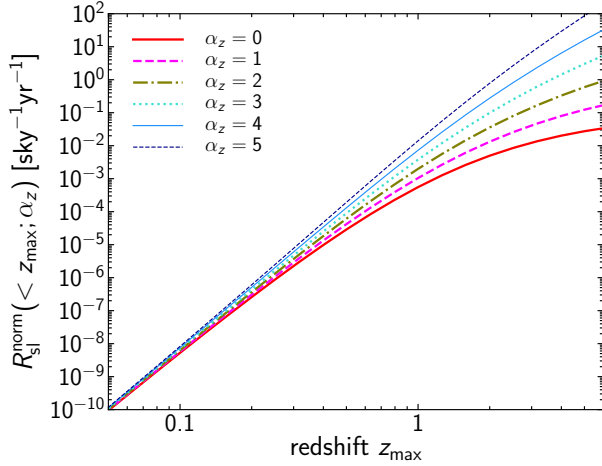


Figure 16. The normalization of the observed strong lensing rate, $R_{\text{sl}}^{\text{norm}}(< z_{\text{max}}; \alpha_z)$ defined in equation (62), as a function of the maximum redshift z_{max} . We show $R_{\text{sl}}^{\text{norm}}$ for several different redshift evolution parameter α_z that is introduced in equation (61). The fitting form of $R_{\text{sl}}^{\text{norm}}$ is given by equation (63).

observed rate (60) is rewritten as

$$R_{\text{sl}}(< z_{\text{max}}) = R_{\text{sl}}^{\text{norm}}(< z_{\text{max}}; \alpha_z) \left(\frac{\Omega_{\text{sky}}}{4\pi} \right) \left(\frac{B}{0.04} \right) \times \left(\frac{R^{\text{loc}}}{1 \text{ Gpc}^{-3} \text{ yr}^{-1}} \right), \quad (62)$$

where $R_{\text{sl}}^{\text{norm}}(< z_{\text{max}}; \alpha_z)$ is calculated by inserting the fiducial values to equation (60) and adopting an approximation given by equation (31).

Figure 16 shows $R_{\text{sl}}^{\text{norm}}(< z_{\text{max}}; \alpha_z)$ for several different choices of α_z . It is found that the expected observed strong lensing rate is a steep function of z_{max} . At low redshift $z_{\text{max}} \ll 1$, we roughly have $R_{\text{sl}}^{\text{norm}}(< z_{\text{max}}; \alpha_z) \propto z_{\text{max}}^6$, in contrast to the unlensed event rate which is proportional to the volume at low redshifts i.e., $\propto z_{\text{max}}^3$.

We find that the results shown in Figure 16 are fitted by the following form

$$R_{\text{sl}}^{\text{norm}}(< z_{\text{max}}; \alpha_z) \approx \frac{a_1 z_{\text{max}}^{a_2} (1 + z_{\text{max}})^{\alpha_z}}{1 + a_3 z_{\text{max}}^{a_4}}, \quad (63)$$

$$a_1 = 3 \times 10^{-3}, \quad (64)$$

$$a_2 = 5.8, \quad (65)$$

$$a_3 = 4.6 + 0.35 \alpha_z \quad (66)$$

$$a_4 = 3.1 + 0.1 \alpha_z^{0.6}. \quad (67)$$

This fitting form is derived in the range $0 \leq \alpha_z \leq 5$ and $z_{\text{max}} < 5$.

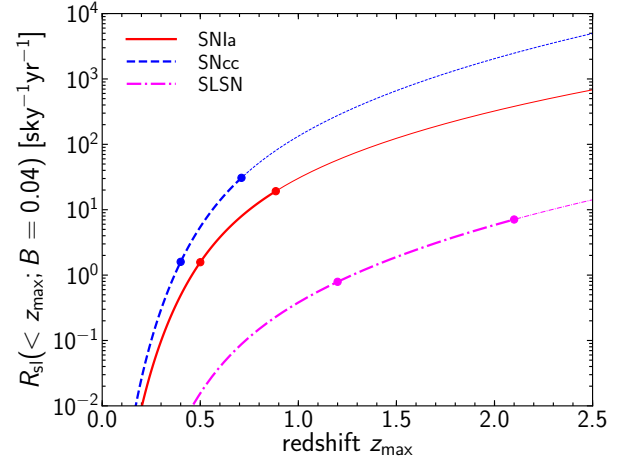


Figure 17. Expected observed rates of strong lensing of supernovae as a function of the maximum redshift z_{max} computed using equation (60). See Table 3 for the fiducial values adopted in the calculation. We show all-sky ($\Omega_{\text{sky}} = 4\pi$) rates with $B = 0.04$ that corresponds to strong lensing events with $\mu_{\text{tot}} \gtrsim 10$. For each supernova type, a rough estimate of z_{lim} and the corresponding z_{max} (see equation 68) for LSST [238] are marked by left and right circles, respectively. Thick lines indicate the rough redshift ranges we can observe with LSST.

We use equations (60) and (63) to compute expected event rates of strong lensing of various explosive transients as a function of z_{max} . For each explosive transient listed in Table 1, we choose a fiducial value of R^{loc} that is consistent with the current estimates. We also choose the redshift evolution parameter defined in equation (61) to $\alpha_z = 1$ or 2 so that it is broadly consistent with the current estimates. Table 3 summarizes our fiducial choices of R^{loc} and α_z , and resulting expected observed rates for $z_{\text{max}} = 0.5, 1, 2$, and 3. Since we adopt $B = 0.04$, these correspond to rates of strong lensing events with $\mu_{\text{tot}} \gtrsim 10$. We note that these predictions can be easily modified to those for other parameter sets by using equation (60).

Results in Table 3 do not take account of the observability. We provide a rough estimate of z_{max} for each survey as follows. For each survey, we first estimate the redshift z_{lim} , out to which normal unlensed events are largely detected. Since we consider strong lensing events $\mu_{\text{tot}} \gtrsim 10$, we assume that each multiple image is magnified by a factor of ~ 4 or so. The magnification factor of 4, for instance, indicates that the event is detected out to a factor of $\sqrt{4} = 2$ larger luminosity distance. Therefore, for each survey and explosive transient with z_{lim} , we assume that the strong lensing events are detected out to z_{max} that satisfies

$$D_{\text{L}}(z_{\text{max}}) = 2 D_{\text{L}}(z_{\text{lim}}). \quad (68)$$

At sufficiently low redshifts, this relation implies $z_{\text{max}} \approx 2z_{\text{lim}}$.

Table 3. Expected observed rates of strong lensing of various transients computed using equation (62). See also Table 1 for the summary of properties of these transients. The columns R^{loc} and α_z show fiducial values of the local event rate and the redshift evolution parameter adopted in the calculation. Expected observed rates R_{sl} for $\Omega_{\text{sky}} = 4\pi$ and $B = 0.04$ (corresponding to $\mu_{\text{tot}} \gtrsim 10$) within the maximum redshift $z_{\text{max}} = 0.5, 1, 2$, and 3 are shown.

Type	Subclass	R^{loc} [Gpc $^{-3}$ yr $^{-1}$]	α_z	$R_{\text{sl}}(< 0.5)$ [sky $^{-1}$ yr $^{-1}$]	$R_{\text{sl}}(< 1)$ [sky $^{-1}$ yr $^{-1}$]	$R_{\text{sl}}(< 2)$ [sky $^{-1}$ yr $^{-1}$]	$R_{\text{sl}}(< 3)$ [sky $^{-1}$ yr $^{-1}$]
Supernova	Ia	3×10^4	1	1.6	30	320	1300
	core-collapse	7×10^4	2	5.4	130	2000	10000
	superluminous	200	2	0.02	0.38	5.8	29
Gamma-ray burst	long	1	2	< 0.01	< 0.01	0.03	0.15
	short	3	1	< 0.01	< 0.01	0.03	0.13
Fast radio burst	...	10^4	2	0.78	19	290	1500
Gravitational wave	BBH	30	2	< 0.01	0.06	0.88	4.4
	BNS	600	1	0.03	0.61	6.5	25
	BHNS	10	1	< 0.01	0.01	0.11	0.4

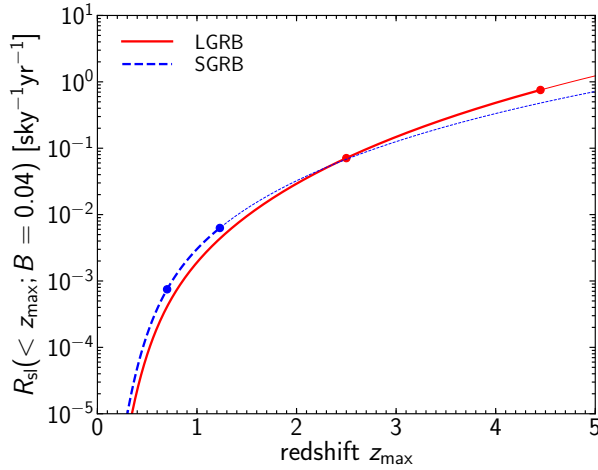


Figure 18. Same as Figure 17, but for strong lensing of gamma-ray bursts and rough estimates of z_{lim} for *Swift* [184].

Figure 17 shows expected observed rates of strong lensing of supernovae along with rough estimates of z_{max} for LSST [238]. The LSST monitors a half sky, but the survey is conducted for 10 years. Therefore in their survey duration we expected to discover the significant number of strongly lensed Type Ia and core-collapse supernovae, which is consistent with more detailed estimates (e.g., [105, 374, 377]). The calculation also suggests that we may be able to discover strongly lensed superluminous supernovae. These are results for the wide survey of LSST, whereas LSST is also planning to conduct deep drilling fields survey where strongly lensed supernovae at higher redshifts may be discovered.

Figure 18 shows expected observed rates of strong lensing of gamma-ray bursts along with rough estimates of z_{max} for *Swift* [184]. Although the event rates of gamma-ray bursts are low, thanks to the high mean redshift strong lensing of long gamma-ray bursts

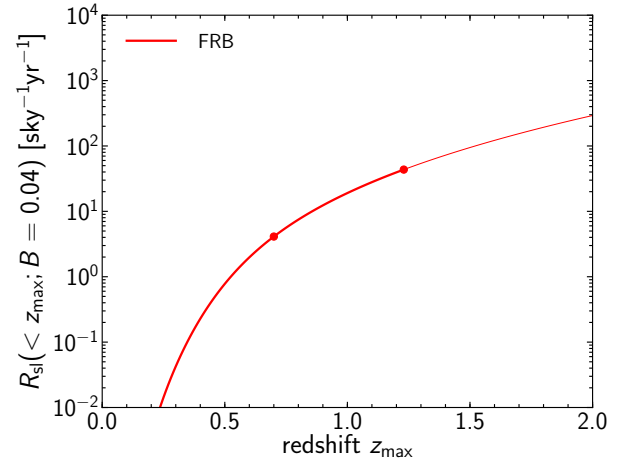


Figure 19. Same as Figure 17, but for strong lensing of fast radio bursts and a rough estimate of z_{lim} for CHIME [211].

can in principle be observed, although one limitation is its inefficient duty cycle as discussed in [378].

Figure 19 shows expected observed rates of strong lensing of fast radio bursts along with a rough estimate of z_{lim} for CHIME [211]. Thanks to the high event rate, the expected rate of strong lensing is also high, but CHIME observes the sky for the area of $\sim 250 \text{ deg}^2$ and therefore a factor of $250/41200 \approx 0.006$ should be multiplied to obtain the actual expected observed rate in CHIME. While this suggests that $\mathcal{O}(1)$ strong lensing events per a few years are expected from CHIME, we caution that this estimate can easily change by an order of magnitude or more given the quite large uncertainties of their event rate and redshift distribution. In addition, we note that CHIME changes observing regions on the sky rapidly as the rotation of the Earth, which is not ideal for identifying multiple images.

Figure 20 shows expected observed rates of

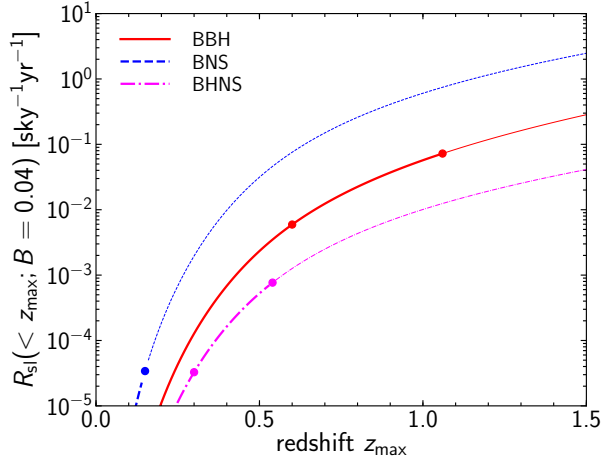


Figure 20. Same as Figure 17, but for strong lensing of gravitational waves and rough estimates of z_{lim} for the Advanced LIGO design sensitivity [223].

strong lensing of gravitational waves along with rough estimates of z_{max} for the Advanced LIGO design sensitivity [223]. This result indicates that, albeit the probability is not very high, it may be possible to detect strongly lensed gravitational waves of binary black hole mergers in Advanced LIGO, which is broadly consistent with more detailed calculations (e.g., [135, 389]).

Finally, we discuss typical magnifications of strongly lensed explosive transients detected in surveys. Table 2 indicates that magnifications of those observed strongly lensed supernovae are high in general, $\mu_{\text{tot}} \gtrsim 30$, which may appear odd given the steep magnification probability distribution of $dP/d\mu \propto \mu^{-3}$. The probability distribution suggests that such highly magnified events are much rarer than strong lensing events with modest magnifications, $\mu_{\text{tot}} < 10$ or so. However, this apparent discrepancy can easily be resolved if we take account of the steep dependence of the expected observed event rate on the redshift. From equation (63), at sufficiently low redshifts we have $R_{\text{sl}}(< z_{\text{max}}) \propto z_{\text{max}}^\eta$ with $\eta \approx 6$. Therefore the differential distribution of R_{sl} at $z = z_{\text{lim}}$ is given by

$$\frac{dR_{\text{sl}}}{dz_{\text{lim}}} \propto z_{\text{lim}}^{\eta-1}. \quad (69)$$

Also from equation (68), again at sufficiently low redshift, we can detect strong lensing events at $z > z_{\text{lim}}$ if the magnification factors satisfy

$$\mu > \left(\frac{z}{z_{\text{lim}}} \right)^2. \quad (70)$$

Since the cumulative probability distribution of the magnification is $P(> \mu) \propto \mu^{-2}$, the differential

distribution of R_{sl} at $z > z_{\text{lim}}$ is approximately given by

$$\frac{dR_{\text{sl}}}{dz} \propto z^{\eta-1} \left(\frac{z_{\text{lim}}}{z} \right)^4 = z^{\eta-5} z_{\text{lim}}^4. \quad (71)$$

By taking the ratio of equations (69) and (71), we have

$$\frac{dR_{\text{sl}}/dz}{dR_{\text{sl}}/dz_{\text{lim}}} \propto \left(\frac{z}{z_{\text{lim}}} \right)^{\eta-5} > 1 \quad (\eta > 5). \quad (72)$$

Since equation (72) is an increasing function of z , we preferentially observe strong lensing events with $z \gg z_{\text{lim}}$ i.e., $\mu \gg 1$, which qualitatively explains the high magnification factors of PS1-10afx and iPTF16geu. In sufficiently deep surveys, on the other hand, Figure 16 implies that the slope of the strong lensing rate becomes shallower, $\eta < 5$, for which this argument no longer holds so that strongly lensing events with modest magnifications are preferentially observed, although the detail depends also on the shape of the luminosity function. We expect that, at least for sufficiently shallow surveys such as CHIME for fast radio bursts and Advanced LIGO for gravitational waves, we typically observe highly magnified events with redshifts well beyond the redshift limit of unlensed events. This point has also discussed in e.g., [135] in the context of strongly lensed gravitational waves.

6. Conclusions

In this article, we have reviewed the science of strong lensing of explosive transients, specifically focusing on supernovae, gamma-ray bursts, fast radio bursts, and gravitational waves from compact binary mergers. Although many strongly lensed quasars and galaxies have already been identified, strong lensing of these explosive transients is complementary to traditional strong lensing and enables new applications that were not possible before. In this article we have discussed possible applications of these new strong lensing events, summarized the current status of strong lens searches, and presented expected rates of strong lensing events adopting a simplified approach.

Rapidly evolving light curves of these transients indicate that we expect a lot of progress in applications of time delays between multiple images. In particular for gamma-ray bursts, fast radio bursts, and gravitational waves, thanks to their very short time scales of $\lesssim 1$ sec we can drastically improve the accuracy of time delay measurements as compared with the current accuracy for strongly lensed quasars, ~ 1 day. The very accurate measurements of time delays open new avenues, including improved constraints on cosmological parameters such as the Hubble constant H_0 , a probe of small-scale perturbations from dark matter substructures, tests of fundamental physics from the propagation speed, and constraints on the

abundance of compact dark matter from the search of pair events with short time delays.

The compact sizes of these explosive transients imply that wave optics effects may play an important role. When the frequency is comparable to the inverse of the typical time delay, wave optics effects induce the interference pattern as a function of the source position and frequency, although in order for this effect to be observed the source size must be smaller than the width of the interference pattern. On the other hand, the frequency is much lower than the inverse of the typical time delay, lensing magnifications are suppressed due to diffraction. We have presented detailed discussions on whether wave optics effects are relevant for strong lensing of these explosive transients, and argued that wave optics effects can become important for strong lensing of gravitational waves, and probably for strong lensing of fast radio bursts as well depending on their actual progenitor sizes.

Strong lensing may also help better understand these explosive transients. Thanks to lensing magnifications, we can detect very high redshift events that are not accessible without lensing magnifications. Lensing magnifications can also be used as a microscope to resolve the fine structure of sources to constrain their progenitor models.

We have presented the current status and future prospect of the strong lens search. We have described recent discoveries of strongly lensed supernovae, PS1-10afx [349], SN Refsdal [350], and iPTF16geu [368]. We have computed expected observed rates of strong lensing of various explosive transients adopting a simple and concise approach. These calculations suggest that strong lensing of gamma-ray bursts, fast radio bursts, and gravitational waves, can be observed in near future. Using this simple model, we have discussed selection effects, and showed that highly magnified strong lensing events are preferentially observed in shallow surveys.

In this review article, we have not covered all explosive transients at cosmological distances. For instance, the tidal disruption event is a disruption of a star by the tidal force of the black hole (see e.g., [403]), which can also act as a source of strong lensing. Furthermore, time-domain surveys may identify new types of transients that are similar to strong lensing of explosive transients. One such example is a caustic crossing. When a star in a gravitationally lensed galaxy passes through a caustic it is magnified by a factor of several thousands or more and hence can be detected even at cosmological distances. Recent discoveries of caustic crossings of individual stars at $z \sim 1 - 1.5$ [404–407] have attracted a lot of attention. The caustic crossing has the time scale of the light curve near the peak as short as several days, and

therefore is definitely an interesting target to find in future time-domain surveys, in addition to strongly lensed explosive transients. In coming years, these new time-variable strong lensing events will deepen our view of the Universe in several ways.

Acknowledgments

I thank Kazumi Kashiyama for useful discussions, and Ariel Goobar, Shaoqi Hou, and Yufeng Li for useful comments. I also thank anonymous referees for many useful comments and suggestions. This work was supported in part by World Premier International Research Center Initiative (WPI Initiative), MEXT, Japan, and JSPS KAKENHI Grant Numbers JP18H04572, JP15H05892, and JP18K03693.

References

- [1] P. Coles, *Einstein, Eddington and the 1919 Eclipse*, in *Historical Development of Modern Cosmology*, V. J. Martínez, V. Trimble and M. J. Pons-Bordería, eds., vol. 252 of *Astronomical Society of the Pacific Conference Series*, p. 21, Jan, 2001, [astro-ph/0102462](#).
- [2] A. Einstein, *Lens-Like Action of a Star by the Deviation of Light in the Gravitational Field*, *Science* **84** (1936) 506.
- [3] F. Zwicky, *Nebulae as Gravitational Lenses*, *Physical Review* **51** (1937) 290.
- [4] F. Zwicky, *On the Probability of Detecting Nebulae Which Act as Gravitational Lenses*, *Physical Review* **51** (1937) 679.
- [5] D. Walsh, R. F. Carswell and R. J. Weymann, *0957 + 561 A, B - Twin quasistellar objects or gravitational lens*, *Nature* **279** (1979) 381.
- [6] R. Lynds and V. Petrosian, *Giant Luminous Arcs in Galaxy Clusters*, in *Bulletin of the American Astronomical Society*, vol. 18 of *Bull. Am. Astron. Soc.*, p. 1014, Sept., 1986.
- [7] G. Soucail, B. Fort, Y. Mellier and J. P. Picat, *A blue ring-like structure, in the center of the A 370 cluster of galaxies*, *Astron. Astrophys.* **172** (1987) L14.
- [8] S. T. Myers, N. J. Jackson, I. W. A. Browne, A. G. de Bruyn, T. J. Pearson, A. C. S. Readhead et al., *The Cosmic Lens All-Sky Survey - I. Source selection and observations*, *Mon. Not. R. Astron. Soc.* **341** (2003) 1 [[astro-ph/0211073](#)].
- [9] I. W. A. Browne, P. N. Wilkinson, N. J. F. Jackson, S. T. Myers, C. D. Fassnacht, L. V. E. Koopmans et al., *The Cosmic Lens All-Sky Survey - II. Gravitational lens candidate selection and follow-up*, *Mon. Not. R. Astron. Soc.* **341** (2003) 13 [[astro-ph/0211069](#)].
- [10] M. Oguri, N. Inada, B. Pindor, M. A. Strauss, G. T. Richards, J. F. Hennawi et al., *The Sloan Digital Sky Survey Quasar Lens Search. I. Candidate Selection Algorithm*, *Astron. J.* **132** (2006) 999 [[astro-ph/0605571](#)].
- [11] N. Inada, M. Oguri, M.-S. Shin, I. Kayo, M. A. Strauss, T. Morokuma et al., *The Sloan Digital Sky Survey Quasar Lens Search. V. Final Catalog from the Seventh Data Release*, *Astron. J.* **143** (2012) 119 [[1203.1087](#)].
- [12] A. More, M. Oguri, I. Kayo, J. Zinn, M. A. Strauss, B. X. Santiago et al., *The SDSS-III BOSS quasar lens*

- survey: discovery of 13 gravitationally lensed quasars, *Mon. Not. R. Astron. Soc.* **456** (2016) 1595 [1509.07917].
- [13] K.-H. Chae, A. D. Biggs, R. D. Blandford, I. W. Browne, A. G. de Bruyn, C. D. Fassnacht et al., *Constraints on Cosmological Parameters from the Analysis of the Cosmic Lens All Sky Survey Radio-Selected Gravitational Lens Statistics*, *Phys. Rev. Lett.* **89** (2002) 151301 [astro-ph/0209602].
- [14] M. Oguri, N. Inada, M. A. Strauss, C. S. Kochanek, I. Kayo, M.-S. Shin et al., *The Sloan Digital Sky Survey Quasar Lens Search. VI. Constraints on Dark Energy and the Evolution of Massive Galaxies*, *Astron. J.* **143** (2012) 120 [1203.1088].
- [15] A. S. Bolton, S. Burles, L. V. E. Koopmans, T. Treu and L. A. Moustakas, *The Sloan Lens ACS Survey. I. A Large Spectroscopically Selected Sample of Massive Early-Type Lens Galaxies*, *Astrophys. J.* **638** (2006) 703 [astro-ph/0511453].
- [16] A. S. Bolton, S. Burles, L. V. E. Koopmans, T. Treu, R. Gavazzi, L. A. Moustakas et al., *The Sloan Lens ACS Survey. V. The Full ACS Strong-Lens Sample*, *Astrophys. J.* **682** (2008) 964 [0805.1931].
- [17] J. F. Hennawi, M. D. Gladders, M. Oguri, N. Dalal, B. Koester, P. Natarajan et al., *A New Survey for Giant Arcs*, *Astron. J.* **135** (2008) 664 [astro-ph/0610061].
- [18] J. M. Kubo, S. S. Allam, J. Annis, E. J. Buckley-Geer, H. T. Diehl, D. Kubik et al., *The Sloan Bright Arcs Survey: Six Strongly Lensed Galaxies at $z = 0.4$ - 1.4* , *Astrophys. J. Lett.* **696** (2009) L61 [0812.3934].
- [19] J. R. Brownstein, A. S. Bolton, D. J. Schlegel, D. J. Eisenstein, C. S. Kochanek, N. Connolly et al., *The BOSS Emission-Line Lens Survey (BELLS). I. A Large Spectroscopically Selected Sample of Lens Galaxies at Redshift ~ 0.5* , *Astrophys. J.* **744** (2012) 41 [1112.3683].
- [20] Y. Shu, A. S. Bolton, C. S. Kochanek, M. Oguri, I. Pérez-Fournon, Z. Zheng et al., *The BOSS Emission-line Lens Survey. III. Strong Lensing of Ly α Emitters by Individual Galaxies*, *Astrophys. J.* **824** (2016) 86 [1604.01842].
- [21] C. Faure, J.-P. Kneib, G. Covone, L. Tasca, A. Leauthaud, P. Capak et al., *First Catalog of Strong Lens Candidates in the COSMOS Field*, *Astrophys. J. Suppl.* **176** (2008) 19 [0802.2174].
- [22] N. Jackson, *Gravitational lenses and lens candidates identified from the COSMOS field*, *Mon. Not. R. Astron. Soc.* **389** (2008) 1311 [0806.3693].
- [23] A. More, R. Cabanac, S. More, C. Alard, M. Limousin, J.-P. Kneib et al., *The CFHTLS-Strong Lensing Legacy Survey (SL2S): Investigating the Group-scale Lenses with the SARCS Sample*, *Astrophys. J.* **749** (2012) 38 [1109.1821].
- [24] M. Negrello, R. Hopwood, G. De Zotti, A. Cooray, A. Verma, J. Bock et al., *The Detection of a Population of Submillimeter-Bright, Strongly Lensed Galaxies*, *Science* **330** (2010) 800 [1011.1255].
- [25] J. L. Wardlow, A. Cooray, F. De Bernardis, A. Amblard, V. Arumugam, H. Aussel et al., *HerMES: Candidate Gravitationally Lensed Galaxies and Lensing Statistics at Submillimeter Wavelengths*, *Astrophys. J.* **762** (2013) 59 [1205.3778].
- [26] J. D. Vieira, D. P. Marrone, S. C. Chapman, C. De Breuck, Y. D. Hezaveh, A. Weiß et al., *Dusty starburst galaxies in the early Universe as revealed by gravitational lensing*, *Nature* **495** (2013) 344 [1303.2723].
- [27] Y. D. Hezaveh, D. P. Marrone, C. D. Fassnacht, J. S. Spilker, J. D. Vieira, J. E. Aguirre et al., *ALMA Observations of SPT-discovered, Strongly Lensed, Dusty, Star-forming Galaxies*, *Astrophys. J.* **767** (2013) 132 [1303.2722].
- [28] L. V. E. Koopmans, T. Treu, A. S. Bolton, S. Burles and L. A. Moustakas, *The Sloan Lens ACS Survey. III. The Structure and Formation of Early-Type Galaxies and Their Evolution since $z \sim 1$* , *Astrophys. J.* **649** (2006) 599 [astro-ph/0601628].
- [29] T. Treu, M. W. Auger, L. V. E. Koopmans, R. Gavazzi, P. J. Marshall and A. S. Bolton, *The Initial Mass Function of Early-Type Galaxies*, *Astrophys. J.* **709** (2010) 1195 [0911.3392].
- [30] M. Postman, D. Coe, N. Benítez, L. Bradley, T. Broadhurst, M. Donahue et al., *The Cluster Lensing and Supernova Survey with Hubble: An Overview*, *Astrophys. J. Suppl.* **199** (2012) 25 [1106.3328].
- [31] J. M. Lotz, A. Koekemoer, D. Coe, N. Grogin, P. Capak, J. Mack et al., *The Frontier Fields: Survey Design and Initial Results*, *Astrophys. J.* **837** (2017) 97 [1605.06567].
- [32] D. Coe, B. Salmon, M. Bradac, L. D. Bradley, K. Sharon, A. Zitrin et al., *RELICS: Reionization Lensing Cluster Survey*, *arXiv e-prints* (2019) [1903.02002].
- [33] C. A. Lemon, M. W. Auger, R. G. McMahon and F. Ostrovski, *Gravitationally lensed quasars in Gaia - II. Discovery of 24 lensed quasars*, *Mon. Not. R. Astron. Soc.* **479** (2018) 5060 [1803.07601].
- [34] C. A. Lemon, M. W. Auger and R. G. McMahon, *Gravitationally lensed quasars in Gaia - III. 22 new lensed quasars from Gaia data release 2*, *Mon. Not. R. Astron. Soc.* **483** (2019) 4242 [1810.04480].
- [35] L. Delchambre, A. Krone-Martins, O. Wertz, C. Ducourant, L. Galluccio, J. Klüter et al., *Gaia GraL: Gaia DR2 Gravitational Lens Systems. III. A systematic blind search for new lensed systems*, *Astron. Astrophys.* **622** (2019) A165 [1807.02845].
- [36] H. T. Diehl, E. J. Buckley-Geer, K. A. Lindgren, B. Nord, H. Gaitsch, S. Gaitsch et al., *The DES Bright Arcs Survey: Hundreds of Candidate Strongly Lensed Galaxy Systems from the Dark Energy Survey Science Verification and Year 1 Observations*, *Astrophys. J. Suppl.* **232** (2017) 15.
- [37] T. Treu, A. Agnello, M. A. Baumer, S. Birrer, E. J. Buckley-Geer, F. Courbin et al., *The STRong lensing Insights into the Dark Energy Survey (STRIDES) 2016 follow-up campaign - I. Overview and classification of candidates selected by two techniques*, *Mon. Not. R. Astron. Soc.* **481** (2018) 1041 [1808.04838].
- [38] T. Anguita, P. L. Schechter, N. Kuropatkin, N. D. Morgan, F. Ostrovski, L. E. Abramson et al., *The STRong lensing Insights into the Dark Energy Survey (STRIDES) 2016 follow-up campaign - II. New quasar lenses from double component fitting*, *Mon. Not. R. Astron. Soc.* **480** (2018) 5017 [1805.12151].
- [39] C. Jacobs, T. Collett, K. Glazebrook, C. McCarthy, A. K. Qin, T. M. C. Abbott et al., *Finding high-redshift strong lenses in DES using convolutional neural networks*, *Mon. Not. R. Astron. Soc.* **484** (2019) 5330 [1811.03786].
- [40] C. E. Petrillo, C. Tortora, G. Vernardos, L. V. E. Koopmans, G. Verdoes Kleijn, M. Bilicki et al., *LinKS: discovering galaxy-scale strong lenses in the Kilo-Degree Survey using convolutional neural networks*, *Mon. Not. R. Astron. Soc.* **484** (2019) 3879 [1812.03168].
- [41] C. E. Rusu, C. T. Bergeha, C. D. Fassnacht, A. More, E. Seman, G. J. Nelson et al., *A search for gravitationally lensed quasars and quasar pairs in*

- Pan-STARRS1: spectroscopy and sources of shear in the diamond 2M1134-2103*, *Mon. Not. R. Astron. Soc.* **486** (2019) 4987 [1803.07175].
- [42] A. Sonnenfeld, J. H. H. Chan, Y. Shu, A. More, M. Oguri, S. H. Suyu et al., *Survey of Gravitationally-lensed Objects in HSC Imaging (SuGOHI). I. Automatic search for galaxy-scale strong lenses*, *Publ. Astron. Soc. Japan* **70** (2018) S29 [1704.01585].
- [43] K. C. Wong, A. Sonnenfeld, J. H. H. Chan, C. E. Rusu, M. Tanaka, A. T. Jaelani et al., *Survey of Gravitationally Lensed Objects in HSC Imaging (SuGOHI). II. Environments and Line-of-Sight Structure of Strong Gravitational Lens Galaxies to $z \sim 0.8$* , *Astrophys. J.* **867** (2018) 107 [1809.07341].
- [44] S. Refsdal, *On the possibility of determining Hubble's parameter and the masses of galaxies from the gravitational lens effect*, *Mon. Not. R. Astron. Soc.* **128** (1964) 307.
- [45] T. Kundić, E. L. Turner, W. N. Colley, J. R. Gott, III, J. E. Rhoads, Y. Wang et al., *A Robust Determination of the Time Delay in 0957+561A, B and a Measurement of the Global Value of Hubble's Constant*, *Astrophys. J.* **482** (1997) 75 [astro-ph/9610162].
- [46] M. Oguri, *Gravitational Lens Time Delays: A Statistical Assessment of Lens Model Dependences and Implications for the Global Hubble Constant*, *Astrophys. J.* **660** (2007) 1 [astro-ph/0609694].
- [47] D. Paraficz and J. Hjorth, *The Hubble Constant Inferred from 18 Time-delay Lenses*, *Astrophys. J.* **712** (2010) 1378 [1002.2570].
- [48] N. Jackson, *The Hubble Constant*, *Living Reviews in Relativity* **18** (2015) 2.
- [49] S. H. Suyu, V. Bonvin, F. Courbin, C. D. Fassnacht, C. E. Rusu, D. Sluse et al., *H0LiCOW - I. H_0 Lenses in COSMOGRAIL's Wellspring: program overview*, *Mon. Not. R. Astron. Soc.* **468** (2017) 2590 [1607.00017].
- [50] V. Bonvin, F. Courbin, S. H. Suyu, P. J. Marshall, C. E. Rusu, D. Sluse et al., *H0LiCOW - V. New COSMOGRAIL time delays of HE 0435-1223: H_0 to 3.8 per cent precision from strong lensing in a flat Λ CDM model*, *Mon. Not. R. Astron. Soc.* **465** (2017) 4914 [1607.01790].
- [51] S. Birrer, T. Treu, C. E. Rusu, V. Bonvin, C. D. Fassnacht, J. H. H. Chan et al., *H0LiCOW - IX. Cosmographic analysis of the doubly imaged quasar SDSS 1206+4332 and a new measurement of the Hubble constant*, *Mon. Not. R. Astron. Soc.* **484** (2019) 4726 [1809.01274].
- [52] K. C. Wong, S. H. Suyu, G. C. F. Chen, C. E. Rusu, M. Millon, D. Sluse et al., *H0LiCOW XIII. A 2.4% measurement of H_0 from lensed quasars: 5.3 σ tension between early and late-Universe probes*, *arXiv e-prints* (2019) arXiv:1907.04869 [1907.04869].
- [53] W. L. Freedman, B. F. Madore, B. K. Gibson, L. Ferrarese, D. D. Kelson, S. Sakai et al., *Final Results from the Hubble Space Telescope Key Project to Measure the Hubble Constant*, *Astrophys. J.* **553** (2001) 47 [astro-ph/0012376].
- [54] A. G. Riess, L. Macri, S. Casertano, H. Lampeitl, H. C. Ferguson, A. V. Filippenko et al., *A 3% Solution: Determination of the Hubble Constant with the Hubble Space Telescope and Wide Field Camera 3*, *Astrophys. J.* **730** (2011) 119 [1103.2976].
- [55] A. G. Riess, L. M. Macri, S. L. Hoffmann, D. Scolnic, S. Casertano, A. V. Filippenko et al., *A 2.4% Determination of the Local Value of the Hubble Constant*, *Astrophys. J.* **826** (2016) 56 [1604.01424].
- [56] A. G. Riess, S. Casertano, W. Yuan, L. M. Macri and D. Scolnic, *Large Magellanic Cloud Cepheid Standards Provide a 1% Foundation for the Determination of the Hubble Constant and Stronger Evidence for Physics beyond Λ CDM*, *Astrophys. J.* **876** (2019) 85 [1903.07603].
- [57] Planck Collaboration, N. Aghanim, Y. Akrami, M. Ashdown, J. Aumont, C. Baccigalupi et al., *Planck 2018 results. VI. Cosmological parameters*, *arXiv e-prints* (2018) arXiv:1807.06209 [1807.06209].
- [58] P. Schneider, J. Ehlers and E. E. Falco, *Gravitational Lenses*. 1992, 10.1007/978-3-662-03758-4.
- [59] R. D. Blandford and R. Narayan, *Cosmological applications of gravitational lensing*, *Ann. Rev. Astron. Astrophys.* **30** (1992) 311.
- [60] A. O. Petters, H. Levine and J. Wambsganss, *Singularity theory and gravitational lensing*. 2001.
- [61] C. S. Kochanek, *Part 2: Strong gravitational lensing*, in *Saas-Fee Advanced Course 33: Gravitational Lensing: Strong, Weak and Micro*, G. Meylan, P. Jetzer, P. North, P. Schneider, C. S. Kochanek and J. Wambsganss, eds., pp. 91–268, 2006.
- [62] M. Bartelmann, *TOPICAL REVIEW Gravitational lensing*, *Classical and Quantum Gravity* **27** (2010) 233001 [1010.3829].
- [63] T. Treu, *Strong Lensing by Galaxies*, *Ann. Rev. Astron. Astrophys.* **48** (2010) 87 [1003.5567].
- [64] J.-P. Kneib and P. Natarajan, *Cluster lenses*, *Astron. Astrophys. Rev.* **19** (2011) 47 [1202.0185].
- [65] M. Meneghetti, M. Bartelmann, H. Dahle and M. Limousin, *Arc Statistics*, *Space Sci. Rev.* **177** (2013) 31 [1303.3363].
- [66] T. Treu and P. J. Marshall, *Time delay cosmography*, *Astron. Astrophys. Rev.* **24** (2016) 11 [1605.05333].
- [67] S. Dodelson, *Gravitational Lensing*. June, 2017.
- [68] A. B. Congdon and C. Keeton, *Principles of Gravitational Lensing: Light Deflection as a Probe of Astrophysics and Cosmology*. 2018.
- [69] A. Barnacka, *Gravitational lenses as high-resolution telescopes*, *Phys. Rep.* **778** (2018) 1 [1810.07265].
- [70] Planck Collaboration, P. A. R. Ade, N. Aghanim, M. Arnaud, M. Ashdown, J. Aumont et al., *Planck 2015 results. XIII. Cosmological parameters*, *Astron. Astrophys.* **594** (2016) A13 [1502.01589].
- [71] S. Weinberg, *Cosmology*. 2008.
- [72] W. L. Burke, *Multiple Gravitational Imaging by Distributed Masses*, *Astrophys. J. Lett.* **244** (1981) L1.
- [73] M. Oguri, *The Mass Distribution of SDSS J1004+4112 Revisited*, *Publ. Astron. Soc. Japan* **62** (2010) 1017 [1005.3103].
- [74] J. F. Navarro, C. S. Frenk and S. D. M. White, *The Structure of Cold Dark Matter Halos*, *Astrophys. J.* **462** (1996) 563 [astro-ph/9508025].
- [75] J. F. Navarro, C. S. Frenk and S. D. M. White, *A Universal Density Profile from Hierarchical Clustering*, *Astrophys. J.* **490** (1997) 493 [astro-ph/9611107].
- [76] M. Bartelmann, *Arcs from a universal dark-matter halo profile.*, *Astron. Astrophys.* **313** (1996) 697 [astro-ph/9602053].
- [77] B. Diemer and A. V. Kravtsov, *A Universal Model for Halo Concentrations*, *Astrophys. J.* **799** (2015) 108 [1407.4730].
- [78] P. Schneider, *A new formulation of gravitational lens theory, time-delay, and Fermat's principle*, *Astron. Astrophys.* **143** (1985) 413.
- [79] R. Blandford and R. Narayan, *Fermat's principle, caustics, and the classification of gravitational lens images*, *Astrophys. J.* **310** (1986) 568.
- [80] C. S. Kochanek, C. R. Keeton and B. A. McLeod, *The*

- Importance of Einstein Rings, *Astrophys. J.* **547** (2001) 50 [astro-ph/0006116].
- [81] T. Treu and L. V. E. Koopmans, *The internal structure of the lens PG1115+080: breaking degeneracies in the value of the Hubble constant*, *Mon. Not. R. Astron. Soc.* **337** (2002) L6 [astro-ph/0210002].
- [82] E. E. Falco, M. V. Gorenstein and I. I. Shapiro, *On model-dependent bounds on $H(0)$ from gravitational images Application of Q0957 + 561A,B*, *Astrophys. J. Lett.* **289** (1985) L1.
- [83] O. Wucknitz, *Degeneracies and scaling relations in general power-law models for gravitational lenses*, *Mon. Not. R. Astron. Soc.* **332** (2002) 951 [astro-ph/0202376].
- [84] P. Schneider and D. Sluse, *Source-position transformation: an approximate invariance in strong gravitational lensing*, *Astron. Astrophys.* **564** (2014) A103 [1306.4675].
- [85] S. Unruh, P. Schneider and D. Sluse, *Ambiguities in gravitational lens models: the density field from the source position transformation*, *Astron. Astrophys.* **601** (2017) A77 [1606.04321].
- [86] P. L. Schechter and J. Wambsganss, *Quasar Microlensing at High Magnification and the Role of Dark Matter: Enhanced Fluctuations and Suppressed Saddle Points*, *Astrophys. J.* **580** (2002) 685 [astro-ph/0204425].
- [87] C. S. Kochanek, *Quantitative Interpretation of Quasar Microlensing Light Curves*, *Astrophys. J.* **605** (2004) 58 [astro-ph/0307422].
- [88] J. Wambsganss, *Part 4: Gravitational microlensing*, in *Saas-Fee Advanced Course 33: Gravitational Lensing: Strong, Weak and Micro*, G. Meylan, P. Jetzer, P. North, P. Schneider, C. S. Kochanek and J. Wambsganss, eds., pp. 453–540, Jan, 2006.
- [89] K. Chang and S. Refsdal, *Flux variations of QSO 0957+561 A, B and image splitting by stars near the light path*, *Nature* **282** (1979) 561.
- [90] M. J. Mortonson, P. L. Schechter and J. Wambsganss, *Size Is Everything: Universal Features of Quasar Microlensing with Extended Sources*, *Astrophys. J.* **628** (2005) 594 [astro-ph/0408195].
- [91] G. Vernardos, C. J. Fluke, N. F. Bate and D. Croton, *GERLUMP Data Release 1: High-resolution Cosmological Microlensing Magnification Maps and eResearch Tools*, *Astrophys. J. Suppl.* **211** (2014) 16 [1401.7711].
- [92] G. Vernardos, C. J. Fluke, N. F. Bate, D. Croton and D. Vohl, *GERLUMP Data Release 2: 2.5 Billion Simulated Microlensing Light Curves*, *Astrophys. J. Suppl.* **217** (2015) 23 [1503.00770].
- [93] J. Diemand, B. Moore and J. Stadel, *Earth-mass dark-matter haloes as the first structures in the early Universe*, *Nature* **433** (2005) 389 [astro-ph/0501589].
- [94] J. S. Bullock and M. Boylan-Kolchin, *Small-Scale Challenges to the Λ CDM Paradigm*, *Ann. Rev. Astron. Astrophys.* **55** (2017) 343 [1707.04256].
- [95] S. Mao and P. Schneider, *Evidence for substructure in lens galaxies?*, *Mon. Not. R. Astron. Soc.* **295** (1998) 587 [astro-ph/9707187].
- [96] C. R. Keeton and L. A. Moustakas, *A New Channel for Detecting Dark Matter Substructure in Galaxies: Gravitational Lens Time Delays*, *Astrophys. J.* **699** (2009) 1720 [0805.0309].
- [97] E. L. Turner, J. P. Ostriker and J. R. Gott, III, *The statistics of gravitational lenses - The distributions of image angular separations and lens redshifts*, *Astrophys. J.* **284** (1984) 1.
- [98] M. Fukugita, T. Futamase, M. Kasai and E. L. Turner, *Statistical properties of gravitational lenses with a nonzero cosmological constant*, *Astrophys. J.* **393** (1992) 3.
- [99] C. S. Kochanek, *Is There a Cosmological Constant?*, *Astrophys. J.* **466** (1996) 638 [astro-ph/9510077].
- [100] M. Chiba and Y. Yoshii, *New Limits on a Cosmological Constant from Statistics of Gravitational Lensing*, *Astrophys. J.* **510** (1999) 42 [astro-ph/9808321].
- [101] K.-H. Chae, *The Cosmic Lens All-Sky Survey: statistical strong lensing, cosmological parameters, and global properties of galaxy populations*, *Mon. Not. R. Astron. Soc.* **346** (2003) 746 [astro-ph/0211244].
- [102] J. L. Mitchell, C. R. Keeton, J. A. Frieman and R. K. Sheth, *Improved Cosmological Constraints from Gravitational Lens Statistics*, *Astrophys. J.* **622** (2005) 81 [astro-ph/0401138].
- [103] D. Huterer, C. R. Keeton and C.-P. Ma, *Effects of Ellipticity and Shear on Gravitational Lens Statistics*, *Astrophys. J.* **624** (2005) 34 [astro-ph/0405040].
- [104] M. Oguri, C. R. Keeton and N. Dalal, *The impact of lens galaxy environments on the image separation distribution*, *Mon. Not. R. Astron. Soc.* **364** (2005) 1451 [astro-ph/0506549].
- [105] M. Oguri and P. J. Marshall, *Gravitationally lensed quasars and supernovae in future wide-field optical imaging surveys*, *Mon. Not. R. Astron. Soc.* **405** (2010) 2579 [1001.2037].
- [106] T. E. Collett, *The Population of Galaxy-Galaxy Strong Lenses in Forthcoming Optical Imaging Surveys*, *Astrophys. J.* **811** (2015) 20 [1507.02657].
- [107] R. Narayan and S. D. M. White, *Gravitational lensing in a cold dark matter universe*, *Mon. Not. R. Astron. Soc.* **231** (1988) 97p.
- [108] J. Wambsganss, R. Cen, J. P. Ostriker and E. L. Turner, *Testing Cosmogonic Models with Gravitational Lensing*, *Science* **268** (1995) 274.
- [109] C. S. Kochanek, *Gravitational Lensing Limits on Cold Dark Matter and Its Variants*, *Astrophys. J.* **453** (1995) 545 [astro-ph/9411082].
- [110] J. S. B. Wyithe, E. L. Turner and D. N. Spergel, *Gravitational Lens Statistics for Generalized NFW Profiles: Parameter Degeneracy and Implications for Self-Interacting Cold Dark Matter*, *Astrophys. J.* **555** (2001) 504 [astro-ph/0007354].
- [111] C. R. Keeton and P. Madau, *Lensing Constraints on the Cores of Massive Dark Matter Halos*, *Astrophys. J. Lett.* **549** (2001) L25 [astro-ph/0101058].
- [112] R. Takahashi and T. Chiba, *Gravitational Lens Statistics and the Density Profile of Dark Halos*, *Astrophys. J.* **563** (2001) 489 [astro-ph/0106176].
- [113] M. Oguri, N. Inada, C. R. Keeton, B. Pindor, J. F. Hennawi, M. D. Gregg et al., *Observations and Theoretical Implications of the Large-Separation Lensed Quasar SDSS J1004+4112*, *Astrophys. J.* **605** (2004) 78 [astro-ph/0312429].
- [114] M. Oguri and C. R. Keeton, *Effects of Triaxiality on the Statistics of Large-Separation Gravitational Lenses*, *Astrophys. J.* **610** (2004) 663 [astro-ph/0403633].
- [115] S. Hilbert, S. D. M. White, J. Hartlap and P. Schneider, *Strong lensing optical depths in a Λ CDM universe*, *Mon. Not. R. Astron. Soc.* **382** (2007) 121 [astro-ph/0703803].
- [116] G. L. Li, S. Mao, Y. P. Jing, W. P. Lin and M. Oguri, *Properties of wide-separation lensed quasars by clusters of galaxies in the Sloan Digital Sky Survey*, *Mon. Not. R. Astron. Soc.* **378** (2007) 469 [astro-ph/0701801].
- [117] Q. E. Minor and M. Kaplinghat, *Effects of galaxy-halo alignment and adiabatic contraction on gravitational lens statistics*, *Mon. Not. R. Astron. Soc.* **391** (2008) 653 [0711.2537].
- [118] T. J. Broadhurst and R. Barkana, *Large Einstein radii: a*

- problem for Λ CDM, *Mon. Not. R. Astron. Soc.* **390** (2008) 1647 [0801.1875].
- [119] M. Oguri and R. D. Blandford, *What is the largest Einstein radius in the universe?*, *Mon. Not. R. Astron. Soc.* **392** (2009) 930 [0808.0192].
- [120] A. Zitrin, T. Broadhurst, M. Bartelmann, Y. Rephaeli, M. Oguri, N. Benítez et al., *The universal Einstein radius distribution from 10 000 SDSS clusters*, *Mon. Not. R. Astron. Soc.* **423** (2012) 2308 [1105.2295].
- [121] M. Redlich, M. Bartelmann, J.-C. Waizmann and C. Fedeli, *The strongest gravitational lenses. I. The statistical impact of cluster mergers*, *Astron. Astrophys.* **547** (2012) A66 [1205.6906].
- [122] J.-C. Waizmann, M. Redlich, M. Meneghetti and M. Bartelmann, *The strongest gravitational lenses. III. The order statistics of the largest Einstein radii*, *Astron. Astrophys.* **565** (2014) A28 [1403.4573].
- [123] C. R. Keeton, II, *Using Gravitational Lenses to Study Galaxies and Cosmology*, Ph.D. thesis, HARVARD UNIVERSITY, 1998.
- [124] C. Porciani and P. Madau, *Gravitational Lensing of Distant Supernovae in Cold Dark Matter Universes*, *Astrophys. J.* **532** (2000) 679.
- [125] C. S. Kochanek and M. White, *Global Probes of the Impact of Baryons on Dark Matter Halos*, *Astrophys. J.* **559** (2001) 531 [astro-ph/0102334].
- [126] L.-X. Li and J. P. Ostriker, *Semianalytical Models for Lensing by Dark Halos. I. Splitting Angles*, *Astrophys. J.* **566** (2002) 652 [astro-ph/0010432].
- [127] M. Oguri, *Constraints on the Baryonic Compression and Implications for the Fraction of Dark Halo Lenses*, *Astrophys. J.* **580** (2002) 2 [astro-ph/0207520].
- [128] C.-P. Ma, *Schechter versus Schechter: Subarcsecond Gravitational Lensing and Inner Halo Profiles*, *Astrophys. J. Lett.* **584** (2003) L1 [astro-ph/0211464].
- [129] D. Huterer and C.-P. Ma, *Constraints on the Inner Cluster Mass Profile and the Power Spectrum Normalization from Strong Lensing Statistics*, *Astrophys. J. Lett.* **600** (2004) L7 [astro-ph/0307301].
- [130] M. Kuhlen, C. R. Keeton and P. Madau, *Gravitational Lensing Statistics in Universes Dominated by Dark Energy*, *Astrophys. J.* **601** (2004) 104 [astro-ph/0310013].
- [131] C. R. Keeton, M. Kuhlen and Z. Haiman, *Gravitational Lensing Magnification without Multiple Imaging*, *Astrophys. J.* **621** (2005) 559 [astro-ph/0405143].
- [132] M. Oguri, *The image separation distribution of strong lenses: halo versus subhalo populations*, *Mon. Not. R. Astron. Soc.* **367** (2006) 1241 [astro-ph/0508528].
- [133] A. Amvrosiadis, S. A. Eales, M. Negrello, L. Marchetti, M. W. L. Smith, N. Bourne et al., *ALMA observations of lensed Herschel sources: testing the dark matter halo paradigm*, *Mon. Not. R. Astron. Soc.* **475** (2018) 4939 [1801.07282].
- [134] E. L. Turner, *The effect of undetected gravitational lenses on statistical measures of quasar evolution*, *Astrophys. J. Lett.* **242** (1980) L135.
- [135] M. Oguri, *Effect of gravitational lensing on the distribution of gravitational waves from distant binary black hole mergers*, *Mon. Not. R. Astron. Soc.* **480** (2018) 3842 [1807.02584].
- [136] M. Bernardi, F. Shankar, J. B. Hyde, S. Mei, F. Marulli and R. K. Sheth, *Galaxy luminosities, stellar masses, sizes, velocity dispersions as a function of morphological type*, *Mon. Not. R. Astron. Soc.* **404** (2010) 2087 [0910.1093].
- [137] P. Torrey, S. Wellons, F. Machado, B. Griffen, D. Nelson, V. Rodriguez-Gomez et al., *An analysis of the evolving comoving number density of galaxies in hydrodynamical simulations*, *Mon. Not. R. Astron. Soc.* **454** (2015) 2770 [1507.01942].
- [138] M. Oguri, Y. Suto and E. L. Turner, *Gravitational Lensing Magnification and Time Delay Statistics for Distant Supernovae*, *Astrophys. J.* **583** (2003) 584 [astro-ph/0210107].
- [139] A. Gould, *Femtolensing of gamma-ray bursters*, *Astrophys. J. Lett.* **386** (1992) L5.
- [140] T. T. Nakamura, *Gravitational Lensing of Gravitational Waves from Inspiring Binaries by a Point Mass Lens*, *Phys. Rev. Lett.* **80** (1998) 1138.
- [141] R. Takahashi and T. Nakamura, *Wave Effects in the Gravitational Lensing of Gravitational Waves from Chirping Binaries*, *Astrophys. J.* **595** (2003) 1039 [astro-ph/0305055].
- [142] A. Mehrabi and S. Rahvar, *Studying wave optics in the light curves of exoplanet microlensing*, *Mon. Not. R. Astron. Soc.* **431** (2013) 1264 [1207.4034].
- [143] H. Niikura, M. Takada, N. Yasuda, R. H. Lupton, T. Sumi, S. More et al., *Microlensing constraints on primordial black holes with Subaru/HSC Andromeda observations*, *Nature Astronomy* **3** (2019) 524 [1701.02151].
- [144] S. Sugiyama, T. Kurita and M. Takada, *Revisiting the wave optics effect on primordial black hole constraints from optical microlensing search*, *arXiv e-prints* (2019) [1905.06066].
- [145] P. Montero-Camacho, X. Fang, G. Vasquez, M. Silva and C. M. Hirata, *Revisiting constraints on asteroid-mass primordial black holes as dark matter candidates*, *arXiv e-prints* (2019) arXiv:1906.05950 [1906.05950].
- [146] T. T. Nakamura and S. Deguchi, *Wave Optics in Gravitational Lensing*, *Progress of Theoretical Physics Supplement* **133** (1999) 137.
- [147] S. Deguchi and W. D. Watson, *Diffraction in gravitational lensing for compact objects of low mass*, *Astrophys. J.* **307** (1986) 30.
- [148] S. Deguchi and W. D. Watson, *Wave effects in gravitational lensing of electromagnetic radiation*, *Phys. Rev. D* **34** (1986) 1708.
- [149] N. Matsunaga and K. Yamamoto, *The finite source size effect and wave optics in gravitational lensing*, *J. Cosmol. Astropart. Phys.* **1** (2006) 023 [astro-ph/0601701].
- [150] A. V. Filippenko, *Optical Spectra of Supernovae*, *Ann. Rev. Astron. Astrophys.* **35** (1997) 309.
- [151] D. Branch and J. C. Wheeler, *Supernova Explosions*. 2017, 10.1007/978-3-662-55054-0.
- [152] D. Maoz, F. Mannucci and G. Nelemans, *Observational Clues to the Progenitors of Type Ia Supernovae*, *Ann. Rev. Astron. Astrophys.* **52** (2014) 107 [1312.0628].
- [153] B. Müller, *The Status of Multi-Dimensional Core-Collapse Supernova Models*, *Publ. Astron. Soc. Aust.* **33** (2016) e048 [1608.03274].
- [154] D. Richardson, D. Branch, D. Casebeer, J. Millard, R. C. Thomas and E. Baron, *A Comparative Study of the Absolute Magnitude Distributions of Supernovae*, *Astron. J.* **123** (2002) 745 [astro-ph/0112051].
- [155] M. M. Phillips, *The absolute magnitudes of Type Ia supernovae*, *Astrophys. J. Lett.* **413** (1993) L105.
- [156] A. G. Riess, A. V. Filippenko, P. Challis, A. Clocchiatti, A. Diercks, P. M. Garnavich et al., *Observational Evidence from Supernovae for an Accelerating Universe and a Cosmological Constant*, *Astron. J.* **116** (1998) 1009 [astro-ph/9805201].
- [157] S. Perlmutter, G. Aldering, G. Goldhaber, R. A. Knop, P. Nugent, P. G. Castro et al., *Measurements of Ω and Λ from 42 High-Redshift Supernovae*, *Astrophys. J.* **517** (1999) 565 [astro-ph/9812133].
- [158] M. Sullivan, J. Guy, A. Conley, N. Regnault, P. Astier, C. Balland et al., *SNLS3: Constraints on Dark Energy*

- Combining the Supernova Legacy Survey Three-year Data with Other Probes, *Astrophys. J.* **737** (2011) 102 [1104.1444].
- [159] M. Sako, B. Bassett, A. C. Becker, P. J. Brown, H. Campbell, R. Wolf et al., *The Data Release of the Sloan Digital Sky Survey-II Supernova Survey*, *Publ. Astron. Soc. Pac.* **130** (2018) 064002 [1401.3317].
- [160] N. M. Law, S. R. Kulkarni, R. G. Dekany, E. O. Ofek, R. M. Quimby, P. E. Nugent et al., *The Palomar Transient Factory: System Overview, Performance, and First Results*, *Publ. Astron. Soc. Pac.* **121** (2009) 1395 [0906.5350].
- [161] N. Suzuki, D. Rubin, C. Lidman, G. Aldering, R. Amanullah, K. Barbary et al., *The Hubble Space Telescope Cluster Supernova Survey. V. Improving the Dark-energy Constraints above $z \gtrsim 1$ and Building an Early-type-hosted Supernova Sample*, *Astrophys. J.* **746** (2012) 85 [1105.3470].
- [162] D. M. Scolnic, D. O. Jones, A. Rest, Y. C. Pan, R. Chornock, R. J. Foley et al., *The Complete Light-curve Sample of Spectroscopically Confirmed SNe Ia from Pan-STARRS1 and Cosmological Constraints from the Combined Pantheon Sample*, *Astrophys. J.* **859** (2018) 101 [1710.00845].
- [163] T. W.-S. Holoien, J. S. Brown, K. Z. Stanek, C. S. Kochanek, B. J. Shappee, J. L. Prieto et al., *The ASAS-SN bright supernova catalogue - III. 2016*, *Mon. Not. R. Astron. Soc.* **471** (2017) 4966 [1704.02320].
- [164] D. Brout, D. Scolnic, R. Kessler, C. B. D'Andrea, T. M. Davis, R. R. Gupta et al., *First Cosmology Results Using SNe Ia from the Dark Energy Survey: Analysis, Systematic Uncertainties, and Validation*, *Astrophys. J.* **874** (2019) 150 [1811.02377].
- [165] N. Yasuda, M. Tanaka, N. Tominaga, J.-a. Jiang, T. J. Moriya, T. Morokuma et al., *The Hyper Suprime-Cam SSP Transient Survey in COSMOS: Overview*, *arXiv e-prints* (2019) [1904.09697].
- [166] J. Guillochon, J. Parrent, L. Z. Kelley and R. Margutti, *An Open Catalog for Supernova Data*, *Astrophys. J.* **835** (2017) 64 [1605.01054].
- [167] A. Gal-Yam, *Luminous Supernovae*, *Science* **337** (2012) 927 [1208.3217].
- [168] T. J. Moriya, E. I. Sorokina and R. A. Chevalier, *Superluminous Supernovae*, *Space Sci. Rev.* **214** (2018) 59 [1803.01875].
- [169] R. M. Quimby, G. Aldering, J. C. Wheeler, P. Höflich, C. W. Akerlof and E. S. Rykoff, *SN 2005ap: A Most Brilliant Explosion*, *Astrophys. J. Lett.* **668** (2007) L99 [0709.0302].
- [170] J. Cooke, M. Sullivan, A. Gal-Yam, E. J. Barton, R. G. Carlberg, E. V. Ryan-Weber et al., *Superluminous supernovae at redshifts of 2.05 and 3.90*, *Nature* **491** (2012) 228 [1211.2003].
- [171] T. J. Moriya, M. Tanaka, N. Yasuda, J.-a. Jiang, C.-H. Lee, K. Maeda et al., *First Release of High-Redshift Superluminous Supernovae from the Subaru HIGH-Z Supernova Campaign (SHIZUCA). I. Photometric Properties*, *Astrophys. J. Suppl.* **241** (2019) 16 [1801.08240].
- [172] W. Li, R. Chornock, J. Leaman, A. V. Filippenko, D. Poznanski, X. Wang et al., *Nearby supernova rates from the Lick Observatory Supernova Search - III. The rate-size relation, and the rates as a function of galaxy Hubble type and colour*, *Mon. Not. R. Astron. Soc.* **412** (2011) 1473 [1006.4613].
- [173] R. M. Quimby, F. Yuan, C. Akerlof and J. C. Wheeler, *Rates of superluminous supernovae at $z \sim 0.2$* , *Mon. Not. R. Astron. Soc.* **431** (2013) 912 [1302.0911].
- [174] L.-D. Liu, B. Zhang, L.-J. Wang and Z.-G. Dai, *Photospheric Radius Evolution of Homologous Explosions*, *Astrophys. J.* **868** (2018) L24 [1809.05048].
- [175] R. W. Klebesadel, I. B. Strong and R. A. Olson, *Observations of Gamma-Ray Bursts of Cosmic Origin*, *Astrophys. J. Lett.* **182** (1973) L85.
- [176] C. A. Meegan, G. J. Fishman, R. B. Wilson, W. S. Paciesas, G. N. Pendleton, J. M. Horack et al., *Spatial distribution of gamma-ray bursts observed by BATSE*, *Nature* **355** (1992) 143.
- [177] E. Costa, F. Frontera, J. Heise, M. Feroci, J. in't Zand, F. Fiore et al., *Discovery of an X-ray afterglow associated with the γ -ray burst of 28 February 1997*, *Nature* **387** (1997) 783 [astro-ph/9706065].
- [178] S. R. Kulkarni, S. G. Djorgovski, A. N. Ramaparakash, R. Goodrich, J. S. Bloom, K. L. Adelberger et al., *Identification of a host galaxy at redshift $z = 3.42$ for the γ -ray burst of 14 December 1997*, *Nature* **393** (1998) 35.
- [179] N. Gehrels, G. Chincarini, P. Giommi, K. O. Mason, J. A. Nousek, A. A. Wells et al., *The Swift Gamma-Ray Burst Mission*, *Astrophys. J.* **611** (2004) 1005 [astro-ph/0405233].
- [180] W. B. Atwood, A. A. Abdo, M. Ackermann, W. Althouse, B. Anderson, M. Axelsson et al., *The Large Area Telescope on the Fermi Gamma-Ray Space Telescope Mission*, *Astrophys. J.* **697** (2009) 1071 [0902.1089].
- [181] C. Meegan, G. Lichti, P. N. Bhat, E. Bissaldi, M. S. Briggs, V. Connaughton et al., *The Fermi Gamma-ray Burst Monitor*, *Astrophys. J.* **702** (2009) 791 [0908.0450].
- [182] T. Piran, *The physics of gamma-ray bursts*, *Reviews of Modern Physics* **76** (2004) 1143 [astro-ph/0405503].
- [183] T. Piran, *Gamma-ray bursts and the fireball model*, *Phys. Rep.* **314** (1999) 575 [astro-ph/9810256].
- [184] E. Berger, *Short-Duration Gamma-Ray Bursts*, *Ann. Rev. Astron. Astrophys.* **52** (2014) 43 [1311.2603].
- [185] C. Kouveliotou, C. A. Meegan, G. J. Fishman, N. P. Bhat, M. S. Briggs, T. M. Koshut et al., *Identification of two classes of gamma-ray bursts*, *Astrophys. J. Lett.* **413** (1993) L101.
- [186] S. Savaglio, K. Glazebrook and D. Le Borgne, *The Galaxy Population Hosting Gamma-Ray Bursts*, *Astrophys. J.* **691** (2009) 182 [0803.2718].
- [187] T. J. Galama, P. M. Vreeswijk, J. van Paradijs, C. Kouveliotou, T. Augusteijn, H. Bönhardt et al., *An unusual supernova in the error box of the γ -ray burst of 25 April 1998*, *Nature* **395** (1998) 670 [astro-ph/9806175].
- [188] J. S. Bloom, S. R. Kulkarni, S. G. Djorgovski, A. C. Eichelberger, P. Côté, J. P. Blakeslee et al., *The unusual afterglow of the γ -ray burst of 26 March 1998 as evidence for a supernova connection*, *Nature* **401** (1999) 453 [astro-ph/9905301].
- [189] S. Nagataki, *Theories of central engine for long gamma-ray bursts*, *Reports on Progress in Physics* **81** (2018) 026901.
- [190] P. Jakobsson, A. Levan, J. P. U. Fynbo, R. Priddey, J. Hjorth, N. Tanvir et al., *A mean redshift of 2.8 for Swift gamma-ray bursts*, *Astron. Astrophys.* **447** (2006) 897 [astro-ph/0509888].
- [191] A. Cucchiara, A. J. Levan, D. B. Fox, N. R. Tanvir, T. N. Ukwatta, E. Berger et al., *A Photometric Redshift of $z \sim 9.4$ for GRB 090429B*, *Astrophys. J.* **736** (2011) 7 [1105.4915].
- [192] D. Wanderman and T. Piran, *The luminosity function and the rate of Swift's gamma-ray bursts*, *Mon. Not. R. Astron. Soc.* **406** (2010) 1944 [0912.0709].
- [193] E. Berger, P. A. Price, S. B. Cenko, A. Gal-Yam, A. M. Soderberg, M. Kasliwal et al., *The afterglow and*

- elliptical host galaxy of the short γ -ray burst GRB 050724, *Nature* **438** (2005) 988 [[astro-ph/0508115](#)].
- [194] D. B. Fox, D. A. Frail, P. A. Price, S. R. Kulkarni, E. Berger, T. Piran et al., *The afterglow of GRB 050709 and the nature of the short-hard γ -ray bursts*, *Nature* **437** (2005) 845 [[astro-ph/0510110](#)].
- [195] D. Wanderman and T. Piran, *The rate, luminosity function and time delay of non-Collapsar short GRBs*, *Mon. Not. R. Astron. Soc.* **448** (2015) 3026 [[1405.5878](#)].
- [196] F. Y. Wang, Z. G. Dai and E. W. Liang, *Gamma-ray burst cosmology*, *New Astron. Rev.* **67** (2015) 1 [[1504.00735](#)].
- [197] E. E. Fenimore and E. Ramirez-Ruiz, *Redshifts For 220 BATSE Gamma-Ray Bursts Determined by Variability and the Cosmological Consequences*, *arXiv Astrophysics e-prints* (2000) [[astro-ph/0004176](#)].
- [198] L. Amati, F. Frontera, M. Tavani, J. J. M. in't Zand, A. Antonelli, E. Costa et al., *Intrinsic spectra and energetics of BeppoSAX Gamma-Ray Bursts with known redshifts*, *Astron. Astrophys.* **390** (2002) 81 [[astro-ph/0205230](#)].
- [199] D. Yonetoku, T. Murakami, T. Nakamura, R. Yamazaki, A. K. Inoue and K. Ioka, *Gamma-Ray Burst Formation Rate Inferred from the Spectral Peak Energy-Peak Luminosity Relation*, *Astrophys. J.* **609** (2004) 935 [[astro-ph/0309217](#)].
- [200] G. Ghirlanda, G. Ghisellini and D. Lazzati, *The Collimation-corrected Gamma-Ray Burst Energies Correlate with the Peak Energy of Their νF_ν Spectrum*, *Astrophys. J.* **616** (2004) 331 [[astro-ph/0405602](#)].
- [201] A. Barnacka and A. Loeb, *A Size-duration Trend for Gamma-Ray Burst Progenitors*, *Astrophys. J.* **794** (2014) L8 [[1409.1232](#)].
- [202] V. Z. Golkhou, N. R. Butler and O. M. Littlejohns, *The Energy Dependence of GRB Minimum Variability Timescales*, *Astrophys. J.* **811** (2015) 93 [[1501.05948](#)].
- [203] A. Katz, J. Kopp, S. Sibiryakov and W. Xue, *Femtolensing by dark matter revisited*, *Journal of Cosmology and Astro-Particle Physics* **2018** (2018) 005 [[1807.11495](#)].
- [204] E. Petroff, J. W. T. Hessels and D. R. Lorimer, *Fast radio bursts*, *Astron. Astrophys. Rev.* **27** (2019) 4 [[1904.07947](#)].
- [205] J. M. Cordes and S. Chatterjee, *Fast Radio Bursts: An Extragalactic Enigma*, *arXiv e-prints* (2019) arXiv:1906.05878 [[1906.05878](#)].
- [206] D. R. Lorimer, M. Bailes, M. A. McLaughlin, D. J. Narkevic and F. Crawford, *A Bright Millisecond Radio Burst of Extragalactic Origin*, *Science* **318** (2007) 777 [[0709.4301](#)].
- [207] D. Thornton, B. Stappers, M. Bailes, B. Barsdell, S. Bates, N. D. R. Bhat et al., *A Population of Fast Radio Bursts at Cosmological Distances*, *Science* **341** (2013) 53 [[1307.1628](#)].
- [208] CHIME/FRB Collaboration, M. Amiri, K. Bandura, P. Berger, M. Bhardwaj, M. M. Boyce et al., *The CHIME Fast Radio Burst Project: System Overview*, *Astrophys. J.* **863** (2018) 48 [[1803.11235](#)].
- [209] A. W. Hotan, J. D. Bunton, L. Harvey-Smith, B. Humphreys, B. D. Jeffs, T. Shimwell et al., *The Australian Square Kilometre Array Pathfinder: System Architecture and Specifications of the Boolardy Engineering Test Array*, *Publ. Astron. Soc. Aust.* **31** (2014) e041 [[1409.1325](#)].
- [210] R. M. Shannon, J. P. Macquart, K. W. Bannister, R. D. Ekers, C. W. James, S. Osłowski et al., *The dispersion-brightness relation for fast radio bursts from a wide-field survey*, *Nature* **562** (2018) 386.
- [211] CHIME/FRB Collaboration, M. Amiri, K. Bandura, M. Bhardwaj, P. Boubel, M. M. Boyce et al., *Observations of fast radio bursts at frequencies down to 400 megahertz*, *Nature* **566** (2019) 230 [[1901.04524](#)].
- [212] L. G. Spitler, J. M. Cordes, J. W. T. Hessels, D. R. Lorimer, M. A. McLaughlin, S. Chatterjee et al., *Fast Radio Burst Discovered in the Arecibo Pulsar ALFA Survey*, *Astrophys. J.* **790** (2014) 101 [[1404.2934](#)].
- [213] L. G. Spitler, P. Scholz, J. W. T. Hessels, S. Bogdanov, A. Brazier, F. Camilo et al., *A repeating fast radio burst*, *Nature* **531** (2016) 202 [[1603.00581](#)].
- [214] CHIME/FRB Collaboration, M. Amiri, K. Bandura, M. Bhardwaj, P. Boubel, M. M. Boyce et al., *A second source of repeating fast radio bursts*, *Nature* **566** (2019) 235 [[1901.04525](#)].
- [215] The CHIME/FRB Collaboration, :, B. C. Andersen, K. Bandura, M. Bhardwaj, P. Boubel et al., *CHIME/FRB Detection of Eight New Repeating Fast Radio Burst Sources*, *arXiv e-prints* (2019) arXiv:1908.03507 [[1908.03507](#)].
- [216] S. P. Tendulkar, C. G. Bassa, J. M. Cordes, G. C. Bower, C. J. Law, S. Chatterjee et al., *The Host Galaxy and Redshift of the Repeating Fast Radio Burst FRB 121102*, *Astrophys. J. Lett.* **834** (2017) L7 [[1701.01100](#)].
- [217] K. W. Bannister, A. T. Deller, C. Phillips, J. P. Macquart, J. X. Prochaska, N. Tejos et al., *A single fast radio burst localized to a massive galaxy at cosmological distance*, *arXiv e-prints* (2019) arXiv:1906.11476 [[1906.11476](#)].
- [218] V. Ravi, M. Catha, L. D'Addario, S. G. Djorgovski, G. Hallinan, R. Hobbs et al., *A fast radio burst localised to a massive galaxy*, *arXiv e-prints* (2019) arXiv:1907.01542 [[1907.01542](#)].
- [219] W. Lu and A. L. Piro, *Implications from ASKAP Fast Radio Burst Statistics*, *arXiv e-prints* (2019) arXiv:1903.00014 [[1903.00014](#)].
- [220] V. Ravi, *The prevalence of repeating fast radio bursts*, *arXiv e-prints* (2019) arXiv:1907.06619 [[1907.06619](#)].
- [221] B. Marcote, Z. Paragi, J. W. T. Hessels, A. Keimpema, H. J. van Langevelde, Y. Huang et al., *The Repeating Fast Radio Burst FRB 121102 as Seen on Milliarcsecond Angular Scales*, *Astrophys. J.* **834** (2017) L8 [[1701.01099](#)].
- [222] B. P. Abbott, R. Abbott, T. D. Abbott, M. R. Abernathy, F. Acernese, K. Ackley et al., *Observation of Gravitational Waves from a Binary Black Hole Merger*, *Phys. Rev. Lett.* **116** (2016) 061102 [[1602.03837](#)].
- [223] LIGO Scientific Collaboration, J. Aasi, B. P. Abbott, R. Abbott, T. Abbott, M. R. Abernathy et al., *Advanced LIGO*, *Classical and Quantum Gravity* **32** (2015) 074001 [[1411.4547](#)].
- [224] M. Maggiore, *Gravitational Waves: Volume 1: Theory and Experiments*. 2008, [10.1093/acprof:oso/9780198570745.001.0001](#).
- [225] M. Maggiore, *Gravitational Waves: Volume 2: Astrophysics and Cosmology*. 2018, [10.1093/oso/9780198570899.001.0001](#).
- [226] The LIGO Scientific Collaboration, the Virgo Collaboration, B. P. Abbott, R. Abbott, T. D. Abbott, S. Abraham et al., *GWTC-1: A Gravitational-Wave Transient Catalog of Compact Binary Mergers Observed by LIGO and Virgo during the First and Second Observing Runs*, *arXiv e-prints* (2018) [[1811.12907](#)].
- [227] B. P. Abbott, R. Abbott, T. D. Abbott, F. Acernese, K. Ackley, C. Adams et al., *GW170817: Observation of Gravitational Waves from a Binary Neutron Star*

- Inspiral*, *Phys. Rev. Lett.* **119** (2017) 161101 [1710.05832].
- [228] B. P. Abbott, R. Abbott, T. D. Abbott, F. Acernese, K. Ackley, C. Adams et al., *GW170814: A Three-Detector Observation of Gravitational Waves from a Binary Black Hole Coalescence*, *Phys. Rev. Lett.* **119** (2017) 141101 [1709.09660].
- [229] F. Acernese, M. Agathos, K. Agatsuma, D. Aisa, N. Allemandou, A. Allocca et al., *Advanced Virgo: a second-generation interferometric gravitational wave detector*, *Classical and Quantum Gravity* **32** (2015) 024001 [1408.3978].
- [230] Y. Aso, Y. Michimura, K. Somiya, M. Ando, O. Miyakawa, T. Sekiguchi et al., *Interferometer design of the KAGRA gravitational wave detector*, *Phys. Rev. D* **88** (2013) 043007 [1306.6747].
- [231] B. P. Abbott, R. Abbott, T. D. Abbott, F. Acernese, K. Ackley, C. Adams et al., *Gravitational Waves and Gamma-Rays from a Binary Neutron Star Merger: GW170817 and GRB 170817A*, *Astrophys. J. Lett.* **848** (2017) L13 [1710.05834].
- [232] B. P. Abbott, R. Abbott, T. D. Abbott, F. Acernese, K. Ackley, C. Adams et al., *Multi-messenger Observations of a Binary Neutron Star Merger*, *Astrophys. J. Lett.* **848** (2017) L12 [1710.05833].
- [233] B. F. Schutz, *Determining the Hubble constant from gravitational wave observations*, *Nature* **323** (1986) 310.
- [234] B. P. Abbott, R. Abbott, T. D. Abbott, F. Acernese, K. Ackley, C. Adams et al., *A gravitational-wave standard siren measurement of the Hubble constant*, *Nature* **551** (2017) 85 [1710.05835].
- [235] T. Kinugawa, A. Miyamoto, N. Kanda and T. Nakamura, *The detection rate of inspiral and quasi-normal modes of Population III binary black holes which can confirm or refute the general relativity in the strong gravity region*, *Mon. Not. R. Astron. Soc.* **456** (2016) 1093 [1505.06962].
- [236] K. Belczynski, T. Ryu, R. Perna, E. Berti, T. L. Tanaka and T. Bulik, *On the likelihood of detecting gravitational waves from Population III compact object binaries*, *Mon. Not. R. Astron. Soc.* **471** (2017) 4702 [1612.01524].
- [237] G. Chartas, C. Rhea, C. Kochanek, X. Dai, C. Morgan, J. Blackburne et al., *Gravitational lensing size scales for quasars*, *Astronomische Nachrichten* **337** (2016) 356 [1509.05375].
- [238] LSST Science Collaboration, P. A. Abell, J. Allison, S. F. Anderson, J. R. Andrew, J. R. P. Angel et al., *LSST Science Book, Version 2.0*, *arXiv e-prints* (2009) arXiv:0912.0201 [0912.0201].
- [239] E. V. Linder, *Lensing time delays and cosmological complementarity*, *Phys. Rev. D* **84** (2011) 123529 [1109.2592].
- [240] M. Tewes, F. Courbin, G. Meylan, C. S. Kochanek, E. Eulaers, N. Cantale et al., *COSMOGRAIL: the COSmological MONitoring of GRAvitational Lenses. XIII. Time delays and 9-yr optical monitoring of the lensed quasar RX J1131-1231*, *Astron. Astrophys.* **556** (2013) A22 [1208.6009].
- [241] E. Eulaers, M. Tewes, P. Magain, F. Courbin, I. Asfandiyarov, S. Ehgamberdiev et al., *COSMOGRAIL: the COSmological MONitoring of GRAvitational Lenses. XII. Time delays of the doubly lensed quasars SDSS J1206+4332 and HS 2209+1914*, *Astron. Astrophys.* **553** (2013) A121 [1304.4474].
- [242] V. Bonvin, J. H. H. Chan, M. Millon, K. Rojas, F. Courbin, G. C. F. Chen et al., *COSMOGRAIL. XVII. Time delays for the quadruply imaged quasar PG 1115+080*, *Astron. Astrophys.* **616** (2018) A183 [1804.09183].
- [243] K. Liao, X.-L. Fan, X. Ding, M. Biesiada and Z.-H. Zhu, *Precision cosmology from future lensed gravitational wave and electromagnetic signals*, *Nature Communications* **8** (2017) 1148 [1703.04151].
- [244] J.-J. Wei and X.-F. Wu, *Strongly lensed gravitational waves and electromagnetic signals as powerful cosmic rulers*, *Mon. Not. R. Astron. Soc.* **472** (2017) 2906 [1707.04152].
- [245] Y. Li, X. Fan and L. Gou, *Constraining Cosmological Parameters in the FLRW Metric with Lensed GW+EM Signals*, *Astrophys. J.* **873** (2019) 37 [1901.10638].
- [246] B. Liu, Z. Li and Z.-H. Zhu, *Complementary constraints on dark energy equation of state from strongly lensed gravitational wave*, *Mon. Not. R. Astron. Soc.* (2019) 1176 [1904.11751].
- [247] E. Mörtzell and C. Sunesson, *Strong lensing, cosmology and lensing halos*, *Journal of Cosmology and Astro-Particle Physics* **2006** (2006) 012 [astro-ph/0510120].
- [248] Z.-X. Li, H. Gao, X.-H. Ding, G.-J. Wang and B. Zhang, *Strongly lensed repeating fast radio bursts as precision probes of the universe*, *Nature Communications* **9** (2018) 3833 [1708.06357].
- [249] A. Zitrin and D. Eichler, *Observing Cosmological Processes in Real Time with Repeating Fast Radio Bursts*, *Astrophys. J.* **866** (2018) 101 [1807.03287].
- [250] D. E. Holz, *Seeing Double: Strong Gravitational Lensing of High-Redshift Supernovae*, *Astrophys. J.* **556** (2001) L71 [astro-ph/0104440].
- [251] S. Huber, S. H. Suyu, U. M. Noebauer, V. Bonvin, D. Rothchild, J. H. H. Chan et al., *Strongly lensed SNe Ia in the era of LSST: observing cadence for lens discoveries and time-delay measurements*, *arXiv e-prints* (2019) arXiv:1903.00510 [1903.00510].
- [252] G. Dobler and C. R. Keeton, *Microlensing of Lensed Supernovae*, *Astrophys. J.* **653** (2006) 1391 [astro-ph/0608391].
- [253] D. A. Goldstein, P. E. Nugent, D. N. Kasen and T. E. Collett, *Precise Time Delays from Strongly Gravitationally Lensed Type Ia Supernovae with Chromatically Microlensed Images*, *Astrophys. J.* **855** (2018) 22 [1708.00003].
- [254] V. Bonvin, O. Tihhonova, M. Millon, J. H. H. Chan, E. Savary, S. Huber et al., *Impact of the 3D source geometry on time-delay measurements of lensed type-Ia supernovae*, *Astron. Astrophys.* **621** (2019) A55 [1805.04525].
- [255] J. D. R. Pierel and S. Rodney, *Turning Gravitationally Lensed Supernovae into Cosmological Probes*, *Astrophys. J.* **876** (2019) 107 [1902.01260].
- [256] K. Liao, *Hubble Constant from LSST Strong-lens Time Delays with Microlensing Systematics*, *Astrophys. J.* **871** (2019) 113.
- [257] J. M. Diego, *The Universe at extreme magnification*, *Astron. Astrophys.* **625** (2019) A84 [1806.04668].
- [258] J. M. Diego, O. A. Hannuksela, P. L. Kelly, G. Pagano, T. Broadhurst, K. Kim et al., *Observational signatures of microlensing in gravitational waves at LIGO/Virgo frequencies*, *Astron. Astrophys.* **627** (2019) A130 [1903.04513].
- [259] A. K. Meena and J. S. Bagla, *Gravitational lensing of gravitational waves: wave nature and prospects for detection*, *arXiv e-prints* (2019) arXiv:1903.11809 [1903.11809].
- [260] A. Yıldırım, S. H. Suyu and A. Halkola, *Next generation cosmography with strong lensing and stellar dynamics*, *arXiv e-prints* (2019) arXiv:1904.07237 [1904.07237].
- [261] S. Birrer and T. Treu, *Astrometric requirements for*

- strong lensing time-delay cosmography, *arXiv e-prints* (2019) arXiv:1904.10965 [[1904.10965](#)].
- [262] M. Oguri and Y. Kawano, *Gravitational lens time delays for distant supernovae: breaking the degeneracy between radial mass profiles and the Hubble constant*, *Mon. Not. R. Astron. Soc.* **338** (2003) L25 [[astro-ph/0211499](#)].
- [263] A. S. Bolton and S. Burles, *Prospects for the Determination of H_0 through Observation of Multiply Imaged Supernovae in Galaxy Cluster Fields*, *Astrophys. J.* **592** (2003) 17 [[astro-ph/0212181](#)].
- [264] T. Riehm, E. Mörtzell, A. Goobar, R. Amanullah, T. Dahlén, J. Jönsson et al., *Near-IR search for lensed supernovae behind galaxy clusters. III. Implications for cluster modeling and cosmology*, *Astron. Astrophys.* **536** (2011) A94 [[1109.6351](#)].
- [265] A. Zitrin, M. Redlich and T. Broadhurst, *Consistent Use of Type Ia Supernovae Highly Magnified by Galaxy Clusters to Constrain the Cosmological Parameters*, *Astrophys. J.* **789** (2014) 51 [[1311.5224](#)].
- [266] X. Wen and K. Liao, *Calibrating the standard candles with strong lensing*, *arXiv e-prints* (2019) arXiv:1907.02693 [[1907.02693](#)].
- [267] M. Foxley-Marrable, T. E. Collett, G. Vernardos, D. A. Goldstein and D. Bacon, *The impact of microlensing on the standardization of strongly lensed Type Ia supernovae*, *Mon. Not. R. Astron. Soc.* **478** (2018) 5081 [[1802.07738](#)].
- [268] M. J. Longo, *New precision tests of the Einstein equivalence principle from SN1987A*, *Phys. Rev. Lett.* **60** (1988) 173.
- [269] A. A. Abdo, M. Ackermann, M. Ajello, K. Asano, W. B. Atwood, M. Axelsson et al., *A limit on the variation of the speed of light arising from quantum gravity effects*, *Nature* **462** (2009) 331 [[0908.1832](#)].
- [270] L. Lombriser and A. Taylor, *Breaking a dark degeneracy with gravitational waves*, *J. Cosmol. Astropart. Phys.* **2016** (2016) 031 [[1509.08458](#)].
- [271] L. M. Krauss and S. Tremaine, *Test of the weak equivalence principle for neutrinos and photons*, *Phys. Rev. Lett.* **60** (1988) 176.
- [272] J.-J. Wei, H. Gao, X.-F. Wu and P. Mészáros, *Testing Einstein's Equivalence Principle With Fast Radio Bursts*, *Phys. Rev. Lett.* **115** (2015) 261101 [[1512.07670](#)].
- [273] M. Biesiada and A. Piórkowska, *Gravitational lensing time delays as a tool for testing Lorentz-invariance violation*, *Mon. Not. R. Astron. Soc.* **396** (2009) 946 [[0712.0941](#)].
- [274] T. E. Collett and D. Bacon, *Testing the Speed of Gravitational Waves over Cosmological Distances with Strong Gravitational Lensing*, *Phys. Rev. Lett.* **118** (2017) 091101 [[1602.05882](#)].
- [275] X.-L. Fan, K. Liao, M. Biesiada, A. Piórkowska-Kurpas and Z.-H. Zhu, *Speed of Gravitational Waves from Strongly Lensed Gravitational Waves and Electromagnetic Signals*, *Phys. Rev. Lett.* **118** (2017) 091102 [[1612.04095](#)].
- [276] T. Baker and M. Trodden, *Multimessenger time delays from lensed gravitational waves*, *Phys. Rev. D* **95** (2017) 063512 [[1612.02004](#)].
- [277] H. Yu and F. Y. Wang, *Testing weak equivalence principle with strongly lensed cosmic transients*, *European Physical Journal C* **78** (2018) 692 [[1801.01257](#)].
- [278] R. Takahashi, *Arrival Time Differences between Gravitational Waves and Electromagnetic Signals due to Gravitational Lensing*, *Astrophys. J.* **835** (2017) 103 [[1606.00458](#)].
- [279] S. Cao, J. Qi, M. Biesiada, X. Zheng, T. Xu and Z.-H. Zhu, *Testing the Speed of Light over Cosmological Distances: The Combination of Strongly Lensed and Unlensed Type Ia Supernovae*, *Astrophys. J.* **867** (2018) 50 [[1810.01287](#)].
- [280] M. Sasaki, T. Suyama, T. Tanaka and S. Yokoyama, *Primordial black holes—perspectives in gravitational wave astronomy*, *Classical and Quantum Gravity* **35** (2018) 063001 [[1801.05235](#)].
- [281] B. Paczynski, *Gravitational Microlensing and Gamma-Ray Bursts*, *Astrophys. J.* **317** (1987) L51.
- [282] O. M. Blaes and R. L. Webster, *Using Gamma-Ray Bursts to Detect a Cosmological Density of Compact Objects*, *Astrophys. J.* **391** (1992) L63.
- [283] S. Mao, *Gravitational Lensing, Time Delay, and Gamma-Ray Bursts*, *Astrophys. J.* **389** (1992) L41.
- [284] S. Mao, *Gravitational microlensing of gamma-ray bursts*, *Astrophys. J.* **402** (1993) 382.
- [285] R. J. Nemiroff and A. Gould, *Probing for MACHOs of Mass 10 -15 M_{sun} to 10 -7 M_{sun} with Gamma-Ray Burst Parallax Spacecraft*, *Astrophys. J.* **452** (1995) L111 [[astro-ph/9505019](#)].
- [286] A. Loeb and R. Perna, *Microlensing of Gamma-Ray Burst Afterglows*, *Astrophys. J.* **495** (1998) 597 [[astro-ph/9708159](#)].
- [287] G. F. Marani, R. J. Nemiroff, J. P. Norris, K. Hurley and J. T. Bonnell, *Gravitationally Lensed Gamma-Ray Bursts as Probes of Dark Compact Objects*, *Astrophys. J.* **512** (1999) L13 [[astro-ph/9810391](#)].
- [288] J. S. B. Wyithe and E. L. Turner, *Gravitational microlensing of gamma-ray bursts at medium optical depth*, *Mon. Not. R. Astron. Soc.* **319** (2000) 1163 [[astro-ph/0008009](#)].
- [289] L. V. E. Koopmans and J. Wambsganss, *On the probability of microlensing in gamma-ray burst afterglows*, *Mon. Not. R. Astron. Soc.* **325** (2001) 1317 [[astro-ph/0011029](#)].
- [290] E. A. Baltz and L. Hui, *Microlensing of Gamma-Ray Bursts by Stars and MACHOs*, *Astrophys. J.* **618** (2005) 403 [[astro-ph/0311569](#)].
- [291] L. Ji, E. D. Kovetz and M. Kamionkowski, *Strong lensing of gamma ray bursts as a probe of compact dark matter*, *Phys. Rev. D* **98** (2018) 123523 [[1809.09627](#)].
- [292] K. Z. Stanek, B. Paczynski and J. Goodman, *Features in the spectra of gamma-ray bursts*, *Astrophys. J. Lett.* **413** (1993) L7.
- [293] A. Ulmer and J. Goodman, *Femtolensing: Beyond the Semiclassical Approximation*, *Astrophys. J.* **442** (1995) 67 [[astro-ph/9406042](#)].
- [294] A. Barnacka, J. F. Glicenstein and R. Moderski, *New constraints on primordial black holes abundance from femtolensing of gamma-ray bursts*, *Phys. Rev. D* **86** (2012) 043001 [[1204.2056](#)].
- [295] J. B. Muñoz, E. D. Kovetz, L. Dai and M. Kamionkowski, *Lensing of Fast Radio Bursts as a Probe of Compact Dark Matter*, *Phys. Rev. Lett.* **117** (2016) 091301 [[1605.00008](#)].
- [296] Y. K. Wang and F. Y. Wang, *Lensing of fast radio bursts by binaries to probe compact dark matter*, *Astron. Astrophys.* **614** (2018) A50 [[1801.07360](#)].
- [297] R. Laha, *Lensing of fast radio bursts: future constraints on primordial black hole density with an extended mass function and a new probe of exotic compact fermion/ boson stars*, *arXiv e-prints* (2018) arXiv:1812.11810 [[1812.11810](#)].
- [298] Z. Zheng, E. O. Ofek, S. R. Kulkarni, J. D. Neill and M. Juric, *Probing the Intergalactic Medium with Fast Radio Bursts*, *Astrophys. J.* **797** (2014) 71 [[1409.3244](#)].
- [299] K.-H. Lai, O. A. Hannuksela, A. Herrera-Martín, J. M. Diego, T. Broadhurst and T. G. F. Li, *Discovering*

- intermediate-mass black hole lenses through gravitational wave lensing, *Phys. Rev. D* **98** (2018) 083005 [1801.07840].
- [300] P. Christian, S. Vitale and A. Loeb, *Detecting stellar lensing of gravitational waves with ground-based observatories*, *Phys. Rev. D* **98** (2018) 103022 [1802.02586].
- [301] S. Jung and C. S. Shin, *Gravitational-Wave Fringes at LIGO: Detecting Compact Dark Matter by Gravitational Lensing*, *Phys. Rev. Lett.* **122** (2019) 041103 [1712.01396].
- [302] K. Liao, M. Biesiada and X.-L. Fan, *The Wave Nature of Continuous Gravitational Waves from Microlensing*, *Astrophys. J.* **875** (2019) 139 [1903.06612].
- [303] Z. Hongsheng and F. Xilong, *Poisson-Arago spot for gravitational waves*, *arXiv e-prints* (2018) arXiv:1809.06511 [1809.06511].
- [304] M. Zumalacárregui and U. Seljak, *Limits on Stellar-Mass Compact Objects as Dark Matter from Gravitational Lensing of Type Ia Supernovae*, *Phys. Rev. Lett.* **121** (2018) 141101 [1712.02240].
- [305] D. Eichler, *Nanolensed Fast Radio Bursts*, *Astrophys. J.* **850** (2017) 159 [1711.04764].
- [306] J. Wagner, J. Liesenborgs and D. Eichler, *Multiply imaged time-varying sources behind galaxy clusters. Comparing fast radio bursts to QSOs, SNe, and GRBs*, *Astron. Astrophys.* **621** (2019) A91 [1811.10618].
- [307] T. S. Kolatt and M. Bartelmann, *Gravitational lensing of type Ia supernovae by galaxy clusters*, *Mon. Not. R. Astron. Soc.* **296** (1998) 763 [astro-ph/9708120].
- [308] J. Nordin, D. Rubin, J. Richard, E. Rykoff, G. Aldering, R. Amanullah et al., *Lensed Type Ia supernovae as probes of cluster mass models*, *Mon. Not. R. Astron. Soc.* **440** (2014) 2742 [1312.2576].
- [309] B. Patel, C. McCully, S. W. Jha, S. A. Rodney, D. O. Jones, O. Graur et al., *Three Gravitationally Lensed Supernovae behind CLASH Galaxy Clusters*, *Astrophys. J.* **786** (2014) 9 [1312.0943].
- [310] S. A. Rodney, B. Patel, D. Scolnic, R. J. Foley, A. Molino, G. Brammer et al., *Illuminating a Dark Lens : A Type Ia Supernova Magnified by the Frontier Fields Galaxy Cluster Abell 2744*, *Astrophys. J.* **811** (2015) 70 [1505.06211].
- [311] K. Liao, X. Ding, M. Biesiada, X.-L. Fan and Z.-H. Zhu, *Anomalies in Time Delays of Lensed Gravitational Waves and Dark Matter Substructures*, *Astrophys. J.* **867** (2018) 69 [1809.07079].
- [312] L. Dai, S.-S. Li, B. Zackay, S. Mao and Y. Lu, *Detecting lensing-induced diffraction in astrophysical gravitational waves*, *Phys. Rev. D* **98** (2018) 104029 [1810.00003].
- [313] D. E. Holz, M. C. Miller and J. M. Quashnock, *Gravitational Lensing Limits on the Average Redshift of Gamma-Ray Bursts*, *Astrophys. J.* **510** (1999) 54 [astro-ph/9804271].
- [314] C. Li and L. Li, *Constraining fast radio burst progenitors with gravitational lensing*, *Science China Physics, Mechanics, and Astronomy* **57** (2014) 1390 [1403.7873].
- [315] G. Aldering, A. G. Kim, M. Kowalski, E. V. Linder and S. Perlmutter, *Snapping supernovae at $z \lesssim 1.7$* , *Astroparticle Physics* **27** (2007) 213 [astro-ph/0607030].
- [316] C.-E. Rydberg, D. J. Whalen, M. Maturi, T. Collett, M. Carrasco, M. Magg et al., *Detecting strongly lensed supernovae at $z \sim 5-7$ with LSST*, *arXiv e-prints* (2018) arXiv:1805.02662 [1805.02662].
- [317] T. Pan and A. Loeb, *Finding core-collapse supernovae from the epoch of reionization behind cluster lenses.*, *Mon. Not. R. Astron. Soc.* **435** (2013) L33 [1303.6960].
- [318] D. J. Whalen, J. Smidt, C.-E. Rydberg, J. L. Johnson, D. E. Holz and M. Stiavelli, *Detecting Ancient Supernovae at $z \sim 5-12$ with CLASH*, *arXiv e-prints* (2013) arXiv:1312.6330 [1312.6330].
- [319] T. Petrushevska, R. Amanullah, A. Goobar, S. Fabbro, J. Johansson, T. Kjellsson et al., *High-redshift supernova rates measured with the gravitational telescope A 1689*, *Astron. Astrophys.* **594** (2016) A54 [1607.01617].
- [320] T. Petrushevska, T. Okamura, R. Kawamata, L. Hangard, G. Mahler and A. Goobar, *Prospects for Strongly Lensed Supernovae Behind Hubble Frontier Fields Galaxy Clusters with the James Webb Space Telescope*, *Astronomy Reports* **62** (2018) 917 [1901.02014].
- [321] T. J. Moriya, K. C. Wong, Y. Koyama, M. Tanaka, M. Oguri, S. Hilbert et al., *Searches for Population III pair-instability supernovae: Predictions for ULTIMATE-Subaru and WFIRST*, *Publ. Astron. Soc. Japan* **71** (2019) 59 [1903.01613].
- [322] K. C. Wong, T. J. Moriya, M. Oguri, S. Hilbert, Y. Koyama and K. Nomoto, *Searches for Population III pair-instability supernovae: Impact of gravitational lensing magnification*, *Publ. Astron. Soc. Japan* **71** (2019) 60 [1903.01614].
- [323] L. Dai, T. Venumadhav and K. Sigurdson, *Effect of lensing magnification on the apparent distribution of black hole mergers*, *Phys. Rev. D* **95** (2017) 044011 [1605.09398].
- [324] Y. Suwa, *Supernova forecast with strong lensing*, *Mon. Not. R. Astron. Soc.* **474** (2018) 2612 [1711.00183].
- [325] E. Babichev and V. Dokuchaev, *Gravitational lensing of relativistic fireball*, *Physics Letters A* **265** (2000) 168 [astro-ph/9912383].
- [326] B. S. Gaudi and A. Loeb, *Resolving the Image of Gamma-Ray Burst Afterglows with Gravitational Microlensing*, *Astrophys. J.* **558** (2001) 643 [astro-ph/0102003].
- [327] K. Ioka and T. Nakamura, *Microlensing of Collimated Gamma-Ray Burst Afterglows*, *Astrophys. J.* **561** (2001) 703 [astro-ph/0102028].
- [328] R. Perna and C. R. Keeton, *Gravitational lensing of anisotropic sources*, *Mon. Not. R. Astron. Soc.* **397** (2009) 1084 [0904.3935].
- [329] A. Barnacka, M. J. Geller, I. P. Dell'Antonio and W. Benbow, *Resolving the High-energy Universe with Strong Gravitational Lensing: The Case of PKS 1830-211*, *Astrophys. J.* **809** (2015) 100 [1504.05210].
- [330] A. Barnacka, M. J. Geller, I. P. Dell'Antonio and A. Zitrin, *The Structure of the Strongly Lensed Gamma-Ray Source B2 0218+35*, *Astrophys. J.* **821** (2016) 58 [1511.02891].
- [331] L. Dai and W. Lu, *Probing Motion of Fast Radio Burst Sources by Timing Strongly Lensed Repeaters*, *Astrophys. J.* **847** (2017) 19 [1706.06103].
- [332] Y. Wang, *Supernova Pencil Beam Survey*, *Astrophys. J.* **531** (2000) 676 [astro-ph/9806185].
- [333] A. Goobar, E. Mörtzell, R. Amanullah and P. Nugent, *Cosmological parameters from lensed supernovae*, *Astron. Astrophys.* **393** (2002) 25 [astro-ph/0207139].
- [334] A. Goobar, E. Mörtzell, R. Amanullah, M. Goliath, L. Bergström and T. Dahlén, *SNOC: A Monte-Carlo simulation package for high- z supernova observations*, *Astron. Astrophys.* **392** (2002) 757 [astro-ph/0206409].
- [335] Z. Kostrzewa-Rutkowska, L. Wyrzykowski and M. Jaroszyński, *On rates of supernovae strongly lensed by galactic haloes in Millennium Simulation*, *Mon.*

- Not. R. Astron. Soc.* **429** (2013) 2392 [1212.1063].
- [336] N. Kaiser, H. Aussel, B. E. Burke, H. Boesgaard, K. Chambers, M. R. Chun et al., *Pan-STARRS: A Large Synoptic Survey Telescope Array*, in *Survey and Other Telescope Technologies and Discoveries*, J. A. Tyson and S. Wolff, eds., vol. 4836 of *Society of Photo-Optical Instrumentation Engineers (SPIE) Conference Series*, pp. 154–164, Dec, 2002, DOI.
- [337] K. C. Chambers, E. A. Magnier, N. Metcalfe, H. A. Flewelling, M. E. Huber, C. Z. Waters et al., *The Pan-STARRS1 Surveys*, *arXiv e-prints* (2016) arXiv:1612.05560 [1612.05560].
- [338] Y. Shu, A. S. Bolton, S. Mao, X. Kang, G. Li and M. Soraism, *Prediction of Supernova Rates in Known Galaxy-Galaxy Strong-lens Systems*, *Astrophys. J.* **864** (2018) 91 [1803.07569].
- [339] M. Sullivan, R. Ellis, P. Nugent, I. Smail and P. Madau, *A strategy for finding gravitationally lensed distant supernovae*, *Mon. Not. R. Astron. Soc.* **319** (2000) 549 [astro-ph/0007228].
- [340] T. D. Saini, S. Raychaudhury and Y. A. Shchekinov, *Observing high-redshift supernovae in lensed galaxies*, *Astron. Astrophys.* **363** (2000) 349 [astro-ph/0002448].
- [341] V. Stanishev, A. Goobar, K. Paech, R. Amanullah, T. Dahlén, J. Jönsson et al., *Near-IR search for lensed supernovae behind galaxy clusters. I. Observations and transient detection efficiency*, *Astron. Astrophys.* **507** (2009) 61 [0908.4176].
- [342] T. Petrushevska, A. Goobar, D. J. Lagattuta, R. Amanullah, L. Hangard, S. Fabbro et al., *Searching for supernovae in the multiply-imaged galaxies behind the gravitational telescope A370*, *Astron. Astrophys.* **614** (2018) A103 [1802.10525].
- [343] A. Goobar, K. Paech, V. Stanishev, R. Amanullah, T. Dahlén, J. Jönsson et al., *Near-IR search for lensed supernovae behind galaxy clusters. II. First detection and future prospects*, *Astron. Astrophys.* **507** (2009) 71 [0810.4932].
- [344] R. Amanullah, A. Goobar, B. Clément, J. G. Cuby, H. Dahle, T. Dahlén et al., *A Highly Magnified Supernova at $z = 1.703$ behind the Massive Galaxy Cluster A1689*, *Astrophys. J.* **742** (2011) L7 [1109.4740].
- [345] D. Rubin, B. Hayden, X. Huang, G. Aldering, R. Amanullah, K. Barbary et al., *The Discovery of a Gravitationally Lensed Supernova Ia at Redshift 2.22*, *Astrophys. J.* **866** (2018) 65 [1707.04606].
- [346] E. Giraud, *A luminosity variation detected in a new pair of arclets in a cluster of galaxies at $Z = 0.424$* , *Astron. Astrophys.* **259** (1992) L49.
- [347] R. Chornock, E. Berger, A. Rest, D. Milisavljevic, R. Lunnan, R. J. Foley et al., *PS1-10afx at $z = 1.388$: Pan-STARRS1 Discovery of a New Type of Superluminous Supernova*, *Astrophys. J.* **767** (2013) 162 [1302.0009].
- [348] R. M. Quimby, M. C. Werner, M. Oguri, S. More, A. More, M. Tanaka et al., *Extraordinary Magnification of the Ordinary Type Ia Supernova PS1-10afx*, *Astrophys. J.* **768** (2013) L20 [1302.2785].
- [349] R. M. Quimby, M. Oguri, A. More, S. More, T. J. Moriya, M. C. Werner et al., *Detection of the Gravitational Lens Magnifying a Type Ia Supernova*, *Science* **344** (2014) 396 [1404.6014].
- [350] P. L. Kelly, S. A. Rodney, T. Treu, R. J. Foley, G. Brammer, K. B. Schmidt et al., *Multiple images of a highly magnified supernova formed by an early-type cluster galaxy lens*, *Science* **347** (2015) 1123 [1411.6009].
- [351] P. L. Kelly, S. A. Rodney, T. Treu, L. G. Strolger, R. J. Foley, S. W. Jha et al., *Deja Vu All Over Again: The Reappearance of Supernova Refsdal*, *Astrophys. J.* **819** (2016) L8 [1512.04654].
- [352] T. Treu, K. B. Schmidt, G. B. Brammer, B. Vulcani, X. Wang, M. Bradač et al., *The Grism Lens-Amplified Survey from Space (GLASS). I. Survey Overview and First Data Release*, *Astrophys. J.* **812** (2015) 114 [1509.00475].
- [353] M. Oguri, *Predicted properties of multiple images of the strongly lensed supernova SN Refsdal*, *Mon. Not. R. Astron. Soc.* **449** (2015) L86 [1411.6443].
- [354] K. Sharon and T. L. Johnson, *Revised Lens Model for the Multiply Imaged Lensed Supernova, “SN Refsdal” in MACS J1149+2223*, *Astrophys. J.* **800** (2015) L26 [1411.6933].
- [355] T. Treu, G. Brammer, J. M. Diego, C. Grillo, P. L. Kelly, M. Oguri et al., *“Refsdal” Meets Popper: Comparing Predictions of the Re-appearance of the Multiply Imaged Supernova Behind MACSJ1149.5+2223*, *Astrophys. J.* **817** (2016) 60 [1510.05750].
- [356] J. M. Diego, T. Broadhurst, C. Chen, J. Lim, A. Zitrin, B. Chan et al., *A free-form prediction for the reappearance of supernova Refsdal in the Hubble Frontier Fields cluster MACSJ1149.5+2223*, *Mon. Not. R. Astron. Soc.* **456** (2016) 356 [1504.05953].
- [357] R. Kawamata, M. Oguri, M. Ishigaki, K. Shimasaku and M. Ouchi, *Precise Strong Lensing Mass Modeling of Four Hubble Frontier Field Clusters and a Sample of Magnified High-redshift Galaxies*, *Astrophys. J.* **819** (2016) 114 [1510.06400].
- [358] M. Jauzac, J. Richard, M. Limousin, K. Knowles, G. Mahler, G. P. Smith et al., *Hubble Frontier Fields: predictions for the return of SN Refsdal with the MUSE and GMOS spectrographs*, *Mon. Not. R. Astron. Soc.* **457** (2016) 2029 [1509.08914].
- [359] C. Grillo, W. Karman, S. H. Suyu, P. Rosati, I. Balestra, A. Mercurio et al., *The Story of Supernova “Refsdal” Told by Muse*, *Astrophys. J.* **822** (2016) 78 [1511.04093].
- [360] S. H. Suyu and A. Halkola, *The halos of satellite galaxies: the companion of the massive elliptical lens SL2S J08544-0121*, *Astron. Astrophys.* **524** (2010) A94 [1007.4815].
- [361] S. H. Suyu, S. W. Hensel, J. P. McKean, C. D. Fassnacht, T. Treu, A. Halkola et al., *Disentangling Baryons and Dark Matter in the Spiral Gravitational Lens B1933+503*, *Astrophys. J.* **750** (2012) 10 [1110.2536].
- [362] M. Meneghetti, P. Natarajan, D. Coe, E. Contini, G. De Lucia, C. Giocoli et al., *The Frontier Fields lens modelling comparison project*, *Mon. Not. R. Astron. Soc.* **472** (2017) 3177 [1606.04548].
- [363] S. A. Rodney, L. G. Strolger, P. L. Kelly, M. Bradač, G. Brammer, A. V. Filippenko et al., *SN Refsdal: Photometry and Time Delay Measurements of the First Einstein Cross Supernova*, *Astrophys. J.* **820** (2016) 50 [1512.05734].
- [364] P. L. Kelly, G. Brammer, J. Selsing, R. J. Foley, J. Hjorth, S. A. Rodney et al., *SN Refsdal: Classification as a Luminous and Blue SN 1987A-like Type II Supernova*, *Astrophys. J.* **831** (2016) 205 [1512.09093].
- [365] J. Vega-Ferrero, J. M. Diego, V. Miranda and G. M. Bernstein, *The Hubble Constant from SN Refsdal*, *Astrophys. J.* **853** (2018) L31 [1712.05800].
- [366] C. Grillo, P. Rosati, S. H. Suyu, I. Balestra, G. B. Caminha, A. Halkola et al., *Measuring the Value of the Hubble Constant “à la Refsdal”*, *Astrophys. J.* **860** (2018) 94 [1802.01584].
- [367] L. L. R. Williams and J. Liesenborgs, *The role of multiple images and model priors in measuring H_0*

- from supernova Refsdal in galaxy cluster MACS J1149.5+2223, *Mon. Not. R. Astron. Soc.* **482** (2019) 5666 [1806.11113].
- [368] A. Goobar, R. Amanullah, S. R. Kulkarni, P. E. Nugent, J. Johansson, C. Steidel et al., *iPTF16geu: A multiply imaged, gravitationally lensed type Ia supernova*, *Science* **356** (2017) 291 [1611.00014].
- [369] S. R. Kulkarni, *The intermediate Palomar Transient Factory (iPTF) begins*, *The Astronomer's Telegram* **4807** (2013) 1.
- [370] A. More, S. H. Suyu, M. Oguri, S. More and C.-H. Lee, *Interpreting the Strongly Lensed Supernova iPTF16geu: Time Delay Predictions, Microlensing, and Lensing Rates*, *Astrophys. J.* **835** (2017) L25 [1611.04866].
- [371] D. A. Yahalomi, P. L. Schechter and J. Wambsganss, *A Quadruply Lensed SN Ia: Gaining a Time-Delay...Losing a Standard Candle*, *arXiv e-prints* (2017) arXiv:1711.07919 [1711.07919].
- [372] E. Mörtzell, J. Johansson, S. Dhawan, A. Goobar, R. Amanullah and D. A. Goldstein, *Lens modelling of the strongly lensed Type Ia supernova iPTF16geu*, *arXiv e-prints* (2019) arXiv:1907.06609 [1907.06609].
- [373] S. Dhawan, J. Johansson, A. Goobar, R. Amanullah, E. Mörtzell, S. B. Cenko et al., *Magnification, dust and time-delay constraints from the first resolved strongly lensed Type Ia supernova*, *arXiv e-prints* (2019) arXiv:1907.06756 [1907.06756].
- [374] D. A. Goldstein, P. E. Nugent and A. Goobar, *Rates and Properties of Supernovae Strongly Gravitationally Lensed by Elliptical Galaxies in Time-domain Imaging Surveys*, *Astrophys. J. Suppl.* **243** (2019) 6 [1809.10147].
- [375] D. A. Goldstein and P. E. Nugent, *How to Find Gravitationally Lensed Type Ia Supernovae*, *Astrophys. J.* **834** (2017) L5 [1611.09459].
- [376] C.-H. Lee, *Identifying Multiply Lensed Supernovae from Ellipticity*, *Research Notes of the American Astronomical Society* **2** (2018) 186.
- [377] R. Wojtak, J. Hjorth and C. Gall, *Magnified or multiply imaged? - Search strategies for gravitationally lensed supernovae in wide-field surveys*, *Mon. Not. R. Astron. Soc.* **487** (2019) 3342 [1903.07687].
- [378] C. Porciani and P. Madau, *On the Association of Gamma-Ray Bursts with Massive Stars: Implications for Number Counts and Lensing Statistics*, *Astrophys. J.* **548** (2001) 522 [astro-ph/0008294].
- [379] J. S. B. Wyithe, S. P. Oh and B. Pindor, *A possible gravitational lensing explanation for the excess of strong Mg II absorbers in gamma-ray burst afterglow spectra*, *Mon. Not. R. Astron. Soc.* **414** (2011) 209 [1004.2081].
- [380] R. J. Nemiroff, W. A. D. T. Wickramasinghe, J. P. Norris, C. Kouveliotou, G. J. Fishman, C. A. Meegan et al., *Null Result in Gamma-Ray Burst Lensed Echo Search*, *Astrophys. J.* **432** (1994) 478 [astro-ph/9403045].
- [381] C. Li and L. Li, *Search for strong gravitational lensing effect in the current GRB data of BATSE*, *Science China Physics, Mechanics, and Astronomy* **57** (2014) 1592 [1406.3102].
- [382] Y. Hirose, M. Umemura, A. Yonehara and J. Sato, *Imprint of Gravitational Lensing by Population III Stars in Gamma-Ray Burst Light Curves*, *Astrophys. J.* **650** (2006) 252 [astro-ph/0605548].
- [383] K. Hurley, A. E. Tsvetkova, D. S. Svinkin, R. L. Aptekar, D. D. Frederiks, S. V. Golenetskii et al., *A Search for Gravitationally Lensed Gamma-Ray Bursts in the Data of the Interplanetary Network and Konus-Wind*, *Astrophys. J.* **871** (2019) 121.
- [384] R. L. Aptekar, D. D. Frederiks, S. V. Golenetskii, V. N. Il'yinskii, E. P. Mazets, V. N. Panov et al., *Konus-W Gamma-Ray Burst Experiment for the GGS Wind Spacecraft*, *Space Sci. Rev.* **71** (1995) 265.
- [385] L. L. R. Williams and R. A. M. J. Wijers, *Distortion of gamma-ray burst light curves by gravitational microlensing*, *Mon. Not. R. Astron. Soc.* **286** (1997) L11 [astro-ph/9701246].
- [386] A. Piórkowska, M. Biesiada and Z.-H. Zhu, *Strong gravitational lensing of gravitational waves in Einstein Telescope*, *Journal of Cosmology and Astro-Particle Physics* **2013** (2013) 022 [1309.5731].
- [387] M. Biesiada, X. Ding, A. Piórkowska and Z.-H. Zhu, *Strong gravitational lensing of gravitational waves from double compact binaries—perspectives for the Einstein Telescope*, *Journal of Cosmology and Astro-Particle Physics* **2014** (2014) 080 [1409.8360].
- [388] X. Ding, M. Biesiada and Z.-H. Zhu, *Strongly lensed gravitational waves from intrinsically faint double compact binaries—prediction for the Einstein Telescope*, *Journal of Cosmology and Astro-Particle Physics* **2015** (2015) 006 [1508.05000].
- [389] S.-S. Li, S. Mao, Y. Zhao and Y. Lu, *Gravitational lensing of gravitational waves: a statistical perspective*, *Mon. Not. R. Astron. Soc.* **476** (2018) 2220 [1802.05089].
- [390] K. K. Y. Ng, K. W. K. Wong, T. Broadhurst and T. G. F. Li, *Precise LIGO lensing rate predictions for binary black holes*, *Phys. Rev. D* **97** (2018) 023012 [1703.06319].
- [391] L. Boco, A. Lapi, S. Goswami, F. Perrotta, C. Baccigalupi and L. Danese, *Merging Rates of Compact Binaries in Galaxies: Perspectives for Gravitational Wave Detections*, *arXiv e-prints* (2019) arXiv:1907.06841 [1907.06841].
- [392] M. Sereno, A. Sesana, A. Bleuler, P. Jetzer, M. Volonteri and M. C. Begelman, *Strong Lensing of Gravitational Waves as Seen by LISA*, *Phys. Rev. Lett.* **105** (2010) 251101 [1011.5238].
- [393] M. Sereno, P. Jetzer, A. Sesana and M. Volonteri, *Cosmography with strong lensing of LISA gravitational wave sources*, *Mon. Not. R. Astron. Soc.* **415** (2011) 2773 [1104.1977].
- [394] T. Broadhurst, J. M. Diego and I. Smoot, George, *Reinterpreting Low Frequency LIGO/Virgo Events as Magnified Stellar-Mass Black Holes at Cosmological Distances*, *arXiv e-prints* (2018) arXiv:1802.05273 [1802.05273].
- [395] T. Broadhurst, J. M. Diego and I. Smoot, George F., *Twin LIGO/Virgo Detections of a Viable Gravitationally-Lensed Black Hole Merger*, *arXiv e-prints* (2019) arXiv:1901.03190 [1901.03190].
- [396] L. Dai and T. Venumadhav, *On the waveforms of gravitationally lensed gravitational waves*, *arXiv e-prints* (2017) arXiv:1702.04724 [1702.04724].
- [397] L. Yang, X. Ding, M. Biesiada, K. Liao and Z.-H. Zhu, *How Does the Earth's Rotation Affect Predictions of Gravitational Wave Strong Lensing Rates?*, *Astrophys. J.* **874** (2019) 139 [1903.11079].
- [398] S. Hou, X.-L. Fan and Z.-H. Zhu, *Gravitational Lensing of Gravitational Waves: Rotation of Polarization Plane*, *arXiv e-prints* (2019) arXiv:1907.07486 [1907.07486].
- [399] O. A. Hannuksela, K. Haris, K. K. Y. Ng, S. Kumar, A. K. Mehta, D. Keitel et al., *Search for Gravitational Lensing Signatures in LIGO-Virgo Binary Black Hole Events*, *Astrophys. J.* **874** (2019) L2 [1901.02674].
- [400] A. K. Y. Li, R. K. L. Lo, S. Sachdev, T. G. F. Li and A. J. Weinstein, *Targeted Sub-threshold Search for Strongly-lensed Gravitational-wave Events*, *arXiv*

- e-prints* (2019) arXiv:1904.06020 [[1904.06020](#)].
- [401] G. P. Smith, M. Jauzac, J. Veitch, W. M. Farr, R. Massey and J. Richard, *What if LIGO's gravitational wave detections are strongly lensed by massive galaxy clusters?*, *Mon. Not. R. Astron. Soc.* **475** (2018) 3823 [[1707.03412](#)].
 - [402] G. P. Smith, M. Bianconi, M. Jauzac, J. Richard, A. Robertson, C. P. L. Berry et al., *Deep and rapid observations of strong-lensing galaxy clusters within the sky localization of GW170814*, *Mon. Not. R. Astron. Soc.* **485** (2019) 5180 [[1805.07370](#)].
 - [403] S. Komossa, *Tidal disruption of stars by supermassive black holes: Status of observations*, *Journal of High Energy Astrophysics* **7** (2015) 148 [[1505.01093](#)].
 - [404] P. L. Kelly, J. M. Diego, S. Rodney, N. Kaiser, T. Broadhurst, A. Zitrin et al., *Extreme magnification of an individual star at redshift 1.5 by a galaxy-cluster lens*, *Nature Astronomy* **2** (2018) 334 [[1706.10279](#)].
 - [405] S. A. Rodney, I. Balestra, M. Bradac, G. Brammer, T. Broadhurst, G. B. Caminha et al., *Two peculiar fast transients in a strongly lensed host galaxy*, *Nature Astronomy* **2** (2018) 324 [[1707.02434](#)].
 - [406] A. A. Kaurov, L. Dai, T. Venumadhav, J. Miralda-Escudé and B. Frye, *Highly Magnified Stars in Lensing Clusters: New Evidence in a Galaxy Lensed by MACS J0416.1-2403*, *Astrophys. J.* **880** (2019) 58 [[1902.10090](#)].
 - [407] W. Chen, P. L. Kelly, J. M. Diego, M. Oguri, L. L. R. Williams, A. Zitrin et al., *Searching for Highly Magnified Stars at Cosmological Distances: Discovery of a Redshift 0.94 Blue Supergiant in Archival Images of the Galaxy Cluster MACS J0416.1-2403*, *Astrophys. J.* **881** (2019) 8 [[1902.05510](#)].